MATHEMATICAL MODELLING OF FLUID FLOW AND HEAT TRANSFER UNDER ELECTROMAGNETIC FORCE IN THE CONTINUOUS STEEL CASTING PROCESS

JUTATIP ARCHAPITAK

A THESIS SUBMITTED IN PARTIAL FULFILLMENT OF THE REQUIREMENTS FOR THE DEGREE OF DOCTOR OF PHILOSOPHY (MATHEMATICS) FACULTY OF GRADUATE STUDIES MAHIDOL UNIVERSITY 2004

ISBN 974-04-5099-7 COPYRIGHT OF MAHIDOL UNIVERSITY

Thesis entitled

MATHEMATICAL MODELLING OF FLUID FLOW AND HEAT TRANSFER UNDER ELECTROMAGNETIC FORCE IN THE CONTINUOUS STEEL CASTING PROCESS

	Miss Jutatip Archapitak
	Candidate
	Assoc. Prof. Benchawan Wiwatanapataphee,
	Ph.D.
	Major-Advisor
	Prof. I Ming Tang,
	Ph.D.
	Co-Advisor
	Assoc. Prof. Yong Hong Wu,
	Ph.D.
	Co-Advisor
Assoc. Prof. Rassmidara Hoonsawat,	Assoc. Prof. Montip Tiensuwan,
Ph.D.	Ph.D.
Dean	Chair
Faculty of Graduate Studies	Doctor of Philosophy Programme
	in Mathematics
	Faculty of Science

Thesis entitled

MATHEMATICAL MODELLING OF FLUID FLOW AND HEAT TRANSFER UNDER ELECTROMAGNETIC FORCE IN THE CONTINUOUS STEEL CASTING PROCESS

was submitted to the Faculty of Graduate Studies, Mahidol University for the degree of Doctor of Philosophy (Mathematics)

on

July 23, 2004

	Miss Jutatip Archapitak
	Candidate
	Assoc. Prof. Benchawan Wiwatanapataphee
	Ph.D.
	Chair
	Prof. I Ming Tang,
	Ph.D.
	Member
Lect. Winai Bodhisuwan,	Assoc. Prof. Yong Hong Wu,
Ph.D.	Ph.D.
Member	Member
Assoc. Prof. Rassmidara Hoonsawat,	Prof. Prasert Sobhon,
Ph.D.	Ph.D.
Dean	Dean
Faculty of Graduate Studies	Faculty of Science
Mahidol University	Mahidol University

ACKNOWLEDGEMENTS

I would like to thank Assoc. Prof. Dr. Benchawan Wiwatanapataphee, my advisor, for her guidance and encouragement. All advices have been of great value to me in the research and preparation of this thesis.

I wish to thank my co-advisor, Prof. Dr. I Ming Tang, for his kindness and his encouragement.

I would like to thank Assoc. Prof. Dr. Yong Hong Wu, my co-advisor, for his kindness, valuable advices, and encouragement during the period of my visit at Curtin University of Technology (Australia) in 2003.

I wish to thank Asst. Prof. Dr. Michael A. Allen for helping me to set up the Mahidol Thesis Latex style file.

I wish to thank the Department of Mathematics, Mahidol University and Department of Mathematics and Statistics, Curtin University of Technology for providing me with the necessary facilities.

I am very grateful to the Thailand Research Fund (TRF) and Development and Promotion of Science and Technology Talents Project (DPST) for the financial support during the period of my study.

Finally, I am greatful to my family and my friends for their encouragement.

Jutatip Archapitak

MATHEMATICAL MODELLING OF FLUID FLOW AND HEAT TRANSFER UNDER ELECTROMAGNETIC FORCE IN THE CONTINUOUS STEEL CASTING PROCESS

JUTATIP ARCHAPITAK 4237665 SCMA/D

Ph.D. (MATHEMATICS)

THESIS ADVISORS: BENCHAWAN WIWATANAPATAPHEE, Ph.D. (APPLIED MATHEMATICS), I MING TANG, Ph.D. (PHYSICS), YONG HONG WU, Ph.D. (APPLIED MATHEMATICS)

ABSTRACT

The continuous steel casting process involves heat transfer, fluid flow and solidification, which effect the quality of steel. Hence, understanding these underlying phenomena is essential for optimizing the casting process and solving problems that have still not been fully understood. I have undertaken a mathematical study to model multi-phase flows including the flux flow and the molten steel flow in the continuous casting process. The work is mainly based on fluid dynamics and electromagnetic theory. The focus of the project is the construction of a mathematical model and the development of robust simulation technique. By incorporating Lorentz force into the model, the influence of an electromagnetic field on heat transfer and fluid flow can be simulated. The model is then illustrated with a numerical example which demonstrates that the thickness of the solidified steel shell critically depends on the magnitude of the Lorentz force. The Lorentz force prevents the molten steel from sticking to the mould wall. The numerical results show that the model is capable of analyzing the influence of an electromagnetic field on the flow pattern of fluid and the solidification profile of steel and could be used in solving technical problems in steel casting.

KEY WORDS : FINITE ELEMENT METHOD / ELECTROMAGNETIC FLUID FLOW / HEAT TRANSFER / MENISCUS

114 pp. ISBN 974-04-5099-7

การจำลองแบบทางคณิตศาสตร์ของการไหลของของเหลวและการถ่ายเทความร้อนด้วยแรง จากสนามแม่เหล็กไฟฟ้าในกระบวนการหล่อเหล็กต่อเนื่อง (MATHEMATICAL MOD-ELLING OF FLUID FLOW AND HEAT TRANSFER UNDER ELECTROMAGNETIC FORCE IN THE CONTINUOUS STEEL CASTING PROCESS)

จุฑาธิป อาชาพิทักษ์ $4237665~\mathrm{SCMA/D}$

ปร.ด. (คณิตศาสตร์)

คณะกรรมการควบคุมวิทยานิพนธ์ : เบญจวรรณ วิวัฒนปฐพี, Ph.D. (APPLIED MATHEMATICS), I Ming Tang, Ph.D. (PHYSICS), YONG HONG WU, Ph.D. (APPLIED MATHEMATICS)

บทคัดย่อ

การหล่อเหล็กต่อเนื่องเกี่ยวกับปรากฏการณ์หลายอย่างเช่น การถ่ายเทความร้อน การ ไหลของของเหลว และการแข็งตัว ซึ่งปรากฏการณ์เหล่านี้มีผลกระทบต่อคุณภาพของเหล็ก ดัง นั้นการเข้าใจปรากฏการณ์เหล่านี้จึงมีความจำเป็นสำหรับการพัฒนากระบวนการหล่อเหล็กต่อ เนื่องให้มีประสิทธิภาพสูงขึ้น และแก้ปัญหาที่ยังคงเกิดขึ้น ดังนั้นการศึกษาในเชิงคณิตศาสตร์ โดยการสร้างแบบจำลองเพื่ออธิบายปรากฏการณ์ต่าง ๆ ที่เกิดขึ้นในกระบวนการหล่อเหล็กโดย อาศัยความรู้ด้านพลศาสตร์ของไหลและทฤษฎีแม่เหล็กไฟฟ้าได้ถูกนำมาใช้ในวิทยานิพนธ์ฉบับ นี้ โดยมีจุดประสงค์เพื่อพัฒนาแบบจำลองทางคณิตศาสตร์ และเทคนิคเชิงคำนวนสำหรับการ วิเคราะห์ปัญหาของการไหลของน้ำเหล็ก การถ่ายเทความร้อนและการเข็งตัวของเหล็กเมื่อมีผล กระทบจากแรง Lorentz เข้ามาเกี่ยวข้อง ผลจากการศึกษาด้วยตัวอย่างการคำนวณแสดงให้ เห็นว่า ขนาดแรงจากสนามแม่เหล็กไฟฟ้ามีผลต่อความหนาของชั้นเหล็กที่แข็งตัวที่บริเวณโดย รอบของเตาหล่อ อีกทั้งแรง Lorentz ช่วยป้องกันไม่ให้น้ำเหล็กติดที่ผนังของเตาหล่อ ดังนั้น ผลเฉลยจากการคำนวณแสดงให้เห็นว่าแบบจำลองทางคณิตศาสตร์ที่ถูกนำเสนอนี้สามารถใช้ใน การวิเคราะห์อิทธิพลของสนามแม่เหล็กไฟฟ้าต่อลักษณะของการไหลของของเหลวและการแข็ง ตัวของเหล็ก อีกทั้งยังสามารถใช้ในการแก้ปัญหาในกระบวนการหล่อเหล็กได้

114 หน้า ISBN 974-04-5099-7

CONTENTS

\mathbf{A}	CKNOWLEDGEMENTS	iii
\mathbf{A}	BSTRACT	iv
\mathbf{T}	HAI ABSTRACT	\mathbf{v}
LI	IST OF TABLES	viii
LI	IST OF FIGURES	ix
1	Introduction	1
	1.1 An Overview of the Continuous Casting Process	1
	1.2 Scope and Objectives	6
	1.3 Outline of the Thesis	6
2	Literature Review	8
	2.1 General Overview	8
	2.2 Modelling of Fluid Flow and Heat Transfer	9
	2.3 Modelling of Electromagnetic Field in Continuous Casting	
	Process	10
	2.4 Modelling of Fluid Flow and Heat Transfer at the Presence of	
	an Electromagnetic Field	11
	2.5 Modelling of Meniscus Phenomena	12
	2.6 Concluding Remarks	13
3	Electromagnetic Field in Continuous Casting Process	14
	3.1 General Overview	14
	3.2 Boundary Value Problem for the Electromagnetic Field	14

	CONTENTS (CONT.)	vii
	3.3 Finite Element Method for the Electromagnetic Field	19
	3.4 Numerical Studies	21
	3.6 Concluding Remarks	22
4	Coupled Fluid Flow-Heat Transfer in Electromagnetic Casting	31
	4.1 General Overview	31
	4.2 Mathematical Model	32
	4.3 Finite Element Formulation	37
	4.4 Numerical Algorithm	49
	4.5 Numerical Studies	52
	5.6 Concluding Remarks	55
5	Dynamic Behavior at Meniscus Region	68
	5.1 General Overview	68
	5.2 Mathematical Model	68
	5.3 Moving Finite Element Formulation	70
	5.4 Numerical Studies	80
	5.5 Concluding Remarks	82
6	Summary and Conclusions	85
	6.1 Concluding Remarks	85
	6.2 Further Works	86
\mathbf{R}	EFERENCES	87
\mathbf{A}	PPENDIX	94
Bl	IOGRAPHY	114

LIST OF TABLES

3.1	Material parameters	23
3.2	Computation schemes	24
4.1	Parameters used in numerical simulation	53
4.2	Computation schemes	54
5.1	Parameters used in numerical simulation	84
5.2	Computation schemes	84

LIST OF FIGURES

1.1	Continuous casting steel plant	2
1.2	The continuous casting process	3
1.3	The layers in the mould during casting	4
1.4	The electromagnetic stirring	5
3.1	The computation domain for the electromagnetic problem	18
3.2	The finite element mesh for the electromagnetic problem	23
3.3	The contour plot of the magnetic vector potential $\mathbf{A}(Wb/m)$ at	
	frequency $f=60$ Hz and source current density $\mathbf{J_s}=1000000~A/m^2.$	25
3.4	The vector plot of the magnetic flux density ${\bf B}$ (Tesla) at frequency	
	$f=60~{\rm Hz}$ and source current density ${\bf J_s}=1000000~A/m^2.$	26
3.5	The contour plot of induced current $\mathbf{J_e}\left(A/m^2\right)$ in the continuous	
	casting mould at frequency $f = 60$ Hz and source current density	
	$J_{s} = 1000000 \ A/m^{2}.$	27
3.6	The vector plot of electromagnetic force $F_{em} (N/m^3)$ in the	
	electromagnetic continuous caster at frequency $f = 60$ Hz and	
	source current density $\mathbf{J_s} = 1000000 \ A/m^2 \dots \dots \dots$	28
3.7	The influence of source current density $\mathbf{J_s} \ (A/m^2)$ on the magnitude	
	of electromagnetic force in the continuous casting process at	
	frequency $f = 60 \text{ Hz.} \dots \dots \dots \dots \dots \dots$	29
3.8	The influence of the frequency of magnetic field $f(Hz)$ on the	
	magnitude of electromagnetic force in the continuous casting	
	process at source current density $\mathbf{J_s} = 1000000 \ A/m^2 \dots$	30
	,	
4.1	Generation of finite element mesh from master element	45
4.2	The computation domain and coordinate system	56
4.3	The finite element mesh for the coupled fluid flow-heat transfer	
	problem	57
4.4	Vector plot of velocity vectors ${\bf u}$ (m/s) and temperature contours	
	$T(^{\circ}C)$ when the coil current is off	58

4.5	Velocity vectors \mathbf{u} (m/s) and temperature contours $T({}^{\circ}C)$ under	
	60 Hz magnetic field and 30000 A source current	59
4.6	Temperature profile $T({}^{\circ}C)$ in the liquid steel pool : (a) without	
	EM force, (b) with EM force under 60 Hz magnetic field and 30000	
	A source current	60
4.7	Thickness of solidified steel shell in (a) with no magnetic field, (b)	
	under 60 Hz magnetic field and 30000 A source current	61
4.8	Temperature distribution of steel strand $T({}^{\circ}C)$ in conventional	
	continuous caster	62
4.9	Temperature distribution of steel strand $T(^{\circ}C)$ in EM caster under	
	60 Hz magnetic field and 30000 A source current	62
4.10	Temperature profile at the end of mould : label $-*-$ for a model	
	without EM force and — for a model with EM force under 60 Hz	
	magnetic field and 30000 A source current	63
4.11	The velocity fields of molten steel in the process for three different	
	source currents : (a) 10000 A, (b) 20000 A, and (c) 30000 A	64
4.12	Temperature distributions of steel in the process for three different	
	source currents : (a) 10000 A, (b) 20000 A, and (c) 30000 A	65
4.13	Thickness of solidified steel shell for different source currents : (a)	
	10000 A, (b) 20000 A, and (c) 30000 A	66
4.14	Temperature profile (° C) at the end of mould for different source	
	currents : label $-*-$ for a model without EM force, and —— for a	
	model with EM force	67
5.1	Computation domain.	71
5.2	Generating mesh for flux and steel	81
5.3	Flow patterns of liquid flux (labelled by black color) and liquid	
	steel (labelled by red color) in (a) conventional casting process and	
	(b) EM casting process	82
5.4	Flow patterns of liquid flux (labelled by black color) and liquid	
	steel (labelled by red color) for different source currents (a) 10000	
	A (b) 20000 A and (c) 30000 A	83

CHAPTER 1

INTRODUCTION

1.1 An Overview of the Continuous Casting Process

Steel making industry is a large-scale industry comprising many production processes ranging from upstream processes to downstream processes as shown in Figure 1.1 [1]. The continuous steel casting process is the process for casting semi-finished steel products such as billet, slab and bloom. The process involves many complex phenomena such as heat transfer, flow of molten steel and flux, formation of oscillation marks on the steel surface, etc. Over the last few decades, the continuous casting process has been increasingly used to produce billet, slab and bloom. Over 80 % of the Western world steel products were casted by the continuous casting process in 1993 [2]. This ratio is expected to increase continuously due to the superiority of the continuous casting over the ingot casting in the following aspects:

- reducing energy consumption;
- savings in manpower;
- reduction in production costs;
- improvement of steel quality.

Although there are many different designs of the continuous steel caster, the schematic diagram of the continuous caster is as shown in Figure 1.2 [3]. The basic principle of the continuous casting process is to pour liquid steel into a water-cooled mould continuously. Due to the intense cooling by water running through channels in the mould wall, the solidified steel shell forms around the edges of mould. The solidified steel shell with a liquid pool at the center is

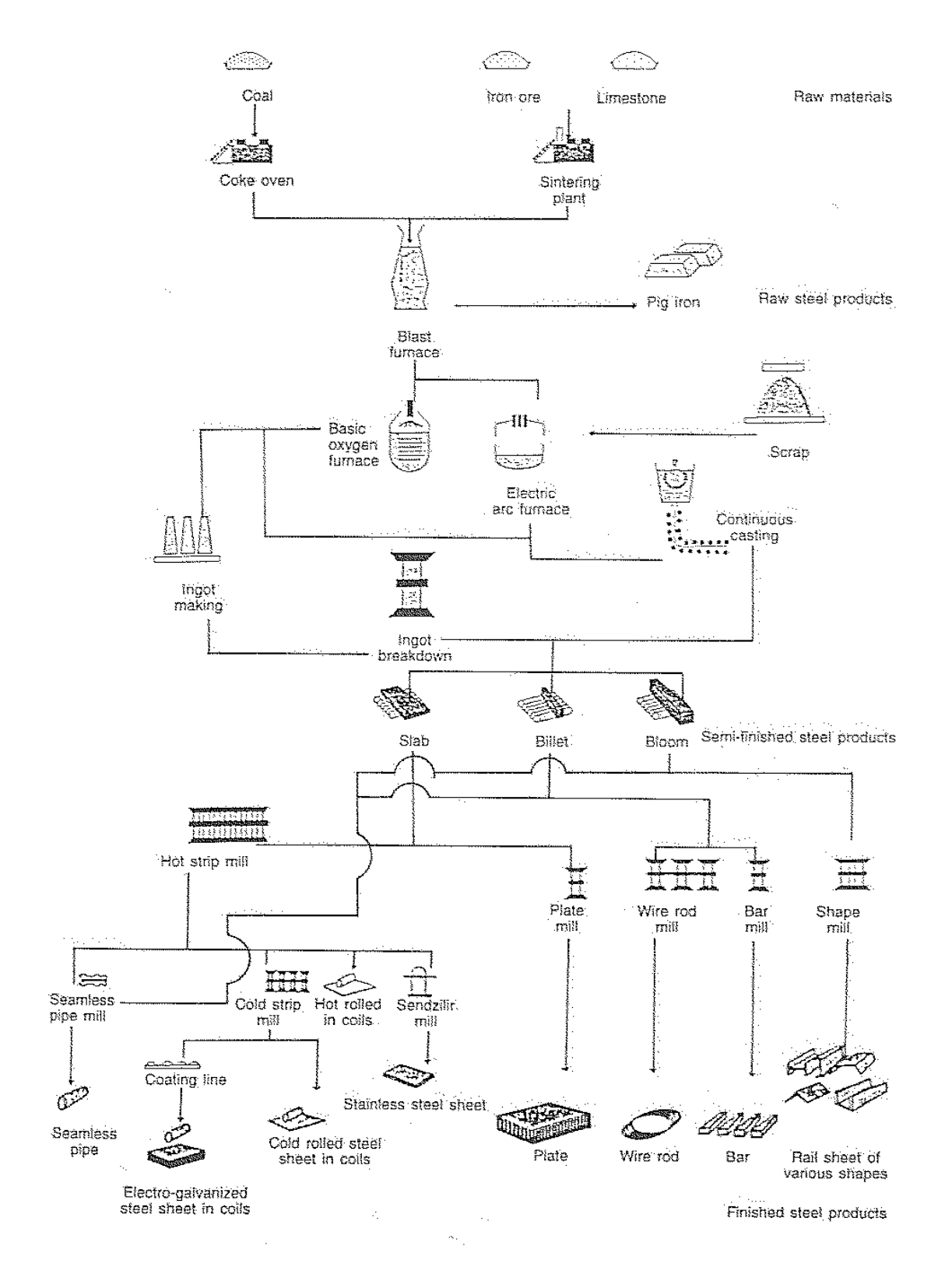


Figure 1.1: Continuous casting steel plant.

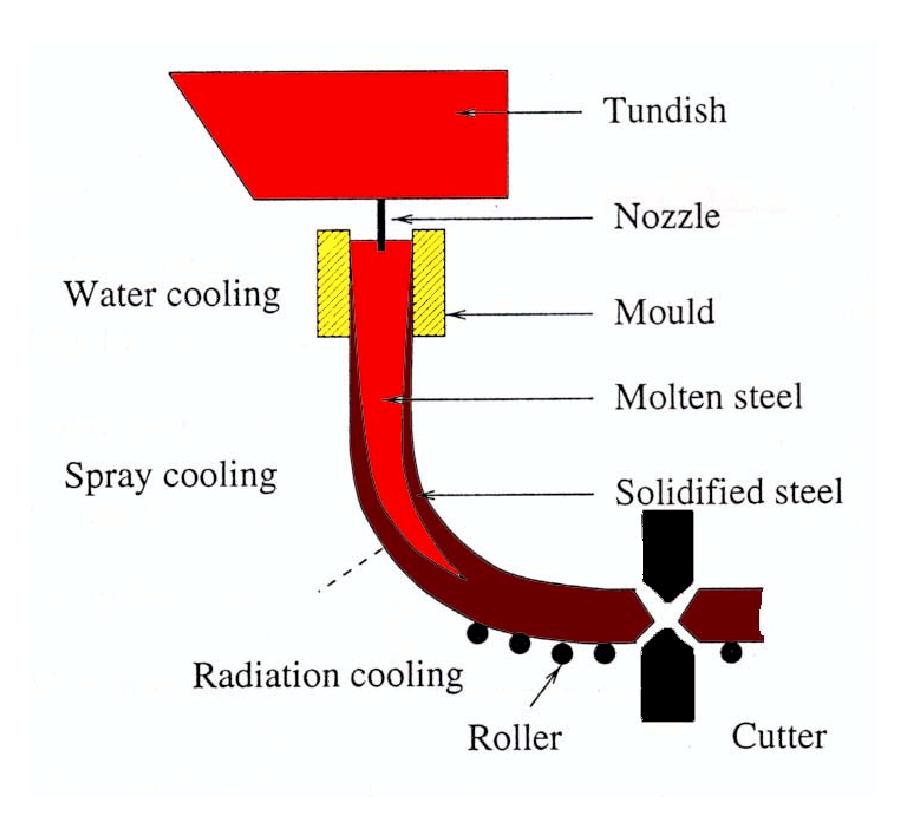


Figure 1.2: The continuous casting process.

withdrawn from the bottom of the mould at the casting speed under support of series of rolls which ensure that it is both rolled into shape and fully solidified at the same time. To facilitate the process and to avoid sticking of the solidified skin to the mould wall, the mould wall itself oscillates vertically. The lubrication oil or mould powder is added continuously at the top of the mould during the process to form a protective liquid flux layer. The liquid flux is drawn into the gap between the steel surface and the mould wall. The various layers formed in the mould during casting are shown in Figure 1.3 [4]. At the cutting point, the casting is cut to the required length.

Over the last few decades, many technologies have been developed and applied to the continuous casting process for improving the quality of the casting product and the production rate. The electromagnetic stirring technology is one of the most promising technologies. It is superior to the conventional continuous casting as it produces casting products with better quality including

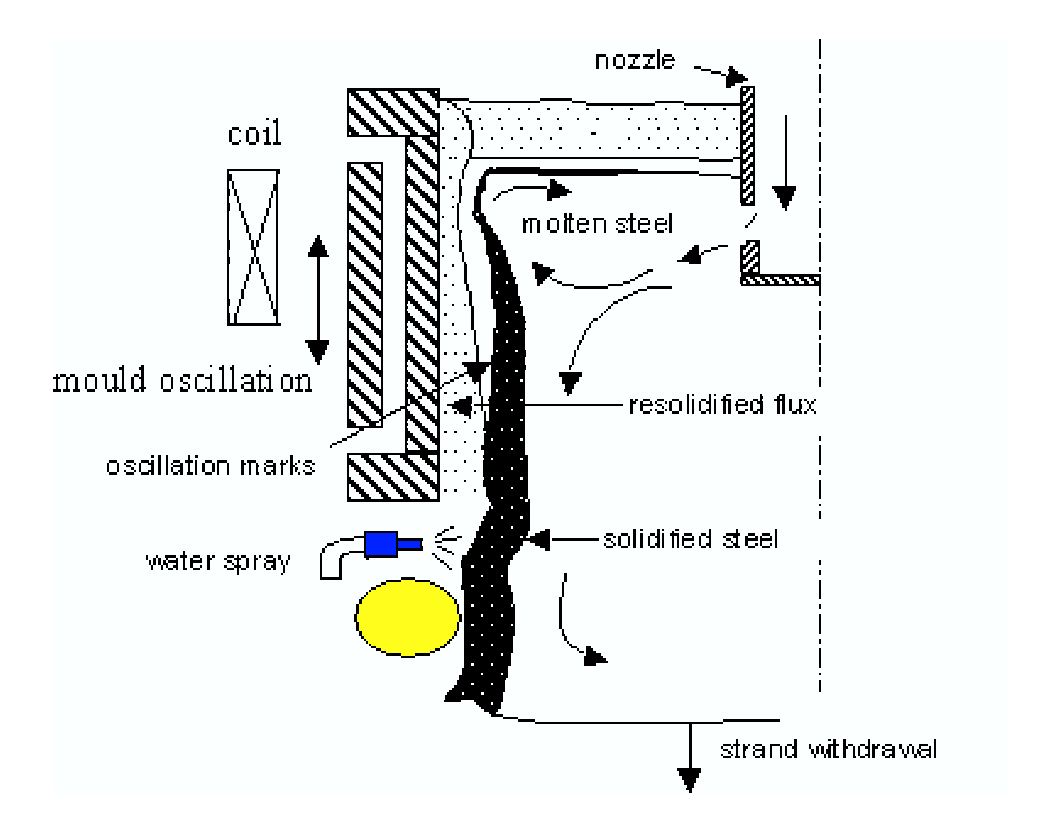


Figure 1.3: The layers in the mould during casting

- improved shearing ability by avoiding structures which cause cracks;
- better hot workability during extrusion forging;
- improved wire rod drawing performance with a low frequency of cup and cone breakages;
- higher and more consistent fatigue properties.

The schematic diagram of electromagnetic casting is shown in Figure 1.4. The basic concept of electromagnetic stirring is to generate induced currents in the steel by applying a moving electromagnetic field to the process. This force affects the flow of liquid steel, and consequently the solidification of the steel. Thus, with the electromagnetic stirring, it is possible to improve the steel surface quality, the internal segregation and structure of the steel [5, 6, 7, 8, 9]. Although this technology has been developed to reduce the occurring of operational problems and to improve the quality of steel products, various crucial problems still

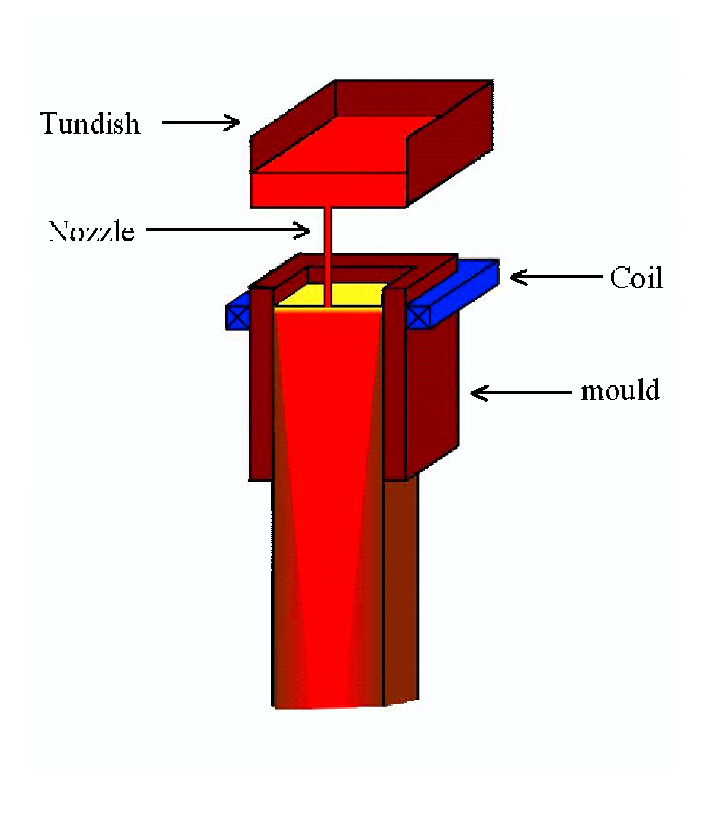


Figure 1.4: The electromagnetic stirring.

frequently occur in the industrial operations such as

- the formation of oscillation marks on the steel surface;
- the generation of cracks on the longitude and transverse of surface and subsurface of steel;
- the breakout of molten steel from the bottom of the mould.

Thus, it is necessary to understand the phenomena occurring in the casting process in order to develop better casting technologies and optimize the process. Although a great deal of work has been carried out to study various aspects of the continuous casting process, very few attempts have been made to study the fluid flow and heat transfer in the meniscus region. The phenomena in this region are still not well understood. Thus, in this work, the meniscus region is included in the computational domain. The aims of this work are to establish a mathematical model for the fluid flow, heat transfer and solidification problem

and to develop a numerical algorithm for simulating the phenomena occurring in the meniscus region in the electromagnetic continuous casting process. In addition, the two-phase flow of steel and flux is studied to predict the meniscus shape. The effect of electromagnetic field on fluid flow and solidification of steel is investigated.

1.2 Scope and Objectives

Although various mathematical models have been developed to describe the phenomena occurring in the continuous casting process [3, 10, 11, 12, 13], the coupled fluid flow-heat transfer process in the meniscus region and the effect of electromagnetic field on the process have still not been fully understood. Thus, this research aims to

- develop a mathematical model to describe the coupled fluid flow and heat transfer with solidification process in the mould region and the meniscus region, taking into account the effect of the electromagnetic field;
- formulate the finite element methods for solving the electromagnetic stirring problem and the coupled fluid flow and heat transfer problem;
- develop a numerical algorithm for simulating the electromagnetic casting process;
- investigate the effect of electromagnetic field on the flow field, temperature field and meniscus shape.

1.3 Outline of the Thesis

This thesis comprises six chapters. In chapter 1, the basic principles of the continuous steel casting and the electromagnetic stirring technology are presented. The scope and objectives are also given in this chapter. In chapter 2, the previous works closely related to our scope and objectives are summarized. Chapter 3 concerns the mathematical model for studying the

two-dimensional electromagnetic stirring problem. The governing equations are Maxwell's equations. A numerical algorithm based on the finite element method is developed to solve the problem. The commercial package FEMLAB is also used to simulate the electromagnetic field in the continuous casting process. The effect of casting parameters such as source current and frequency of magnetic field on the electromagnetic force are investigated. In chapter 4, the effect of electromagnetic field on the coupled fluid flow and heat transfer process is studied. The governing equations consist of the Navier-Stokes equations, the continuity equation and the convection-diffusion equation. A numerical algorithm based on the finite element method is developed to solve the problem. The effect of various casting parameters and electromagnetic parameters on the flow field and temperature field are investigated. In chapter 5, we present a 2-D mathematical model of steel-flux flow in the meniscus region to predict the meniscus shape. An algorithm based on the pressure balance and the moving finite element method are developed to solve this problem. The effect of electromagnetic fields on the flow field is studied in this chapter.

The conclusions gained from this work are given in chapter 6, together with some suggestions for further work.

CHAPTER 2

LITERATURE REVIEW

2.1 General Overview

Many complex phenomena, such as solidification of steel, formation of oscillation marks on steel surface, breakout of molten steel at the bottom of the mould and flow of flux, occur in the continuous steel casting process. All these phenomena have effect on the quality of steel product. To improve the product quality, new technologies using electromagnetic field in the process have been developed to cast steel products.

Over the last few decades, extensive research has been carried out to study the various phenomena occurring in the continuous steel casting process, including experimental studies, analytical studies and numerical studies. Numerical investigation has been the dominant approach, as experimental studies are limited due to the high temperature involved in the process and analytical approach could only solve very simple problems. The previous studies mainly focused on the following areas [3, 6, 9, 15]:

- the meniscus phenomena,
- flux flow and formation of oscillation marks on the steel surface,
- heat transfer with solidification of steel,
- flow of molten steel,
- the coupled fluid flow and heat transfer,
- the effect of an electromagnetic field on molten steel flow and heat transfer with solidification.

2.2 Modelling of Fluid Flow and Heat Transfer

Various mathematical models and numerical algorithms for fluid flow and heat transfer have been developed to study the pattern of molten steel flow and the temperature distribution in the continuous steel casting process. In 1997, Li [14] developed a numerical algorithm based on the finite element method and the Lagrangian Eulerian formulation for solving the transient evolution of the fluid flow, heat transfer and solidification phenomena in the ingot and spreading casting. His model is based on Scheil's equation to predict temperature distribution and fluid flow of steel. His results lead to better understanding of the process and provide useful information which can be used to improve the design of the casting process and equipment. Wiwatanapataphee (1998) [3] presented a coupled turbulent fluid flow-heat transfer with solidification model to analyze the effect of turbulence on the solidification of steel and the flow of molten steel. She developed a finite element algorithm to solve the problem and investigated the effect of some casting parameters on the solidification profile and the flow field of fluid. Yang et al. (1998) [15] developed a coupled model for the fluid flow, heat transfer, solidification and solute redistribution in the continuous casting process. The porous media theory is used to model the blockage of fluid flow by columna dendrites in the mushy zone. The output shows the close relationship between the flow pattern of molten steel and the shape of the solid shell. In the work of Lee et al. (1999) [16], the finite difference method is used to analyze the turbulent fluid flow in a round billet and the finite element method is used to analyze the thermo-elastic plastic deformation. The simulation results are in good agreement with the experimental observations. The cracks on surface were predicted in the work and the effect of casting speed was investigated. In 2001, Takatani et al. [17] developed a mathematical model for simulating the transient fluid flow in a continuous casting mould. The argon gas injected from the nozzle, the molten steel and the solidified shell are all taken into account in the calculation. They also used a water model in their experimental study and compared experimental results with the simulation results. An algorithm based

on the SOLA method was used to solve the problem. In 2002, Thomas *et al.* [18] presented four different methods for evaluating velocity of fluid flow in the liquid pool. The computations are based on PIV, CFX and LES, and electromagnetic sensors at the mould wall are used to measure the flow velocity. The turbulence effect is modelled by using the standard $K - \varepsilon$ model.

2.3 Modelling of Electromagnetic Field in Continuous Casting Process

Major reviews on the application of electromagnetic field in the continuous casting process are given in many papers due to Birat and Chonè (1983) [6], Garnier (1990) [19], Kolesnichenko (1990) [20] and Nakanishi (1996) [21]. Various studies have been undertaken to develop mathematical models and numerical algorithms to study the electromagnetic problem in the continuous casting process. Makarov et al. (2000) [22] analyzed the conventional method for electromagnetic separation of small inclusion in metal casting with high electric conductivity. The separation technique for the electromagnetic force was presented and analyzed in each case. It is noted that a direct current superconduction coil can drastically improve the power loss in the process. Trindade et al. (2002) [23] introduced a low-frequency numerical model for the electromagnetic field in the continuous casting process. A finite element algorithm based on the ELEKTRA/OPERA-3D Package was used to solve the problem. They compared the simulation outputs with experimental measurements and the results were in agreement. In the same year, Na et al. (2002) [24] used a high frequency magnetic field in a soft contact continuous casting mould in the continuous steel casting process. The distribution of electromagnetic field, the electromagnetic body force and the effect of magnetic field frequency on the solidification were discussed in their work.

2.4 Modelling of Fluid Flow and Heat Transfer at the Presence of an Electromagnetic Field

Over the last two decades, the electromagnetic casting has been developed to cast steel products. In 1989, the influence of an electromagnetic field on the solidification was investigated in the work of Miyoshino et al. [9]. They introduced the fundamental of magnetohydrodynamic phenomena through experimental and numerical studies. A low frequency magnetic field (60 Hz) was used in the experimental system. In the same year, Ganma et al. [25] studied the pattern of fluid flow in the mould with the effect of electromagnetic stirring in the slab caster. The experimental results and the simulation results The results show that the velocity of molten steel were given in the work. that is injected from the nozzle is decelerated when the electromagnetic field is applied. In 1996, Trophime et al. [26] presented a mathematical model for the magnetrohydrodynamic problem. The electromagnetic model $(A - \phi \text{ model})$ and the fluid flow model are developed and the finite element method is used to solve the problem. In 1997, Toh et al.[8] presented a mathematical model for controlling the solidification of steel in the continuous steel casting process with the effect of electromagnetic field. The low-frequency magnetic field used in the simulation was of 60 Hz. The numerical results show that the surface of the steel is improved by the use of the magnetic field. As in the works of Fujisaki et al. [27, 28], they presented the mathematical model for In-Mold electromagnetic stirring in the continuous casting process. The experimental results and simulation results are in good agreement and show that the electromagnetic stirring leads to more uniform velocity field near the mould wall. In 1998, Li [29] used an electromagnetic field in a model for the coupled fluid flow, heat transfer and solidification process. Maxwell's equations were used to model the electromagnetic field. The results show that an electromagnetic field can reduce the fluid motion and affect the quality of the steel. Dumont and Gagnoud (2000) [30] presented a model for the molten metal shape in the electromagnetic casting to analyze the interactions between the shape of a molten metal and a magnetic field distribution. They developed a numerical algorithm based on a moving finite element mesh with impedance boundary condition to solve the problem, and determined the free surface under the equilibrium of the electromagnetic and hydrostatic pressures. Fujisaki (2000) [31] developed a three-dimension magnetohydrodynamic calculation model for the heat transfer and solidification problem. The electromagnetic force is calculated using the shadow method when the flow of molten steel changes. The results of this calculation show that the electromagnetic stirring makes the solidified steel shell uniform and the dynamic deviation of temperature stable. Li et al. (2000) [32] developed a mathematical model for the fluid flow with the effect of an electromagnetic field. The effect of argon gas injection was also investigated in this work. The computational results show that the argon gas injection affects the flow pattern of molten steel. In 2001, Park et al. [33] presented a mathematical model for the fluid flow and heat transfer analysis. The effect of varying the nozzle angle is taken into account to investigate the flow pattern in the mould. In 2002, Park et al. [34] and Kim et al. [35] studied the effect of a high frequency magnetic field in the electromagnetic casting technology. The experimental study was carried out to examine the effect of mould shape on the quality of the steel billet surface. They also investigated the effect of current source, casting speed and mould oscillation pattern on the surface quality of steel.

2.5 Modelling of Meniscus Phenomena

The study of the meniscus phenomena in the continuous casting process has been undertaken by many researchers. The flow of molten steel, lubrication flux, and heat transfer at the top surface were studied by McDavid and Thomas (1996) [36]. A three-dimensional finite element formulation was presented in their work. The effect of various material parameters on the formation of the flux layer was also investigated. The model gave reasonable results of the flux layer in the operating slab casting. The melting behavior of mould powders and the formation of the mould powder liquid pool were studied by Nakano et al. [37] in

1970. They proposed a one-dimensional heat conduction equation taking into account the difference in material properties of the various forms of the flux. In the work of Nakata and Etay (1992)[38], the two-dimensional meniscus shape under an alternating magnetic field was simulated. The finite difference method was used to solve the problem. The frequency of magnetic field and coil current are taken into account to investigate the height of meniscus layer. Li et al. (1995) [39] studied the behavior on the meniscus region and the properties of the surface on the billet casting in the presence of a magnetic field. The relations between the meniscus behavior and the surface quality were investigated in their work. The effect of a high-frequency magnetic field, mould oscillation on meniscus behavior was presented. The experimental results using molten gallium and molten tin were used to confirm the given concepts. The results of the study also showed that the use of a magnetic field improves the quality of the steel surface. Lucus (1998) [40] proposed a three-dimensional model for the fluid flow problem. The meniscus interface was studied by using the commercial package CFX. His results gave a flow field similar to that simulated using PIV by Thomas (2001) [41]. Sha et al. (1996) [42] investigated the behavior of meniscus on the mercury and silicon oil with the effect of oscillation wall. A two-dimensional mathematical model was presented in the work, together with the initial and boundary conditions. The Marker and Cell (MAC) method has been used to solve the problem. The experimental results and the computation results on the meniscus shape were in good agreement.

2.6 Concluding Remarks

Many models concerning about the phenomena in the continuous casting process have been developed to describe the complex phenomena. Many researchers focused only on subproblems of heat transfer, fluid flow and solidification. Further work is needed to investigate the influence of electromagnetic field on the coupled fluid flow and heat transfer with solidification process occurring in the continuous steel casting process.

CHAPTER 3

ELECTROMAGNETIC FIELD IN CONTINUOUS CASTING PROCESS

3.1 General Overview

Over the last few decades, the electromagnetic continuous casting process, as shown in Figure 1.4, has been used to cast steel products. The electromagnetic field will generate eddy currents and electromagnetic forces which consequently influence the flow of molten steel and heat transfer with solidification. As steel is a good conductor, the magnetic Reynold's number is very small. The change in the magnetic flux density caused by the fluid flow can thus be neglected. Hence, the electromagnetic problem is uncoupled from the fluid flow problem and solved separately.

In this chapter, we establish a mathematical model for the electromagnetic problem in the continuous casting process. The $A - \phi$ model based on Maxwell's equations and boundary conditions are presented in section 3.2. In section 3.3, the Bubnov-Galerkin finite element method for the solution of the electromagnetic problem is presented. In section 3.4, the influences of various parameters on the electromagnetic field in the continuous casting process are investigated.

3.2 Boundary Value Problem for the Electromagnetic Field

The governing equations for the electromagnetic field include the Maxwell's equations and the constitutive equations. Let H and E denote respectively the magnetic field and the electric field. The Maxwell's equations are

$$\nabla \times \mathbf{H} = \mathbf{J} + \frac{\partial \mathbf{D}}{\partial t},\tag{3.1}$$

Fac. of Grad. Studies, Mahidol Univ.

$$\nabla \times \mathbf{E} = -\frac{\partial \mathbf{B}}{\partial t},\tag{3.2}$$

$$\nabla \cdot \mathbf{B} = 0, \tag{3.3}$$

$$\nabla \cdot \mathbf{D} = \rho_d, \tag{3.4}$$

where \mathbf{J} is the total current density, \mathbf{D} is the electric displacement, ρ_d is the free charge density, and \mathbf{B} is the magnetic flux density. The magnetic flux density \mathbf{B} and the electric displacement \mathbf{D} are respectively related to the magnetic field \mathbf{H} and the electric field \mathbf{E} by the following constitutive equations

$$\mathbf{B} = \mu \mathbf{H},\tag{3.5}$$

$$\mathbf{D} = \varepsilon \mathbf{E},\tag{3.6}$$

where μ and ε are magnetic permeability and electric permeability, respectively. Another constitutive equation relating the induced current density with \mathbf{E} , \mathbf{B} and the velocity \mathbf{v} is as follows

$$\mathbf{J_e} = \sigma(\mathbf{E} + \mathbf{v} \times \mathbf{B}) + \rho_d \mathbf{v},\tag{3.7}$$

where σ is the electric conductivity. For metal material (good conductors), we could assume that the field changed in one part of the system radiates to other parts instantaneously. Thus, the term $\frac{\partial \mathbf{D}}{\partial t}$ in the equation (3.1) can be neglected and the equation (3.1) becomes

$$\nabla \times \mathbf{H} = \mathbf{J},\tag{3.8}$$

from which and noting that the divergence of the curl of a vector field is identical to zero, we have

$$\nabla \cdot \mathbf{J} = 0. \tag{3.9}$$

Furthermore, in the case that the magnetic Reynolds number $(R_m = \mu \sigma \mathbf{v} L)$ is sufficiently small ($\ll 1$), the term $(\mathbf{v} \times \mathbf{B})$ in equation (3.7) due to fluid flow can be neglected. Under the above approximation and neglecting the displacement current ρ_d , the field equations are simplified as follows

$$\nabla \times \mathbf{H} = \mathbf{J},\tag{3.10}$$

$$\nabla \times \mathbf{E} = -\frac{\partial \mathbf{B}}{\partial t},\tag{3.11}$$

$$\nabla \cdot \mathbf{B} = 0, \tag{3.12}$$

$$\nabla \cdot \mathbf{D} = 0, \tag{3.13}$$

$$\mathbf{B} = \mu \mathbf{H},\tag{3.14}$$

$$\mathbf{J_e} = \sigma \mathbf{E}.\tag{3.15}$$

The Maxwell's equations and the constitutive equations can also be formulated in terms of potential functions. From equation (3.12) and noting that the divergence of the curl of a vector field is identical to zero, we can introduce the magnetic flux density \mathbf{B} in terms of a magnetic vector potential \mathbf{A} such that

$$\mathbf{B} = \nabla \times \mathbf{A}.\tag{3.16}$$

Using equations (3.14) and (3.16), we have from equation (3.10) that

$$\nabla \times (\frac{1}{\mu} \nabla \times \mathbf{A}) = \mathbf{J}. \tag{3.17}$$

Substituting equation (3.16) into equation (3.11), we have

$$\nabla \times (\mathbf{E} + \frac{\partial \mathbf{A}}{\partial t}) = 0. \tag{3.18}$$

Thus, the field $\mathbf{E} + \frac{\partial \mathbf{A}}{\partial t}$ is conservative and consequently there exists a scalar potential ϕ such that

$$\mathbf{E} + \frac{\partial \mathbf{A}}{\partial t} = -\nabla \phi. \tag{3.19}$$

Hence, the electric field can be determined by

$$\mathbf{E} = -\frac{\partial \mathbf{A}}{\partial t} - \nabla \phi. \tag{3.20}$$

The total current density J is defined as the sum of the induced current density J_e and the source current density J_s , namely

$$\mathbf{J} = \mathbf{J_e} + \mathbf{J_s} = -\sigma \frac{\partial \mathbf{A}}{\partial t} - \sigma \nabla \phi + \mathbf{J_s}.$$
 (3.21)

Substituting equation (3.21) into (3.17), we end up with the Maxwell's equations in terms of the magnetic vector potential \mathbf{A} and the electric scalar potential ϕ as follows

$$\nabla \times (\frac{1}{\mu} \nabla \times \mathbf{A}) = -\sigma \frac{\partial \mathbf{A}}{\partial t} - \sigma \nabla \phi + \mathbf{J_s}, \tag{3.22}$$

$$\nabla \cdot (-\sigma \frac{\partial \mathbf{A}}{\partial t} - \sigma \nabla \phi + \mathbf{J_s}) = 0. \tag{3.23}$$

In the case that sinusoidal current is applied for the problem, the solution may be assumed to have the form of $\mathbf{A}(\mathbf{x})e^{j\omega t}$. Thus, the partial derivative of the vector potential with respect to time may be replaced by $j\omega \mathbf{A}$. Hence equations (3.22) and (3.23) become

$$\nabla \times (\frac{1}{\mu} \nabla \times \mathbf{A}) = -\sigma j \omega \mathbf{A} - \sigma \nabla \phi + \mathbf{J_s}, \tag{3.24}$$

$$\nabla \cdot (-\sigma j\omega \mathbf{A} - \sigma \nabla \phi + \mathbf{J_s}) = 0. \tag{3.25}$$

These equations with a set of suitable boundary conditions describe the general 3-D electromagnetic field. Based on the FEMLAB user guide [43], the gauge transformation is applied to obtain the unique solution of the system. Let \mathbf{A} and ϕ be the solutions, the fields $\widetilde{\mathbf{A}} = \mathbf{A} + \nabla \mathbf{\Psi}$ and $\widetilde{\phi} = \phi - j\omega \mathbf{\Psi}$ also satisfy the equations for any scalar field $\mathbf{\Psi}$ such chosen that $\widetilde{\mathbf{A}}$ and $\widetilde{\phi}$ satisfy the boundary conditions. The system of equations can be reduced by choosing $\mathbf{\Psi} = -\frac{j\phi}{\omega}$, as for this case, $\widetilde{\mathbf{A}} = \mathbf{A} - \frac{j}{\omega} \nabla \phi$ and $\widetilde{\phi} = 0$. The particular choice of $\mathbf{\Psi}$ fixes the gauge and makes $\widetilde{\mathbf{A}}$ unique. The electric field and magnetic field are not affected by this choice of gauge, hence we can reduce the system to one equation as follows

$$\nabla \times (\frac{1}{\mu} \nabla \times \mathbf{A}) = -\sigma j \omega \mathbf{A} + \mathbf{J_s}. \tag{3.26}$$

In the real world applications, many problems, such as axisymmetric problems and the problem of one dimension being very large in comparision with others, can be modelled as two dimensional. For rectangular (x, y, z) coordinates, we can construct an approximate two-dimensional model to describe the electromagnetic field on the plane parallel to the x-z plane. For this case, Let $\mathbf{A}=(0,A_y(x,z),0)$ and $\mathbf{J}=(0,J_y(x,z),0)$, and $\phi=constant$. Thus,

$$\nabla \times \mathbf{A} = \left(-\frac{\partial A_y}{\partial z}, 0, \frac{\partial A_y}{\partial x}\right),\tag{3.27}$$

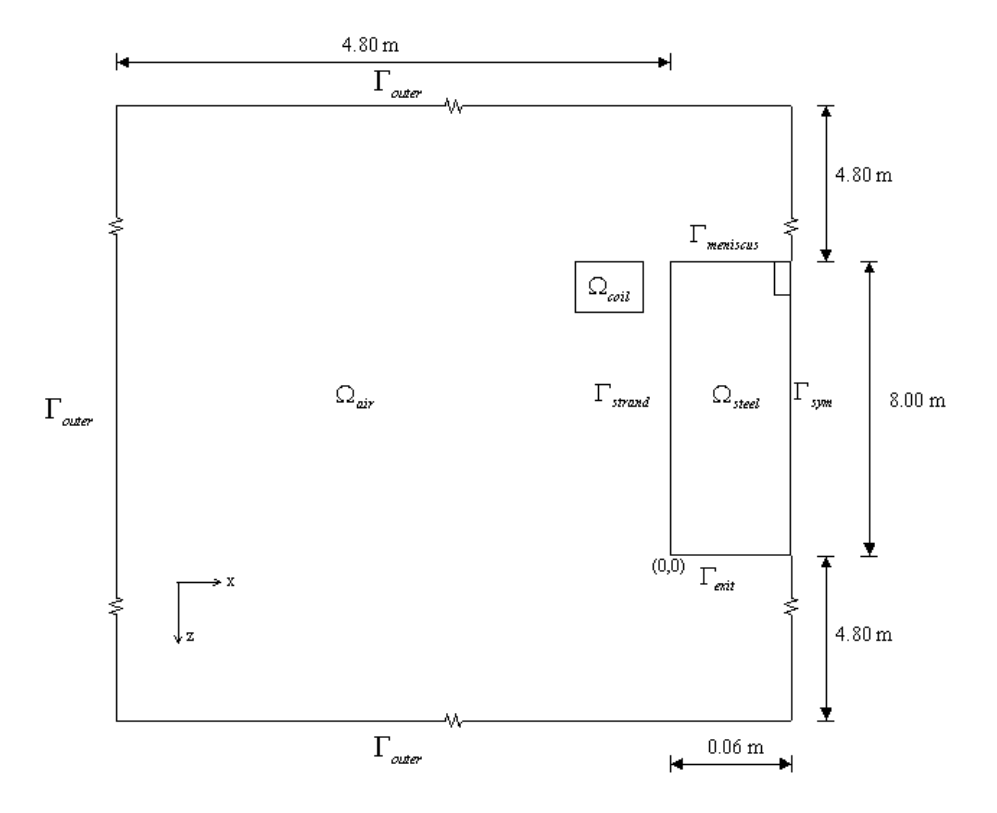


Figure 3.1: The computation domain for the electromagnetic problem.

$$\nabla \times (\nabla \times \mathbf{A}) = (0, -\nabla^2 A_y, 0). \tag{3.28}$$

Hence, equation (3.22) becomes

$$\sigma \mu \frac{\partial A_y}{\partial t} = \nabla^2 A_y - \mu J_{s_y}. \tag{3.29}$$

For the case of sinusoidal current, we let $A_y = A_y e^{i\omega t}$ and consequently equation (3.24) becomes

$$\sigma\mu\omega j A_y = \nabla^2 A_y - \mu J_{s_y}. (3.30)$$

For the continuous casting problem, we consider a typical computation domain as shown in Figure 3.1. On the symmetric plane, the restriction that the magnetic flux cannot penetrate the face is imposed. This means $A_y = 0$ on the symmetric boundary. On the outer boundary, the vector potential are all set to zero. This implies that the effect of an inductor on the magnetic field at these points is negligible. An appropriate distance from the inductors is needed to insure high accuracy.

Fac. of Grad. Studies, Mahidol Univ.

In summary, the boundary value problem of the two-dimensional electromagnetic field is as follows

BVP: Find A_y such that the field equation (3.30) is satisfied in the computation domain Ω and all boundary conditions are satisfied.

3.3 Finite Element Method for the Electromagnetic Field

Firstly, we consider the general case, namely, the problem governed by equation (3.29). To solve this problem by the finite element method, we need to develop a variational statement of the problem. For this purpose, we multiply both sides of equation (3.29) by the test function and then integrate over Ω , namely

$$\left(\sigma\mu\frac{\partial A_y}{\partial t}, W_A\right) = ((A_{y,j})_{,j}, W_A) - (\mu J_{s_y}, W_A), \tag{3.31}$$

where (\cdot,\cdot) denotes the inner product on space $L^2(\Omega)$. As

$$W_A \nabla^2 A_y = \nabla \cdot (W_A \nabla A_y) - \nabla W_A \cdot \nabla A_y, \tag{3.32}$$

substituting equation (3.32) into equation (3.31) yields

$$\int_{\Omega} \sigma \mu \frac{\partial A_y}{\partial t} W_A d\Omega = -\int_{\Omega} (\nabla W_A) \cdot (\nabla A_y) d\Omega + \int_{\Gamma} W_A \nabla A_y \cdot \mathbf{n} \, d\mathbf{s} - \int_{\Omega} \mu J_{s_y} W_A d\Omega.$$
(3.33)

By choosing $W_A = 0$ on the boundary where $A_y = 0$, we have

$$\int_{\Omega} \sigma \mu \frac{\partial A_y}{\partial t} W_A d\Omega = -\int_{\Omega} (\nabla W_A) \cdot (\nabla A_y) d\Omega - \int_{\Omega} \mu J_{s_y} W_A d\Omega, \tag{3.34}$$

or

$$\left(\sigma\mu \frac{\partial A_y}{\partial t}, W_A\right) = (A_{y,j}, W_{A,j}) - (\mu J_{s_y}, W_A). \tag{3.35}$$

Thus, the variational statement for the problem is as follows

VBVP: Find $A_y \in H_0^1(\Omega)$ such that for all the test function $W_A \in H_0^1(\Omega)$, equation (3.35) holds, where $H_0^1(\Omega) = \{v \in H^1(\Omega) | v = 0 \text{ on } \partial\Omega\}$.

To solve this problem numerically, we pose the problem into an N-dimensional subspace A_y and W_A , namely approximate A_y and W_A by

$$A_y = \sum_{i=1}^{N} (A_y)_i \phi_i$$
 , $W_A = \sum_{k=1}^{N} (W_A)_k \phi_k$. (3.36)

Substituting equation (3.36) into equation (3.35), we have

$$\left\{ \left(\sigma \mu \frac{\partial A_y}{\partial t}, \phi_k \right) + \left(A_{y,j}, \phi_{k,j} \right) + \left(J_{s_y}, \phi_k \right) \right\} W_{A_k} = 0,$$
(3.37)

where k = 1, 2, ..., N and j = 1, 2. Then

$$\sum_{i=1}^{N} (\sigma \mu \phi_i, \phi_k) \frac{\partial A_{y_i}}{\partial t} + \sum_{i=1}^{N} (\phi_{i,j}, \phi_{k,j}) A_{y_i} = -(J_{s_y}, \phi_k), \tag{3.38}$$

which can be written in matrix form as

$$\mathbf{M}\frac{\partial \mathbf{A_y}}{\partial t} + \mathbf{L}\mathbf{A_y} = \mathbf{F},\tag{3.39}$$

where

$$\mathbf{M} = \{m_{ik}\} \text{ with } m_{ik} = (\sigma \mu \phi_i, \phi_k) = \int_{\Omega} \sigma \mu \phi_k \phi_i d\Omega,$$

$$\mathbf{L} = \{L_{ik}\} \text{ with } l_{ik} = (\phi_{i,j}, \phi_{k,j}) = \int_{\Omega} \phi_{i,j} \phi_{k,j} d\Omega,$$

$$\mathbf{F} = \{f_k\} = -(J_{s_y}, \phi_k) = -\int_{\Omega} \phi_k J_{s_y} d\Omega.$$

For the time-harmonic problem, the first term of equation (3.38) can be written as

$$\sum_{i=1}^{N} (j\omega \sigma \mu \phi_i, \phi_k) A_{y_i}. \tag{3.40}$$

Therefore, we have

$$\sum_{i=1}^{N} \left[\left(j\omega \sigma \mu \phi_i, \phi_k \right) + \left(\phi_{i,j}, \phi_{k,j} \right) \right] A_{y_i} = -(J_{s_y}, \phi_k), \tag{3.41}$$

which can be written in the matrix form as

$$\overline{\mathbf{M}}\mathbf{A}_{\mathbf{y}} = \mathbf{F},\tag{3.42}$$

where

$$\overline{\mathbf{M}} = \{m_{ik}\}$$
 with $m_{ik} = \int_{\Omega} (j\omega\sigma\mu\phi_i\phi_k + \phi_{i,j}\phi_{k,j}) d\Omega$.

Once A_y is determined by solving the linear system of equation (3.42), \mathbf{B} and $\mathbf{J_e}$ can be determined from equations (3.16) and (3.21) and consequently the electromagnetic force at each node can be determined by $\mathbf{F_{em}} = \mathbf{J_e} \times \mathbf{B}$.

3.4 Numerical Studies

The example under the investigation is a square billet continuous caster which has a width of 0.12 m and a depth of 0.8 m. The computation domain for this problem is given in Figure 3.1. The finite element mesh, constructed from FEMLAB, has 23180 elements and 11856 nodes as shown in Figure 3.2. The parameters used in this problem is as given in Table 3.1. The computation schemes for investigating the effect of varying current source and frequency of magnetic field on the electromagnetic force are given in Table 3.2. The computation results are shown in Figure 3.3-3.7.

Figure 3.3 shows the contour plot of the magnetic vector potential A_y (Wb/m) in the computation domain. All values of magnetic vector potential are negative. Negative values mean sign of values gives the same direction as the source current. It indicates that the magnitude of A_y is between 0 and 0.004 Wb/m which reduces 60% from the original source (coil) to the steel strand while it reduces only 20% to environment.

Figure 3.4 shows the vector plot of the magnetic flux density corresponding to the magnetic vector potential obtained from Figure 3.3. The distribution of the magnetic flow field corresponds to the right hand spiral rule (RHS). The magnitude of the magnetic flux in the steel strand is larger than that in the environment because of the higher electric conductivity.

The contour plot of induce currents in the molten steel pool is shown in Figure 3.5. Its direction is in the opposite way of the source current. The magnitude of \mathbf{J}_e is between 0 and $1.14 \times 10^5 A/m^2$. Its value reduces almost 100% from strand surface to the symmetry plane because we assume that the magnetic flux cannot penetrate to the symmetry plane.

Figure 3.6 shows the vectors plot of the electromagnetic force generated

by the magnetic field and the induced current in the steel. The direction of the electromagnetic force is in-mould direction. The electromagnetic flux flows into the mould with higher intensity in the top part of mould than that in other parts. There is no significant electromagnetic force present at 3 meters below the meniscus. It is noted that the magnitude of the electromagnetic force decreases with the increase of distance from the mould wall.

The effect of source current on the intensity of electromagnetic force is investigated by using three different source current densities those are 1000000 A/m^2 , 2000000 A/m^2 and 3000000 A/m^2 . The results as shown in Figure 3.7 indicate that the larger source current generates the larger magnitude of electromagnetic force. By increasing the source current from 1000000 A/m^2 to 3000000 A/m^2 in a horizontal section 0.05 meters below the meniscus, the magnitude of electromagnetic force increases about 89% on the strand surface. It is clear that the intensity of electromagnetic force decreases with decreasing the source current.

Figure 3.8 shows the effect of the frequency of magnetic field on the magnitude of electromagnetic force. The results of the investigation, by using three different frequencies of 60 Hz, 80 Hz and 100 Hz, indicate that the higher magnetic frequency generates the larger magnitude of electromagnetic force. By increasing the frequency of the magnetic field from 60 Hz to 100 Hz at 5 cm below meniscus, the magnitude of electromagnetic force increases about 56% on strand surface. It is noted that the magnitude of electromagnetic body force decreases with the decrease of the frequency of the magnetic field.

3.5 Concluding Remarks

The mathematical model for simulating the electromagnetic problem in the continuous casting process is governed by the $A-\phi$ model, derived from

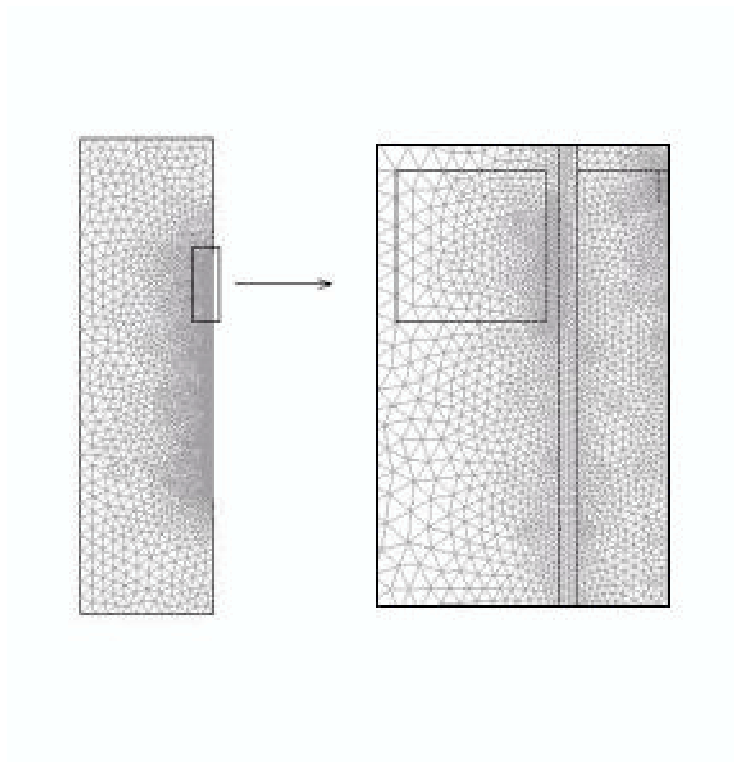


Figure 3.2: The finite element mesh for the electromagnetic problem.

Table 3.1: Material parameters

Parameter	Value	Unit
Conductivity of molten steel σ_s	7.14×10^5	$\Omega^{-1}m^{-1}$
Magnetic permeability in a vacuum μ	$4\pi \times 10^{-7}$	Henry/m
Magnetic permittivity in a vacuum ε	8.8541×10^{-12}	Farad/m

the Maxwell's equations. A finite element technique based on the Bubnov-finite element method is used to study the electromagnetic field in the continuous casting process.

The study shows that the electromagnetic force in molten steel generated by an external magnetic field directs toward the central plane

Scheme Source Current density Frequency J_s f $(Ampere/m^2)$ (Hz)1 100000060 2 2000000 60 3 3000000 60 4 2000000 80 5 2000000 100

Table 3.2: Computation schemes

of the mould and its magnitude decreases with increasing distance from the mould wall. This force will contribute to the improvement of steel surface quality.

The study also shows that the source current density and the magnetic frequency have considerable effect on the magnitude of the electromagnetic force. By decreasing the source current density or the magnetic frequency, the magnitude of the electromagnetic force in the molten steel decreases significantly.

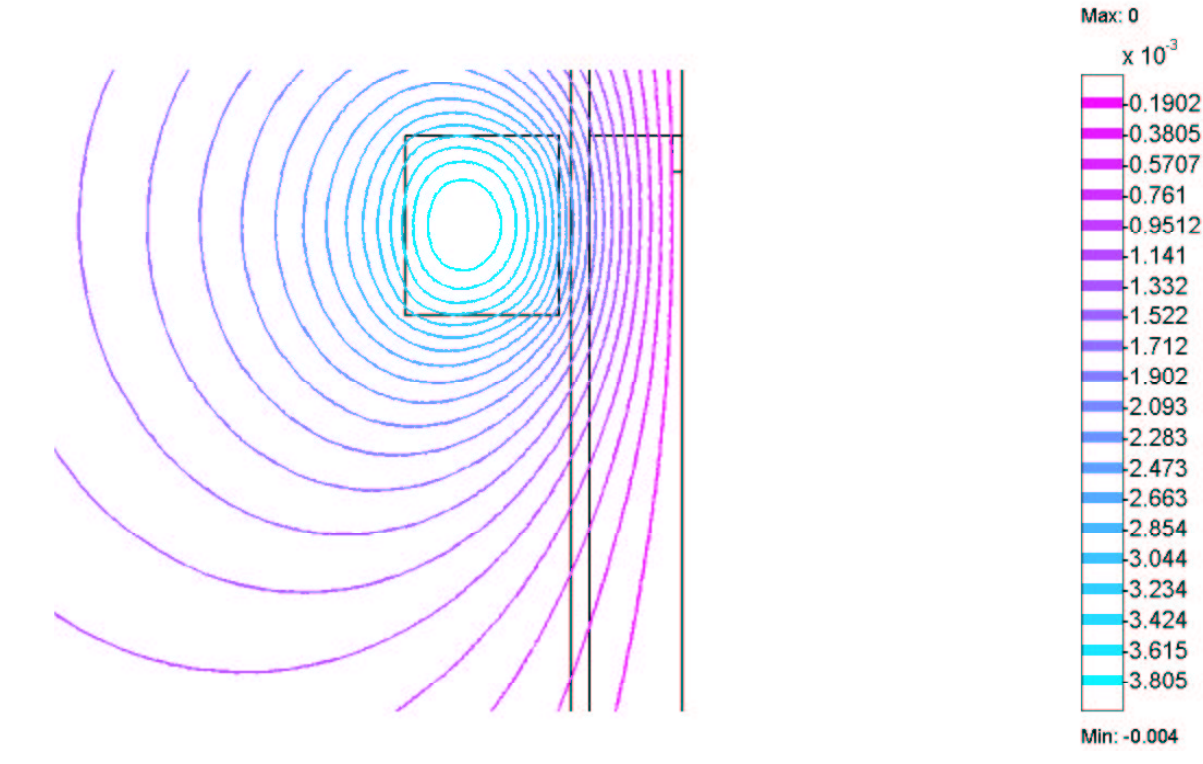


Figure 3.3: The contour plot of the magnetic vector potential $\mathbf{A}(Wb/m)$ at frequency f=60 Hz and source current density $\mathbf{J_s}=1000000$ A/m^2 .

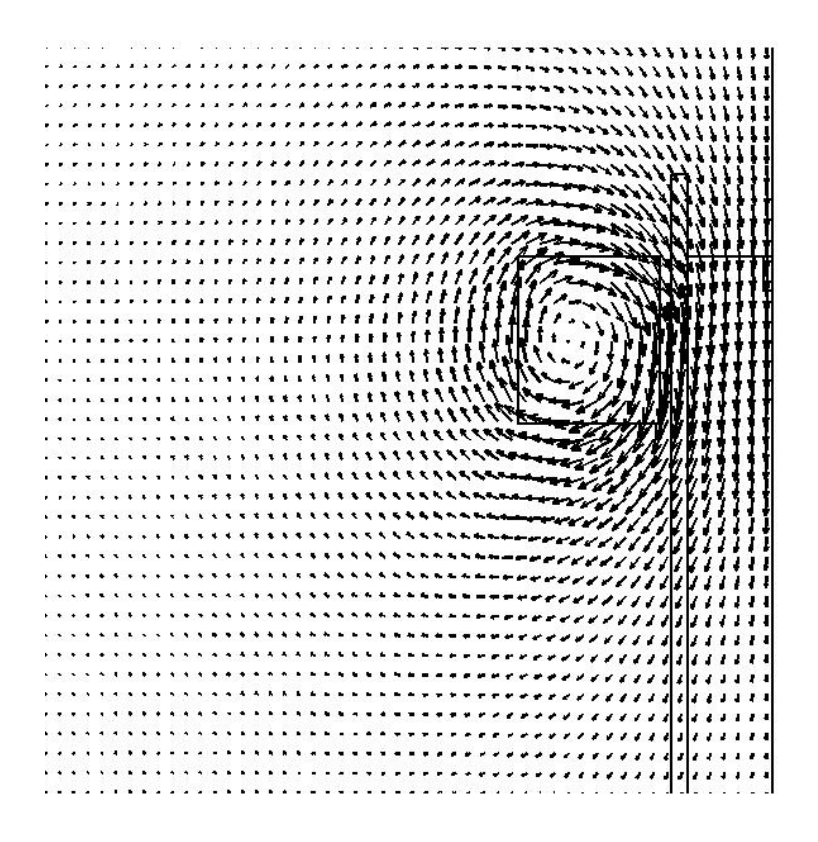


Figure 3.4: The vector plot of the magnetic flux density ${\bf B}$ (Tesla) at frequency f=60 Hz and source current density ${\bf J_s}=1000000~A/m^2$.

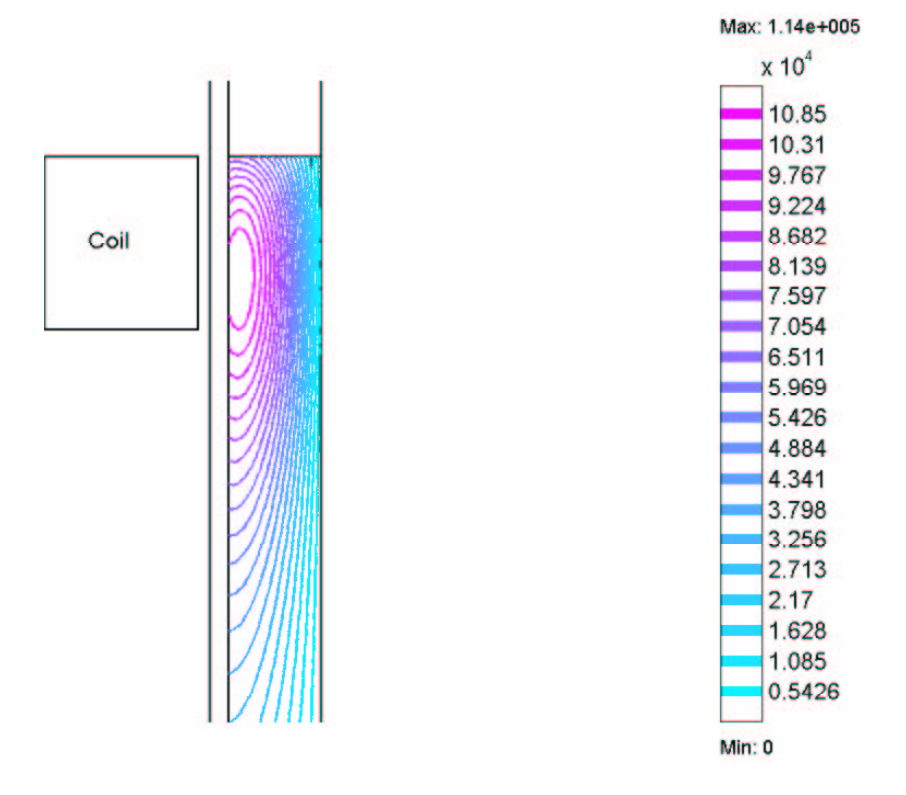


Figure 3.5: The contour plot of induced current ${\bf J_e}\,(A/m^2)$ in the continuous casting mould at frequency f=60 Hz and source current density ${\bf J_s}=1000000~A/m^2.$

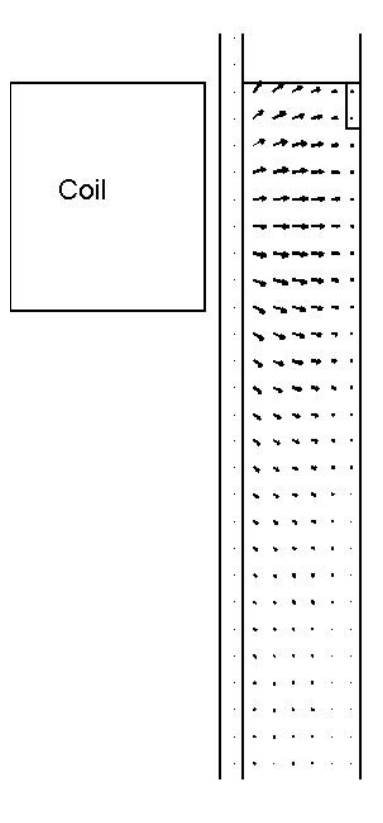


Figure 3.6: The vector plot of electromagnetic force $F_{em} (N/m^3)$ in the electromagnetic continuous caster at frequency f=60 Hz and source current density $\mathbf{J_s}=1000000~A/m^2$.

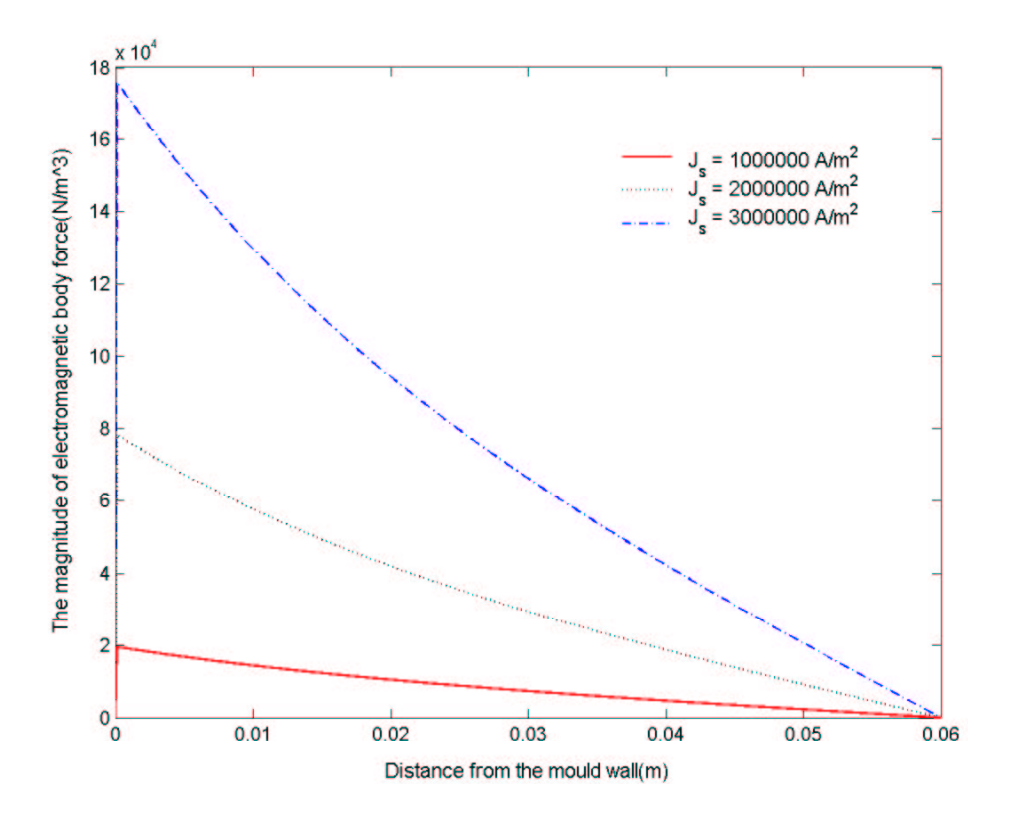


Figure 3.7: The influence of source current density J_s (A/m^2) on the magnitude of electromagnetic force in the continuous casting process at frequency $f=60~\mathrm{Hz}$.

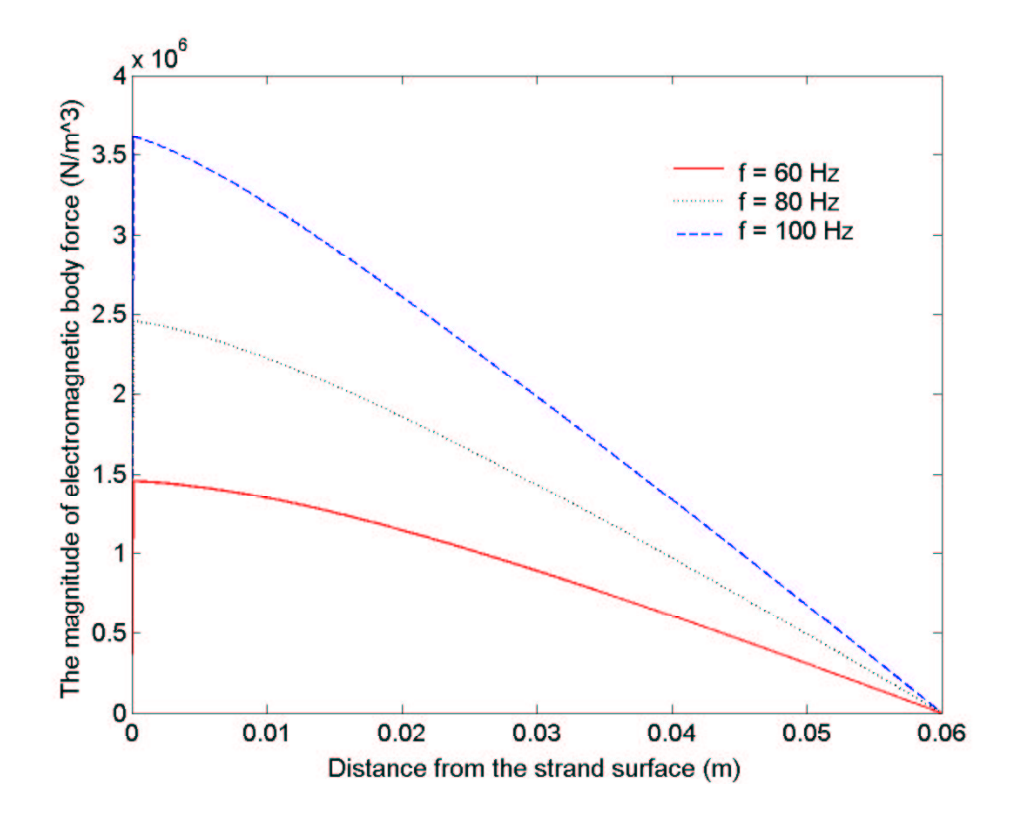


Figure 3.8: The influence of the frequency of magnetic field f(Hz) on the magnitude of electromagnetic force in the continuous casting process at source current density $J_s = 1000000 \ A/m^2$.

CHAPTER 4

COUPLED FLUID FLOW-HEAT TRANSFER IN ELECTROMAGNETIC CASTING

4.1 General Overview

The electromagnetic continuous casting process has been developed to cast steel over the last few decades. Various mathematical models and numerical algorithms have been developed to simulate the heat transfer, fluid flow and electromagnetic stirring occurring in the casting process. A number of commercial packages, such as FIDAP, PHONIC, PIV, SOLA, OPERA-3D and MORDY, have been used for the simulation. However, only a few attempts have been made to study the coupled fluid flow, heat transfer and solidification problem taking into account the effect of electromagnetic stirring.

As the effect of molten steel flow on the magnetic flux density is negligible, the electromagnetic problem is decoupled from the fluid flow problem and is solved in chapter 3. The influence of electromagnetic field on the coupled fluid flow-heat transfer process is taken into account by adding the electromagnetic force to the fluid flow model. The molten steel is assumed to be an incompressible Newtonian fluid and the flow in the mushy region is modelled on the basis of Darcy's flow in porous media. The influence of turbulence on the fluid flow and heat transfer process is taken into account in this work. A single domain enthalpy method is used for the heat transfer-solidification problem in the continuous casting process. The complete set of equations for the coupled fluid flow, heat transfer and solidification process at the presence of an electromagnetic field is presented in section 4.2. In section 4.3-4.4, a numerical algorithm based on a Bubnov-Galerkin finite element method is established. In

section 4.5, a numerical investigation is carried out to study the influence of electromagnetic field on the fluid flow, heat transfer and solidification process.

4.2 Mathematical Model

In this section, the mathematical model for the coupled fluid flow, heat transfer and solidification process occurring in the electromagnetic continuous casting process is described. The governing equations for the problem include the Navier-Stokes equations, the continuity equation and the energy equation. The effect of electromagnetic field and turbulence on the flow field and the temperature field are taken into account.

To simulate the heat transfer process, a single-domain enthalpy method is used. From the principle of energy conservation, the heat transfer in the region undergoing a phase change is

$$\rho \left(\frac{\partial H_t}{\partial t} + u_j H_{t,j} \right) = \left(k_0 T_{,j} \right)_{,j} \tag{4.1}$$

where $(\cdot)_{,j}$ denotes differentiation with respect to x_j , u_j represents the velocity component of fluid in the x_j direction, ρ and k_0 are respectively the density of steel and the thermal conductivity of steel. The enthalpy H_t is defined as the sum of sensible heat h = cT and latent heat H as follows

$$H_t = cT + H, (4.2)$$

where c is the specific heat of liquid steel and the latent heat H is defined by

$$H = \begin{cases} 0 & \text{if } T \leq T_S \\ L\left(\frac{T - T_S}{T_L - T_S}\right) & \text{if } T_S < T < T_L \end{cases}, \tag{4.3}$$

$$L & \text{if } T \geq T_L$$

in which L is the latent heat of steel, T_s and T_l are respectively the solidification temperature and the melting temperature of steel.

Substituting equation (4.2) to equation (4.1), we have

$$\rho c \left(\frac{\partial T}{\partial t} + u_j T_{,j} \right) = (k_0 T_{,j})_{,j} - \rho \left(\frac{\partial H}{\partial t} + u_j H_{,j} \right). \tag{4.4}$$

From equation (4.3), it is obviously that the last term in equation (4.4) is equal to zero everywhere except in the region where phase-change occurs. Consequently, the equation can be applied to all the regions including the solid region, the mushy region and the liquid region and there are no conditions to be satisfied at the phase-change boundary. Thus, the heat transfer-phase change problem can be solved by using a single domain approach.

For the flow of fluid in the electromagnetic caster, the molten steel is assumed to be a incompressible Newtonian fluid. The influence of turbulence on the transport of momentum and energy is modelled by the addition of the turbulent viscosity μ_t to the laminar viscosity μ_0 and the turbulent conductivity k_t to the molecular conductivity k_0 , yielding the effective viscosity μ_f and the effective thermal conductivity k_f given by

$$\mu_f = \mu_0 + \mu_t, \qquad k_f = k_0 + k_t,$$
(4.5)

where $k_t = \frac{c\mu_t}{\sigma_t}$, σ_t is the turbulent Prandtl number [11, 13, 16, 44, 45]. To simulate the influence of an electromagnetic field on the flow field in the electromagnetic continuous casting process, the electromagnetic force \mathbf{F}_{em} is incorporated into the fluid flow model. The flow field in the mushy region is modelled by Darcy's law for porous media. Thus, the unified field equations governing the multi-phases heat transfer and fluid flow with turbulence and electromagnetic effects, for all the regions with or without phase change are as follows

$$u_{i,i} = 0, (4.6)$$

$$\rho \left(\frac{\partial u_i}{\partial t} + u_j u_{i,j} \right) + p_{,i} - (\mu_f (u_{i,j} + u_{j,i}))_{,j} = F_i(u_i, T) + \rho g_i + F_{em_i}, \tag{4.7}$$

$$\rho c \left(\frac{\partial T}{\partial t} + u_j T_{,j} \right) = (k_f T_{,j})_{,j} - \rho \left(\frac{\partial H}{\partial t} + u_j H_{,j} \right), \tag{4.8}$$

where Darcy's law for porous media [3, 44, 46] has been used for modeling the flow in the mushy region and $F_i(u_i, T)$ is determined by

$$F_i(u_i, T) = C \frac{\mu_f \left[1 - f(T)\right]^2}{\rho f(T)^3} (u_i - (U_{cast})_i)$$
(4.9)

in which f(T) is the local liquid fraction which is approximated by the linear function

$$f(T) = \begin{cases} 0 & \text{if } T \le T_S \\ \frac{T - T_S}{T_L - T_S} & \text{if } T_S < T < T_L. \\ 1 & \text{if } T \ge T_L \end{cases}$$

$$(4.10)$$

The electromagnetic force F_{em_i} in the Navier-stokes equations (4.7) can be determined by

$$F_{em_i} = (\mathbf{J_e} \times \mathbf{B})_i \tag{4.11}$$

which is calculated from the results in chapter 3.

Equations (4.6)-(4.8) do not constitute a closed system as both μ_f and k_f are related to an unknown function μ_t . Various models, such as the mixing-length type model, the one-equation model [47, 48] and the two-equation $(K-\varepsilon)$ model [3, 49, 50, 51, 52, 53], have been proposed for calculating μ_t . Launder [45] and Ferziger [54], based on a critical review, suggested that the simple mixing-length type model is suitable for most boundary-layer type flows in the absence of recirculation; the one-equation model can be used to model simple recirculation flow; but for more complex flow fields, the two-equation model should be used. As the flow field in the continuous casting mould is complex with circulation, μ_t is calculated by using the two equation $K - \varepsilon$ model. As the phase change is taken into account in the heat transfer problem, the computation region has three sub-regions including the solidified steel region, the mushy region and the molten steel region. Consequently, the standard $K-\varepsilon$ model, which is suitable for the far-wall highly turbulent region, cannot be applied to the problem for the continuous casting process. Thus, some

modification to the standard $K - \varepsilon$ model is needed. According to the work by Wiwatanapataphee [3], the low-Reynold number $K - \varepsilon$ model is used in this project for the turbulent flow of molten steel in the continuous casting process, namely

$$\rho\left(\frac{\partial K}{\partial t} + u_j K_{,j}\right) - \left(\left(\mu_0 + \frac{\mu_t}{\sigma_K}\right) K_{,j}\right)_{,j} = -\frac{\mu_t}{\sigma_t} \beta g_j T_{,j} + \mu_t G - \rho \varepsilon, \tag{4.12}$$

$$\rho\left(\frac{\partial\varepsilon}{\partial t} + u_{j}\varepsilon_{,j}\right) - ((\mu_{0} + \frac{\mu_{t}}{\sigma_{\varepsilon}})\varepsilon_{,j})_{,j} = C_{1}(1 - C_{3})\frac{\varepsilon\mu_{t}}{K\sigma_{t}}\beta g_{j}T_{,j} + C_{1}\frac{\varepsilon}{K}\mu_{t}G - \rho C_{2}f_{\varepsilon}\frac{\varepsilon^{2}}{K}, \qquad (4.13)$$

where $G = 2\epsilon_{ij}\epsilon_{ij}$ with $\epsilon_{ij} = \frac{u_{i,j} + u_{j,i}}{2}$. The constants involved in equations (4.5)-(4.13) are empirical constants. Extensive examination of turbulent flows has resulted in a recommended set of values for these constants [3, 50], namely $\sigma_t = 0.9$, $\sigma_k = 1$, $\sigma_{\varepsilon} = 1.25$, $C_1 = 1.44$, $C_2 = 1.92$, and $C_3 = 0.8$.

Equations (4.12)-(4.13) are used to accommodate the region with relatively low local turbulent Reynolds number and to reduce the effect of turbulent across the various sub-layers. The turbulent viscosity μ_t is determined by [3, 45, 54]

$$\mu_t = \frac{0.09 f_\mu \rho K^2}{\varepsilon},\tag{4.14}$$

where the generalized damping mechanism of turbulent transport in both the liquid and mushy regions f_{μ} is determined [3] by

$$f_{\mu} = \sqrt{f(T)} exp(-3.4/(1 + R_t/50)^2),$$
 (4.15)

where f(T) is the liquid fraction as defined before in equation (4.10), R_t denotes the local turbulent Reynolds number defined by

$$R_t = \frac{\rho K^2}{\mu \varepsilon}. (4.16)$$

To ensure that all the terms in equations (4.12)-(4.13) will not tend to infinity as K approaches zero in the near-wall region, the last term of the right hand side of

equation (4.13) includes a damping function f_{ε} defined by

$$f_{\varepsilon} = 1 - A_{\varepsilon} e^{-R_t^2}, \tag{4.17}$$

where A_{ε} is a constant and is chosen as one if $K < 10^{-4}$ or otherwise $A_{\varepsilon} = 0.3$ [3, 55, 56]. By choosing $A_{\varepsilon} = 1$ in equation (4.17), the term $\frac{\rho C_2 f_{\varepsilon} \varepsilon_2}{K}$ in equation (4.13) approaches zero as K becomes small. To completely define the problem, boundary and initial conditions for velocity, temperature, turbulent kinetic energy, and dissipation rate must be given. The computation region and the boundary conditions for the problem are shown in Figure 4.2, as detailed below. On the nozzle inlet Γ_{in} , the velocity, the temperature of steel, the turbulent kinetic energy and the rate of dissipation are respectively determined by

$$\mathbf{u} = \mathbf{u}_{in}, \quad T = T_{in}, \quad K = K_{in}, \quad \varepsilon = \varepsilon_{in}.$$
 (4.18)

On the solidified strand surface Γ_{wall} , the velocity is set to the casting speed, the heat transfer is determined by the convection boundary condition, the turbulent kinetic energy K and the rate of dissipation ε are assumed to be zero, namely

$$\mathbf{u} = (0, U_{cast}), \quad -k_f \frac{\partial T}{\partial \mathbf{n}} = h_{\infty}(T - T_{\infty}), \quad K = \varepsilon = 0.$$
 (4.19)

On the meniscus surface Γ_0 and the nozzle wall $\bar{\Gamma}_n$, the derivatives of the turbulent kinetic energy and the rate of dissipation in the normal direction are set to zero. The velocity is set to zero and the temperature is taken to be the inlet molten steel temperature, namely

$$\mathbf{u} = \mathbf{0}, \quad T = T_{in}, \quad \frac{\partial K}{\partial n} = \frac{\partial \varepsilon}{\partial n} = 0.$$
 (4.20)

On the plane of symmetry Γ_{sym} , the normal velocity \mathbf{v}_n is zero and the derivatives of the tangential velocity \mathbf{u}_t and temperature T in the normal direction are both zero; the derivatives of the turbulent kinetic energy and the rate of dissipation in the normal direction are also set to zero, namely

Fac. of Grad. Studies, Mahidol Univ.

$$\mathbf{u}_n = 0, \quad \frac{\partial \mathbf{u}_t}{\partial n} = \frac{\partial T}{\partial n} = 0, \quad \frac{\partial K}{\partial n} = \frac{\partial \varepsilon}{\partial n} = 0,$$
 (4.21)

where n is the unit vector normal to the boundary.

In summary, the boundary value problem for the turbulent fluid flow-heat transfer problem is as follows :

BVP: Find u_i, p, T, K and ε such that the field equations (4.6)-(4.8) and (4.12)-(4.13) are satisfied in the computation domain Ω and all boundary conditions (4.18)-(4.21) are satisfied.

4.3 Finite Element Formulation

To solve the BVP, firstly we use the penalty function method to weaken the continuity equation as follows

$$u_{i,i} = -\delta p^*, (4.22)$$

where δ is a small positive number and p^* is denoted by

$$p^* = p - \rho gz. \tag{4.23}$$

The variational statement corresponding to the BVP can now be described as the following variational boundary value problem.

VBVP: Find u_i, p^*, T, K and $\varepsilon \in H^1(\Omega)$ such that for all w_i^u, w^p, w^T, w^K and $w^{\varepsilon} \in H^1_0(\Omega)$, all boundary conditions including (4.18)-(4.21) are satisfied and

$$(u_{i,i}, w^p) = (-\delta p^*, w^p),$$

$$(\frac{\partial u_i}{\partial t}, w^{u_i}) + (u_j u_{i,j}, w^{u_i}) - ((\frac{\mu_f}{\rho} (u_{i,j} + u_{j,i}))_{,j}, w^{u_i})$$

$$+ (\frac{1}{\rho} p_{,i}^*, w^{u_i}) = (\frac{1}{\rho} F_i, w^{u_i}) + (\frac{1}{\rho} F_{em_i}, w^{u_i}),$$

$$\left(\frac{\partial T}{\partial t}, w^{T}\right) + \left(u_{j}T_{,j}, w^{T}\right) - \left(\left(\frac{k_{f}}{\rho c}T_{,j}\right)_{,j}, w^{T}\right) = -\frac{1}{c}\left\{\left(\frac{\partial H}{\partial t}, w^{T}\right) + \left(u_{j}H_{,j}, w^{T}\right)\right\},$$

$$\left(\frac{\partial K}{\partial t}, w^{K}\right) + \left(u_{j}K_{,j}, w^{K}\right) - \left(\left(\left(\frac{\mu_{0}}{\rho} + \frac{\mu_{t}}{\rho\sigma_{K}}\right)K_{,j}\right)_{,j}, w^{K}\right) = -\left(\frac{\mu_{t}}{\rho\sigma_{t}}\beta g_{j}T_{,j} - \frac{\mu_{t}}{\rho}G + \varepsilon, w^{K}\right),$$

$$\left(\frac{\partial \varepsilon}{\partial t}, w^{\varepsilon}\right) + \left(u_{j}\varepsilon_{,j}, w^{\varepsilon}\right) - \left(\left(\left(\frac{\mu_{0}}{\rho} + \frac{\mu_{t}}{\rho\sigma_{\varepsilon}}\right)\varepsilon_{,j}\right)_{,j}, w^{\varepsilon}\right) = \left(C_{1}(1 - C_{3})\frac{\varepsilon\mu_{t}}{K\rho\sigma_{t}}\beta g_{j}T_{,j}\right)$$

$$+ C_{1}\frac{\varepsilon\mu_{t}}{K\rho}G - C_{2}f_{\varepsilon}\frac{\varepsilon^{2}}{K}, w^{\varepsilon},$$

$$(4.24)$$

where $H^1(\Omega)$ is the Sobolev space $W^{1,2}(\Omega)$ with norm $||\cdot||_{1,2,\Omega}$, $H^1_0(\Omega) = \{v \in H^1(\Omega)|v=0 \text{ on } \partial\Omega_v \text{ where } \partial\Omega_v \text{ denote a Dirichlet type boundary for } v\}$, and the inner product (\cdot,\cdot) is defined by

$$(\mathbf{a}, \mathbf{b}) = \int_{\Omega} \mathbf{a} \cdot \mathbf{b} \ d\Omega. \tag{4.25}$$

Using Green's formula, the second order derivatives in (4.24) can be reduced to order one, namely

$$\left(\frac{1}{\rho}p_{,i}^{*}, w^{u_{i}}\right) = -\left(\frac{1}{\rho}p_{,i}^{*}, w_{,i}^{u_{i}}\right) + B_{p}\left(w^{u_{i}}\right),$$

$$\left(\left(\frac{\mu_{f}}{\rho}\left(u_{i,j} + u_{j,i}\right)\right)_{,j}, w^{u_{i}}\right) = -\left(\left(\frac{\mu_{f}}{\rho}\left(u_{i,j} + u_{j,i}\right)\right), w_{,j}^{u_{i}}\right) + B_{u}\left(w^{u_{i}}\right),$$

$$\left(\left(\frac{k_{f}}{\rho c}T_{,j}\right)_{,j}, w^{T}\right) = -\left(\left(\frac{k_{f}}{\rho c}T_{,j}\right), w_{,j}^{T}\right) + B_{T}\left(w^{T}\right),$$

$$\left(\left(\left(\frac{\mu_{0}}{\rho} + \frac{\mu_{t}}{\rho\sigma_{K}}\right)K_{,j}\right)_{,j}, w^{K}\right) = -\left(\left(\left(\frac{\mu_{0}}{\rho} + \frac{\mu_{t}}{\rho\sigma_{K}}\right)K_{,j}\right), w_{,j}^{K}\right) + B_{K}\left(w^{K}\right),$$

$$\left(\left(\left(\frac{\mu_{0}}{\rho} + \frac{\mu_{t}}{\rho\sigma_{\varepsilon}}\right)\varepsilon_{,j}\right)_{,j}, w^{\varepsilon}\right) = -\left(\left(\left(\frac{\mu_{0}}{\rho} + \frac{\mu_{t}}{\rho\sigma_{\varepsilon}}\right)\varepsilon_{,j}\right), w_{,j}^{\varepsilon}\right) + B_{\varepsilon}\left(w^{\varepsilon}\right),$$

$$\left(\left(\left(\frac{\mu_{0}}{\rho} + \frac{\mu_{t}}{\rho\sigma_{\varepsilon}}\right)\varepsilon_{,j}\right)_{,j}, w^{\varepsilon}\right) = -\left(\left(\left(\frac{\mu_{0}}{\rho} + \frac{\mu_{t}}{\rho\sigma_{\varepsilon}}\right)\varepsilon_{,j}\right), w_{,j}^{\varepsilon}\right) + B_{\varepsilon}\left(w^{\varepsilon}\right),$$

$$\left(\left(\frac{\mu_{0}}{\rho} + \frac{\mu_{t}}{\rho\sigma_{\varepsilon}}\right)\varepsilon_{,j}\right)_{,j}, w^{\varepsilon}\right) = -\left(\left(\left(\frac{\mu_{0}}{\rho} + \frac{\mu_{t}}{\rho\sigma_{\varepsilon}}\right)\varepsilon_{,j}\right), w_{,j}^{\varepsilon}\right) + B_{\varepsilon}\left(w^{\varepsilon}\right),$$

$$\left(\left(\frac{\mu_{0}}{\rho} + \frac{\mu_{t}}{\rho\sigma_{\varepsilon}}\right)\varepsilon_{,j}\right)_{,j}, w^{\varepsilon}\right) = -\left(\left(\frac{\mu_{0}}{\rho} + \frac{\mu_{t}}{\rho\sigma_{\varepsilon}}\right)\varepsilon_{,j}\right), w_{,j}^{\varepsilon}\right) + B_{\varepsilon}\left(w^{\varepsilon}\right),$$

$$\left(\left(\frac{\mu_{0}}{\rho} + \frac{\mu_{t}}{\rho\sigma_{\varepsilon}}\right)\varepsilon_{,j}\right)_{,j}, w^{\varepsilon}\right) = -\left(\left(\frac{\mu_{0}}{\rho} + \frac{\mu_{t}}{\rho\sigma_{\varepsilon}}\right)\varepsilon_{,j}\right), w_{,j}^{\varepsilon}\right) + B_{\varepsilon}\left(w^{\varepsilon}\right),$$

$$\left(\left(\frac{\mu_{0}}{\rho} + \frac{\mu_{t}}{\rho\sigma_{\varepsilon}}\right)\varepsilon_{,j}\right)_{,j}, w^{\varepsilon}\right) = -\left(\left(\frac{\mu_{0}}{\rho} + \frac{\mu_{t}}{\rho\sigma_{\varepsilon}}\right)\varepsilon_{,j}\right), w_{,j}^{\varepsilon}\right) + B_{\varepsilon}\left(w^{\varepsilon}\right),$$

Fac. of Grad. Studies, Mahidol Univ.

where B_p, B_u, B_T, B_K , and B_{ε} are as follows

$$B_{p}(w^{u_{i}}) = \int_{\Gamma} \frac{1}{\rho} p^{*} w^{u_{i}} \cdot \mathbf{n} \, d\Gamma,$$

$$B_{u}(w^{u_{i}}) = \int_{\Gamma} \frac{\mu_{f}}{\rho} \left(u_{i,j} + u_{j,i} \right) w^{u_{i}} \cdot \mathbf{n} \, d\Gamma,$$

$$B_{T}(w^{T}) = \int_{\Gamma} \frac{k_{f}}{\rho c} T_{,j} w^{T} \cdot \mathbf{n} \, d\Gamma,$$

$$B_{K}(w^{K}) = \int_{\Gamma} \left(\frac{\mu_{0}}{\rho} + \frac{\mu_{t}}{\rho \sigma_{K}} \right) K_{,j} w^{K} \cdot \mathbf{n} \, d\Gamma,$$

$$B_{\varepsilon}(w^{\varepsilon}) = \int_{\Gamma} \left(\frac{\mu_{0}}{\rho} + \frac{\mu_{t}}{\rho \sigma_{\varepsilon}} \right) \varepsilon_{,j} w^{\varepsilon} \cdot \mathbf{n} \, d\Gamma.$$

$$(4.27)$$

To find the solution of the above VBVP problem, the Bubnov-Galerkin finite element method is used to solve the problem. The problem is posed into an N-dimensional subspace for u_i, T, K and ε and an N'-dimensional subspace for p^* . Let H_{γ} be an N-dimensional subspace of $H^1(\Omega)$ with basis functions $\{\gamma_1, \gamma_2, \dots, \gamma_n\}$ and H_{β} be an N'-dimensional subspace of $H^1(\Omega)$ with basis function $\{\beta_1, \beta_2, \dots, \beta_n\}$. Then $w^{u_i}, w^T, w^K, w^{\varepsilon}$ and w^p are approximated by

$$w^{u_i} \approx \hat{w}^{u_i} = \sum_{m=1}^{N} \gamma_m w_m^{u_i}, \quad w^T \approx \hat{w}^T = \sum_{m=1}^{N} \gamma_m w_m^T,$$

$$w^K \approx \hat{w}^K = \sum_{m=1}^{N} \gamma_m w_m^K, \quad w^\varepsilon \approx \hat{w}^\varepsilon = \sum_{m=1}^{N} \gamma_m w_m^\varepsilon,$$

$$w^p \approx \hat{w}^p = \sum_{p=1}^{N'} \beta_p w_p.$$

$$(4.28)$$

Substituting equations (4.26) - (4.28) into equation (4.24) and noting that the test function is arbitrary, we have

$$(u_{i,i}, \beta_p) = -(\delta p^*, \beta_p),$$

$$\begin{split} \left(\frac{\partial u_{i}}{\partial t}, \gamma_{m}\right) + \left(u_{j}u_{i,j}, \gamma_{m}\right) + \left(\left(\frac{\mu_{f}}{\rho}\left(u_{i,j} + u_{j,i}\right)\right), \gamma_{m,j}\right) - \left(\frac{1}{\rho}p^{*}, \gamma_{m,i}\right) \\ &= \left(\frac{1}{\rho}F_{i}, \gamma_{m}\right) + \left(\frac{1}{\rho}F_{em_{i}}, \gamma_{m}\right) + B_{u}(\gamma_{m}) - B_{p}(\gamma_{m}), \\ \left(\frac{\partial T}{\partial t}, \gamma_{m}\right) + \left(u_{j}T_{,j}, \gamma_{m}\right) + \left(\left(\frac{k_{f}}{\rho c}T_{,j}\right), \gamma_{m,j}\right) \\ &= -\frac{1}{c}\left\{\left(\frac{\partial H}{\partial t}, \gamma_{m}\right) + \left(u_{j}H_{,j}, \gamma_{m}\right)\right\} + B_{T}(\gamma_{m}), \\ \left(\frac{\partial K}{\partial t}, \gamma_{m}\right) + \left(u_{j}K_{,j}, \gamma_{m}\right) + \left(\left(\left(\frac{\mu_{0}}{\rho} + \frac{\mu_{t}}{\rho\sigma_{K}}\right)K_{,j}\right), \gamma_{m,j}\right) \\ &= -\left(\frac{\mu_{t}}{\rho\sigma_{t}}\beta g_{j}T_{,j} - \frac{\mu_{t}}{\rho}G + \varepsilon, \gamma_{m}\right) + B_{K}(\gamma_{m}), \\ \left(\frac{\partial \varepsilon}{\partial t}, \gamma_{m}\right) + \left(u_{j}\varepsilon_{,j}, \gamma_{m}\right) + \left(\left(\left(\frac{\mu_{0}}{\rho} + \frac{\mu_{t}}{\rho\sigma_{\varepsilon}}\right)\varepsilon_{,j}\right), \gamma_{m,j}\right) \\ &= \left(C_{1}(1 - C_{3})\frac{\varepsilon\mu_{t}}{K\rho\sigma_{t}}\beta g_{j}T_{,j} + C_{1}\frac{\varepsilon\mu_{t}}{K\rho}G - C_{2}f_{\varepsilon}\frac{\varepsilon^{2}}{K}, \gamma_{m}\right) + B_{\varepsilon}(\gamma_{m}), \quad (4.29) \end{split}$$

Similarly, u_i, T, K, ε and p^* are approximated by

$$u_{i}(\mathbf{x},t) \approx \hat{u}_{i} = \sum_{l=1}^{N} (u_{i})_{l}(t)\gamma_{l}(\mathbf{x}),$$

$$T(\mathbf{x},t) \approx \hat{T} = \sum_{l=1}^{N} T_{l}(t)\gamma_{l}(\mathbf{x}),$$

$$K(\mathbf{x},t) \approx \hat{K} = \sum_{l=1}^{N} K_{l}(t)\gamma_{l}(\mathbf{x}),$$

$$\varepsilon(\mathbf{x},t) \approx \hat{\varepsilon} = \sum_{l=1}^{N} \varepsilon_{l}(t)\gamma_{l}(\mathbf{x}),$$

$$p^{*}(\mathbf{x},t) = \sum_{k=1}^{N'} p_{k}^{*}(t)\beta_{k}(\mathbf{x}).$$

$$(4.30)$$

Substituting equation (4.30) into equation (4.29), we have

$$\sum_{l=1}^{N} (\gamma_{l,i}, \beta_{p}) u_{il} = -\sum_{l=1}^{N'} (\delta \beta_{l}, \beta_{p}) p_{l}^{*},$$

$$\begin{split} \sum_{l=1}^{N} \left\{ (\gamma_{l}, \gamma_{m}) \dot{u}_{il} + (u_{j} \gamma_{l,j}, \gamma_{m}) u_{il} + \frac{\mu_{f}}{\rho} (\gamma_{l,j}, \gamma_{m,j}) u_{il} + \frac{\mu_{f}}{\rho} (\gamma_{l,i}, \gamma_{m,j}) u_{jl} \right\} \\ - \frac{1}{\rho} \sum_{l=1}^{N'} \left\{ (\beta_{l}, \gamma_{m,i}) p_{l}^{*} - \rho B_{p} (\gamma_{m}) \right\} &= \left(\frac{1}{\rho} F_{i}, \gamma_{m} \right) + \left(\frac{1}{\rho} F_{em_{i}}, \gamma_{m} \right) + B_{u} (\gamma_{m}), \\ \sum_{l=1}^{N} \left\{ (\gamma_{l}, \gamma_{m}) \dot{T}_{l} + (u_{j} \gamma_{l,j}, \gamma_{m}) T_{l} + \left(\frac{k_{f}}{\rho c} \gamma_{l,j}, \gamma_{m,j} \right) T_{l} \right\} - B_{T} (\gamma_{m}) \\ &= -\frac{1}{c} \sum_{l=1}^{N} \left\{ (\gamma_{l}, \gamma_{m}) \dot{H}_{l} + (u_{j} \gamma_{l,j}, \gamma_{m}) H_{l} \right\}, \\ \sum_{l=1}^{N} \left\{ (\gamma_{l}, \gamma_{m}) \dot{K}_{l} + (u_{j} \gamma_{l,j}, \gamma_{m}) K_{l} + \left(\left(\frac{\mu_{0}}{\rho} + \frac{\mu_{t}}{\rho \sigma_{K}} \right) \gamma_{l,j}, \gamma_{m,j} \right) K_{l} \right\} \\ &= -\left(\frac{\mu_{t}}{\rho \sigma_{t}} \beta g_{j} T_{,j} - \frac{\mu_{t}}{\rho} G + \varepsilon, \gamma_{m} \right) + B_{K} (\gamma_{m}), \\ \sum_{l=1}^{N} \left\{ (\gamma_{l}, \gamma_{m}) \dot{\varepsilon}_{l} + (u_{j} \gamma_{l,j}, \gamma_{m}) \varepsilon_{l} + \left(\left(\frac{\mu_{0}}{\rho} + \frac{\mu_{t}}{\rho \sigma_{\varepsilon}} \right) \gamma_{l,j}, \gamma_{m,j} \right) \varepsilon_{l} \right\} \\ &= \left(C_{1} (1 - C_{3}) \frac{\varepsilon \mu_{t}}{K \rho \sigma_{t}} \beta g_{j} T_{,j} + C_{1} \frac{\varepsilon \mu_{t}}{K \rho} G - C_{2} f_{\varepsilon} \frac{\varepsilon^{2}}{K}, \gamma_{m} \right) + B_{\varepsilon} (\gamma_{m}), \quad (4.31) \end{split}$$

for m = 1, 2, 3, ..., N and p = 1, 2, 3, ..., N'. The Newmann type and Robin type boundary conditions in (4.18)-(4.21) can now be introduced into system (4.31). Thus, we have

$$B_{p}(\gamma_{m}) = \int_{\Gamma_{exit}} \frac{1}{\rho} \gamma_{m} \beta_{l} d\Gamma p_{l}^{*},$$

$$B_{T}(\gamma_{m}) = -\int_{\Gamma_{wall}} \frac{1}{\rho c} h_{\infty} \gamma_{l} \gamma_{m} d\Gamma T_{l} + \int_{\Gamma_{wall}} \frac{1}{\rho c} h_{\infty} \gamma_{m} T_{\infty} d\Gamma.$$

$$(4.32)$$

The system of equations (4.31) can be expressed in matrix form as follows

$$\begin{bmatrix}
C_1^T & C_2^T \\
U_2
\end{bmatrix} = -\delta M_p p^*,
S\dot{U}_i + BU_i + A_{u_i}^1 U_1 + A_{u_i}^2 U_2 - C_i^* p^* = F_{u_i} + F_{em_i},
S\dot{T} + BT + A_T T + A_b T = F_T + S' \dot{H} + B' H,
S\dot{K} + BK + A_K K = F_K,
S\dot{E} + BE + A_{\varepsilon} E = F_{\varepsilon},$$
(4.33)

From equation $(4.33)_1$, we can write p^* in terms of U_i as follow

$$p^* = -\frac{1}{\delta} M_p^{-1} \left(C_1^T U_1 + C_2^T U_2 \right).$$

Thus, the pressure term in the system of equations (4.33) can be eliminated so that we have

$$S\dot{U}_i + BU_i + A_{u_i}^1 U_1 + A_{u_i}^2 U_2 + \frac{1}{\delta} C_i^* M_p^{-1} \left(C_1^T U_1 + C_2^T U_2 \right) = F_{u_i} + F_{em_i}. \tag{4.34}$$

The system of equations (4.34) then can be written into two groups in matrix form

$$\begin{bmatrix} S & 0 & 0 \\ 0 & S & 0 \\ 0 & 0 & S \end{bmatrix} \begin{bmatrix} \dot{U}_1 \\ \dot{U}_2 \\ \dot{T} \end{bmatrix}$$

$$+ \begin{bmatrix} B + A_{u_1}^1 + \frac{1}{\delta} C_1^* M_p^{-1} C_1^T & A_{u_1}^1 + \frac{1}{\delta} C_1^* M_p^{-1} C_2^T & 0 \\ A_{u_2}^1 + \frac{1}{\delta} C_2^* M_p^{-1} C_1^T & B + A_{u_2}^1 + \frac{1}{\delta} C_2^* M_p^{-1} C_2^T & 0 \\ 0 & 0 & B + A_T + A_b \end{bmatrix} \begin{bmatrix} U_1 \\ U_2 \\ T \end{bmatrix}$$

$$= \begin{bmatrix} F_{u_1} \\ F_{u_2} \end{bmatrix} + \begin{bmatrix} F_{em_1} \\ F_{em_2} \end{bmatrix} + \begin{bmatrix} 0 \\ 0 \\ 0 \end{bmatrix}, \quad (4.35)$$

Fac. of Grad. Studies, Mahidol Univ.

$$\begin{bmatrix} S & 0 \\ 0 & S \end{bmatrix} \begin{bmatrix} \dot{K} \\ \dot{E} \end{bmatrix} + \begin{bmatrix} B + A_k & 0 \\ 0 & B + A_{\varepsilon} \end{bmatrix} \begin{bmatrix} K \\ E \end{bmatrix} = \begin{bmatrix} F_K \\ F_{\varepsilon} \end{bmatrix}, \tag{4.36}$$

where the coefficient matrices are defined by

$$M_p = ((m_p)_{lm})_{N' \times N'} \quad \text{with} \quad (m_p)_{lm} = \int_{\Omega} \beta_l \beta_m \, d\Omega,$$

$$C_i = \left\{ c_{lm}^i \right\}_{N \times N'} \quad \text{with} \quad c_{lm}^i = \int_{\Omega} \frac{\partial \gamma_l}{\partial x_i} \beta_m \, d\Omega \quad (i = 1, 2),$$

$$C_i^* = \frac{1}{\rho} \left\{ c_{lm}^i - c_{lm}^* \right\}_{N \times N'} \quad \text{with} \quad c_{lm}^* = \int_{\Gamma_{exit}} \gamma_l \beta_m \, d\Gamma,$$

$$S = (s_{lm})_{N \times N}, S' = -\frac{1}{c} (s_{lm})_{N \times N} \quad \text{with} \quad s_{lm} = \int_{\Omega} \gamma_l \gamma_m \, d\Omega,$$

$$B = (b_{lm})_{N \times N}, B' = -\frac{1}{c}(b_{lm})_{N \times N} \quad \text{with} \quad b_{lm} = \int_{\Omega} \gamma_l(u_j \frac{\partial \gamma_m}{\partial x_j}) d\Omega, \quad (j = 1, 2)$$

$$A_{u} = \begin{bmatrix} A_{u_{1}}^{1} & A_{u_{1}}^{2} \\ A_{u_{2}}^{1} & A_{u_{2}}^{2} \end{bmatrix} = \begin{bmatrix} 2a_{lm}^{11} + d_{lm}^{22} & a_{lm}^{12} \\ a_{lm}^{21} & a_{lm}^{11} + 2a_{lm}^{22} \end{bmatrix}_{2N \times 2N} \text{ with } a_{lm}^{ij} = \int_{\Omega} \frac{\mu_{f}}{\rho} \frac{\partial \gamma_{l}}{\partial x_{i}} \frac{\partial \gamma_{m}}{\partial x_{j}} d\Omega ,$$

$$(i, j = 1, 2)$$

$$A_T = (a_{lm}^T)_{N \times N}$$
 with $a_{lm}^T = \int_{\Omega} \frac{k_f}{\rho c} (\frac{\partial \gamma_l}{\partial x_j} \frac{\partial \gamma_m}{\partial x_j}) d\Omega$; $(j = 1, 2)$,

$$A_k = (a_{lm}^k)_{N \times N} \quad \text{with} \quad a_{lm}^k = \int\limits_{\Omega} (\frac{\mu_0}{\rho} + \frac{\mu_t}{\rho \sigma_K}) (\frac{\partial \gamma_l}{\partial x_j} \frac{\partial \gamma_m}{\partial x_j}) \, d\Omega \ ; (j = 1, 2),$$

$$A_{\varepsilon} = (a_{lm}^{\varepsilon})_{N \times N} \quad \text{with} \quad a_{lm}^{\varepsilon} = \int_{\Omega} (\frac{\mu_0}{\rho} + \frac{\mu_t}{\sigma_{\varepsilon}}) (\frac{\partial \gamma_l}{\partial x_j} \frac{\partial \gamma_m}{\partial x_j}) \ d\Omega \ ; (j = 1, 2),$$

$$F_{u} = \begin{bmatrix} f_{l}^{1} \\ f_{l}^{2} \end{bmatrix}_{2N \times 1} \quad \text{with} \quad f_{l}^{1} = \int_{\Omega} \frac{\mu_{f}}{\rho \kappa} u \gamma_{l} d\Omega, \quad f_{l}^{2} = \int_{\Omega} \frac{\mu_{f}}{\rho \kappa} (v - U_{cast}) \gamma_{l} d\Omega,$$

$$F_{em} = \begin{bmatrix} f_{em_l}^1 \\ f_{em_l}^2 \end{bmatrix}_{2N \times 1} \quad \text{with} \quad f_{em_l}^1 = \int_{\Omega} \frac{1}{\rho} F_{em_x} \gamma_l \, d\Omega, \quad f_{em_l}^2 = \int_{\Omega} \frac{1}{\rho} F_{em_z} \gamma_l \, d\Omega,$$

$$A_b = (a_{lm}^b)_{N \times N}$$
 with $a_{ij}^b = \frac{1}{\rho c} \int_{\Gamma_{wall}} h_{\infty} \gamma_l \gamma_m \, d\Gamma$,

$$F_T = (f_l^T)_{N \times 1} \text{ with } f_l^T = \frac{1}{\rho c} \int_{\Gamma_{wall}} h_\infty T_\infty \gamma_l \, d\Gamma,$$

$$F_K = (f_l^K)_{N \times 1}$$
 with $f_l^K = \int_{\Omega} (\nu_t G - \varepsilon - \frac{\nu_t}{\sigma_t} \beta g \frac{\partial T}{\partial z}) \gamma_l d\Omega$,

$$F_{\varepsilon} = (f_l^{\varepsilon})_{N \times 1} \quad \text{with} \quad f_l^{\varepsilon} = \int_{\Omega} (C_1 \frac{\varepsilon}{K} \nu_t G + C_1 (1 - C_3) \frac{\varepsilon \nu_t}{K \sigma_t} \beta g \frac{\partial T}{\partial z} - C_2 f_{\varepsilon} \frac{\varepsilon^2}{K}) \gamma_l \, d\Omega.$$

$$(4.37)$$

To find the finite element solutions of (4.35) and (4.36), we discretize the computation domain Ω into M elements Ω_e , namely

$$\Omega = \bigcup_{e=1}^{M} \Omega_e,$$

where $\Omega_i \cap \Omega_j = 0 \ \forall i \neq j$. The basis functions $\gamma_l(\mathbf{x}_j)$ are chosen to be piecewise continuous and to have a value of one at its their node and zero at other nodes. Then, the integral terms defined in (4.37) can be obtained by assembling the contribution from each element. For example,

$$\int_{\Omega} \gamma_l \gamma_m \, d\Omega = \sum_{e=1}^M \int_{\Omega_e} \gamma_l^e \gamma_m^e \, d\Omega_e. \tag{4.38}$$

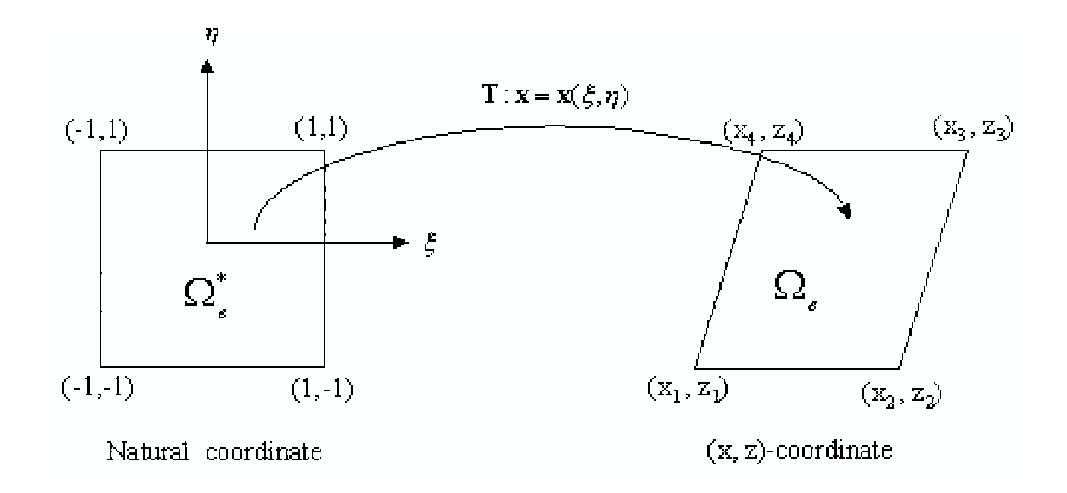


Figure 4.1: Generation of finite element mesh from master element.

To evaluate the integrals over each element Ω_e , the coordinate transformation in Figure 4.1 is used to map a master element Ω_e^* to Ω_e ,

$$T: x = x(\xi, \eta)$$

$$z = z(\xi, \eta).$$
(4.39)

The inverse transformation is as follows

$$T^{-1}$$
: $\xi = \xi(x, z)$
 $\eta = \eta(x, z)$

By using this coordinate transformation, the integral domain for every element Ω_e is the same with respect to the new integration variables ξ and η .

The computational domain Ω is divided into M rectangular elements Ω_e . Let $\{x_i, z_i\}_{i=1}^4$ and $\{\gamma_i\}_{i=1}^4$ be the corner points and the element shape functions at the nodes, respectively. To transform the points $\{x_i, z_i\}_{i=1}^4$ and $\{\gamma_i\}_{i=1}^4$ in Ω_e to the points and functions in element Ω_e^* , the transformation for mapping is given by

$$x = \sum_{i=1}^{4} x_i N_i(\xi, \eta)$$

$$T_e: z = \sum_{i=1}^{4} z_i N_i(\xi, \eta)$$
(4.40)

where the shape functions $N_i(\xi, \eta)$ are as follows

$$N_i(\xi, \eta) = \frac{1}{4} (1 + \xi \xi_i)(1 + \eta \eta_i). \tag{4.41}$$

To approximate the unknown variables, u, v, T, K and ε , we use the Lagrange polynomial to interpolate the unknown functions as follows

$$u(\xi, \eta) = \sum_{i=1}^{4} u_i N_i(\xi, \eta),$$
 (4.42)

where $\{u_i\}_{i=1}^4$ denote the values of the unknown function u at the four corner nodes of Ω_e^* . For the pressure field, we choose the center of Ω_e as the node and the pressure $p^* = p_e^* \gamma_e$ with $\gamma_e = 1$ to ensure the convergence of solution for our problem [3]. To perform the element calculation, the chain rule of differentiation is applied to equation (4.39). We then have

$$dx = \frac{\partial x}{\partial \xi} d\xi + \frac{\partial x}{\partial \eta} d\eta,$$

$$dz = \frac{\partial z}{\partial \xi} d\xi + \frac{\partial z}{\partial \eta} d\eta,$$
(4.43)

or

$$\begin{bmatrix} dx \\ dz \end{bmatrix} = \begin{bmatrix} \frac{\partial x}{\partial \xi} & \frac{\partial x}{\partial \eta} \\ \frac{\partial z}{\partial \xi} & \frac{\partial z}{\partial \eta} \end{bmatrix} \begin{bmatrix} d\xi \\ d\eta \end{bmatrix} = \mathbf{J}^* \begin{bmatrix} d\xi \\ d\eta \end{bmatrix}$$
(4.44)

where \mathbf{J}^* is the Jacobian matrix. From equation (4.44), after some calculations, we have

$$\frac{\partial \xi}{\partial x} = \frac{1}{|\mathbf{J}^*|} \frac{\partial z}{\partial \eta}, \qquad \frac{\partial \xi}{\partial z} = -\frac{1}{|\mathbf{J}^*|} \frac{\partial x}{\partial \eta},
\frac{\partial \eta}{\partial x} = -\frac{1}{|\mathbf{J}^*|} \frac{\partial z}{\partial \xi}, \qquad \frac{\partial \eta}{\partial z} = \frac{1}{|\mathbf{J}^*|} \frac{\partial x}{\partial \xi},
(4.45)$$

where $|\mathbf{J}^*|$ is the determinant of the Jacobian matrix \mathbf{J}^* . We use the composite rule for differentiation to calculate the following derivatives

$$\frac{\partial \gamma_{j}}{\partial x} = \frac{\partial N_{j}}{\partial \xi} \frac{\partial \xi}{\partial x} + \frac{\partial N_{j}}{\partial \eta} \frac{\partial \eta}{\partial x},$$

$$\frac{\partial \gamma_{j}}{\partial z} = \frac{\partial N_{j}}{\partial \xi} \frac{\partial \xi}{\partial z} + \frac{\partial N_{j}}{\partial \eta} \frac{\partial \eta}{\partial z}.$$
(4.46)

Thus, the entries of the global matrices in (4.47) can be evaluated over the master element Ω_e^* by

$$(m_{p})_{lm}^{e} = \int_{-1}^{1} \int_{-1}^{1} |\mathbf{J}^{*}| \ d\xi d\eta,$$

$$(c_{lm}^{i})^{e} = \int_{-1}^{1} \int_{-1}^{1} Q_{i}^{l} |\mathbf{J}^{*}| \ d\xi d\eta,$$

$$(c_{lm}^{*})^{e} = \int_{-1}^{1} \int_{-1}^{1} N_{i}(\xi, 1) \ |\mathbf{J}^{*}| \ d\xi,$$

$$(s_{lm})^{e} = \int_{-1}^{1} \int_{-1}^{1} N_{l}N_{m} \ |\mathbf{J}^{*}| \ d\xi d\eta,$$

$$(b_{lm})^{e} = \int_{-1}^{1} \int_{-1}^{1} N_{l}(uQ_{1}^{l} + vQ_{2}^{l}) \ |\mathbf{J}^{*}| \ d\xi d\eta,$$

$$(a_{lm}^{ij})^{e} = \int_{-1}^{1} \int_{-1}^{1} \frac{\mu_{f}}{\rho} (Q_{i}^{l}Q_{i}^{m} + Q_{1}^{l}Q_{1}^{m}) \ |\mathbf{J}^{*}| \ d\xi d\eta,$$

$$(a_{lm}^{T})^{e} = \int_{-1}^{1} \int_{-1}^{1} \frac{k_{f}}{\rho c} (Q_{1}^{l}Q_{1}^{m} + Q_{2}^{l}Q_{2}^{m}) \ |\mathbf{J}^{*}| \ d\xi d\eta,$$

$$(a_{lm}^{e})^{e} = \int_{-1}^{1} \int_{-1}^{1} (\frac{\mu_{0}}{\rho} + \frac{\mu_{t}}{\rho \sigma_{K}}) (Q_{1}^{l}Q_{1}^{m} + Q_{2}^{l}Q_{2}^{m}) \ |\mathbf{J}^{*}| \ d\xi d\eta,$$

$$(a_{lm}^{\varepsilon})^{e} = \int_{-1}^{1} \int_{-1}^{1} (\frac{\mu_{0}}{\rho} + \frac{\mu_{t}}{\rho \sigma_{K}}) (Q_{1}^{l}Q_{1}^{m} + Q_{2}^{l}Q_{2}^{m}) \ |\mathbf{J}^{*}| \ d\xi d\eta,$$

$$f_{l}^{1} = \int_{-1}^{1} \int_{-1}^{1} \frac{\mu_{f}}{\rho \kappa} uN_{l} \ |\mathbf{J}^{*}| \ d\xi d\eta,$$

$$f_{l}^{2} = \int_{-1}^{1} \int_{-1}^{1} \frac{\mu_{f}}{\rho \kappa} (v - U_{cast}) N_{l} |\mathbf{J}^{*}| d\xi d\eta,$$

$$f_{em_{l}}^{1} = \int_{-1}^{1} \int_{-1}^{1} \frac{1}{\rho} F_{em_{x}} N_{l} |\mathbf{J}^{*}| d\xi d\eta,$$

$$f_{em_{l}}^{2} = \int_{-1}^{1} \int_{-1}^{1} \frac{1}{\rho} F_{em_{x}} N_{l} |\mathbf{J}^{*}| d\xi d\eta,$$

$$(a_{ij}^{b})^{e} = \frac{1}{\rho c} \int_{-1}^{1} h_{\infty} N_{l} (-1, \eta) N_{m} (-1, \eta) |\mathbf{J}^{*}| d\eta,$$

$$(f_{l}^{T})^{e} = \frac{1}{\rho c} \int_{-1}^{1} h_{\infty} T_{\infty} N_{l} (-1, \eta) |\mathbf{J}^{*}| d\eta,$$

$$(f_{l}^{K})^{e} = \int_{-1}^{1} \int_{-1}^{1} (\nu_{t} G - \varepsilon - \frac{\nu_{t}}{\sigma_{t}} \beta g \frac{\partial T}{\partial z}) N_{l} |\mathbf{J}^{*}| d\xi d\eta,$$

$$(f_{l}^{\varepsilon})^{e} = \int_{-1}^{1} \int_{-1}^{1} (C_{1} \frac{\varepsilon}{K} \nu_{t} G + C_{1} (1 - C_{3}) \frac{\varepsilon \nu_{t}}{K \sigma_{t}} \beta g \frac{\partial T}{\partial z} - C_{2} f_{\varepsilon} \frac{\varepsilon^{2}}{K}) N_{l} |\mathbf{J}^{*}| d\xi d\eta,$$

$$(4.47)$$

where Q_i^j is defined by

$$Q_i^l(\xi,\eta) = \frac{\partial \gamma_l}{\partial x_i}.$$

The integrals in (4.47) are then evaluated numerically by the Gaussian quadrature formula.

4.4 Numerical Algorithm

Numerical Algorithm for Transient Problems

The system (4.44) can be written as

$$S\dot{\mathbf{U}} + B_{u}\mathbf{U} = \mathbf{F}_{u} + \mathbf{F}_{em},$$

$$S\dot{\mathbf{T}} + B_{T}\mathbf{T} = \mathbf{F}_{T} + S'\dot{\mathbf{H}} + B'\mathbf{H},$$

$$S\dot{\mathbf{K}} + B_{K}\mathbf{K} = \mathbf{F}_{K},$$

$$S\dot{\mathbf{E}} + B_{\varepsilon}\mathbf{E} = \mathbf{F}_{\varepsilon}.$$

$$(4.48)$$

By using the backward Euler differentiation scheme for a typical time step $(t_n \to t_{n+1})$, we have the following nonlinear system of equations

$$\left(\frac{S}{\Delta t_n} + B_u\right) \mathbf{U}_{n+1} = \mathbf{F}_{u_{n+1}} + \mathbf{F}_{em_{n+1}} + \frac{S}{\Delta t_n} \mathbf{U}_n,$$

$$\left(\frac{S}{\Delta t_n} + B_T\right) \mathbf{T}_{n+1} = \mathbf{F}_{T_{n+1}} + \frac{1}{\Delta t_n} \left(S \mathbf{T}_n - S' \mathbf{H}_n\right) + \left(\frac{S'}{\Delta t_n} + B'\right) \mathbf{H}_{n+1},$$

$$\left(\frac{S}{\Delta t_n} + B_K\right) \mathbf{K}_{n+1} = \mathbf{F}_{K_{n+1}} + \frac{S}{\Delta t_n} \mathbf{K}_n,$$

$$\left(\frac{S}{\Delta t_n} + B_\varepsilon\right) \mathbf{E}_{n+1} = \mathbf{F}_{\varepsilon_{n+1}} + \frac{S}{\Delta t_n} \mathbf{E}_n.$$
(4.49)

In this work, all quantities except for \mathbf{H}_{n+1} are frozen at values of $\mathbf{U}_n, \mathbf{T}_n, \mathbf{K}_n$ and \mathbf{E}_n corresponding to the previous time step. For \mathbf{H}_{n+1} , we have a nonlinearity to deal with. One way of treating this discontinuous source term for an iterative solution of (4.49) would be to use the iterative update

$$\left(\frac{S}{\Delta t_n} + B_u\right) \mathbf{U}_{n+1}^{i+1} = \mathbf{F}_{u_{n+1}}^i + \mathbf{F}_{em_{n+1}}^i + \frac{S}{\Delta t_n} \mathbf{U}_n,
\left(\frac{S}{\Delta t_n} + B_T\right) \mathbf{T}_{n+1}^{i+1} = \mathbf{F}_{T_{n+1}}^i + \frac{1}{\Delta t_n} \left(S\mathbf{T}_n - S'\mathbf{H}_n\right) + \left(\frac{S'}{\Delta t_n} + B'\right) \mathbf{H}_{n+1}^i,
\left(\frac{S}{\Delta t_n} + B_K\right) \mathbf{K}_{n+1}^{i+1} = \mathbf{F}_{K_{n+1}}^i + \frac{S}{\Delta t_n} \mathbf{K}_n,
\left(\frac{S}{\Delta t_n} + B_\varepsilon\right) \mathbf{E}_{n+1}^{i+1} = \mathbf{F}_{\varepsilon_{n+1}}^i + \frac{S}{\Delta t_n} \mathbf{E}_n.$$
(4.50)

where the superscript i refers to evaluation at the ith iteration step. As found by Wu et al. [57], the above iterative scheme is not reliable especially when the difference between the solidification temperature and the liquid temperature is small. This is because, during the iterations, the temperature near the solidification interface may oscillate and convergence will not be achieved. To overcome this problem, the relaxation scheme developed by Wu et al. [57] for multi-phase heat transfer problems has been generalized to solve system (4.48). Thus, the algorithm for finding $\mathbf{U}_{n+1}, \mathbf{T}_{n+1}, \mathbf{K}_{n+1}$ and \mathbf{E}_{n+1} from (4.48) is as follows

Set
$$\mathbf{T}_{n+1}^0 = \mathbf{T}_n$$
, $\mathbf{H}_{n+1}^0 = \mathbf{H}_n$,

For i = 0, 1, 2, ...

Calculate

$$\theta = \mathbf{H}_{n+1}^{i} + \beta c \left\{ \mathbf{T}_{n+1}^{i} - \left[\frac{T_{L} - T_{S}}{L} \mathbf{H}_{n+1}^{i} + T_{S} \right] \right\}$$

$$\mathbf{H}_{n+1}^{i+1} = \begin{cases} L & \text{if } \theta \ge L \\ \theta & 0 < \theta < L \\ 0 & \theta \le 0. \end{cases}$$

Calculate \mathbf{T}_{n+1}^{i+1} by solving $(4.48)_2$ with \mathbf{H}_{n+1}^i replaced by \mathbf{H}_{n+1}^{i+1} .

Fac. of Grad. Studies, Mahidol Univ.

Repeat the above two steps until $\|\mathbf{T}_{n+1}^{i+1} - \mathbf{T}_{n+1}^i\| < \text{Tolerance}$.

For i = 0, 1, 2, ...

Calculate \mathbf{U}_{n+1}^{i+1} by solving $(4.48)_1$

Repeat the above steps until $\|\mathbf{U}_{n+1}^{i+1} - \mathbf{U}_{n+1}^i\| < \text{Tolerance}.$

For i = 0, 1, 2, ...

Calculate \mathbf{K}_{n+1}^{i+1} and \mathbf{E}_{n+1}^{i+1} by solving $(4.48)_{3,4}$

Repeat the above steps until $\|\mathbf{K}_{n+1}^{i+1} - \mathbf{K}_{n+1}^i\|$ < Tolerance and $\|\mathbf{E}_{n+1}^{i+1} - \mathbf{E}_{n+1}^i\|$ < Tolerance.

By repeatedly using the above procedure for n = 0, 1, 2, ..., we can determine the state $(\mathbf{U}_n, \mathbf{T}_n, \mathbf{K}_n, \mathbf{E}_n)$ of the system at $t_0, t_1, t_2, ...$ If $\|\mathbf{T}_{n+1} - \mathbf{T}_n\|$, $\|\mathbf{U}_{n+1} - \mathbf{U}_n\|$, $\|\mathbf{K}_{n+1} - \mathbf{K}_n\|$ and $\|\mathbf{E}_{n+1} - \mathbf{E}_n\|$ are all sufficiently small, then the system approaches the so-called steady state.

Numerical Algorithm for Steady State Problems

Under a steady state condition, the time derivatives of temperature, velocity, turbulent kinetic energy and rate of dissipation are all zero and hence the discretized finite element equations governing the nodal temperature, velocity, turbulent kinetic energy and rate of dissipation are

$$\mathbf{B}_{u}(U, K, E)\mathbf{U} = \mathbf{F}_{u}(T) + \mathbf{F}_{\mathbf{em}}, \tag{4.51}$$

$$\mathbf{B}_T(U, K, E)\mathbf{T} = \mathbf{F}_T + \mathbf{B}'\mathbf{H},\tag{4.52}$$

$$\mathbf{B}_K(U, K, E)\mathbf{K} = \mathbf{F}_K(T), \tag{4.53}$$

$$\mathbf{B}_{\varepsilon}(U, K, E)\mathbf{E} = \mathbf{F}_{\varepsilon}(T), \tag{4.54}$$

which constitute a highly nonlinear system of equations. An iterative scheme based on Broyden's Quasi-Newton method has been developed for the solution of the system. In each iteration, we first solve equations (4.53) and (4.54) simultaneously for K and E. Using the K and E obtained, equations (4.51) and (4.52) are updated and then solved simultaneously to obtain the U and T vectors.

4.5 Numerical Studies

In this section, a computer program developed based on the presented algorithm is used to simulate the coupled fluid flow, heat transfer and solidification process, taking into account the effect of electromagnetic field. The simulation results, including the flow patterns, the temperature field and the steel solidification profiles, are presented in this section. Numerical investigations have also been undertaken to analyze the effect of source current on the flow field and temperature field in the continuous casting mould. The flow pattern and the thickness of the solidified steel shell obtained from the model with an electromagnetic field imposed are compared with those obtained from the model without an electromagnetic field imposed to the system.

The electromagnetic continuous caster under investigation has the same size as the one in chapter 3. The solution is limited to the region within 8 meters below the meniscus. The computation domain for the problem is limited to only one quadrant as shown in Figure 4.2 because the mould is symmetrical about two planes. The parameters used and the investigation schemes are given in Table 4.1 and Table 4.2, respectively. The finite element mesh consists of 1324 elements and 1410 nodes which is shown in Figure 4.3.

The simulation results for a coupled fluid flow-heat transfer problem in the continuous casting process are presented in Figures 4.4 - 4.12. The vector plot of steel velocity and the temperature contour without the effect of electromagnetic field and with the effect of electromagnetic field are shown in Figure 4.4 and Figure 4.5, respectively. The flow pattern on the top part of the mould in Figure 4.4(a) and 4.5(a) separates into two recirculation zones. A larger zone occurs below the nozzle inlet while a smaller zone occurs near the mould wall and meniscus. Figure 4.4(b) and 4.5(b) show how the heat in molten steel flows with the fluid. Temperature drops a few degree in the liquid pool in the conventional caster.

Table 4.1: Parameters used in numerical simulation

Parameter	symbol	Value	Unit
Pouring temperature	T_{in}	1530	°C
Molten temperature	T_L	1525	°C
Solidified temperature	T_S	1465	°C
Temperature of cooling water	T_{∞}	20	°C
External temperature	T_{ext}	100	^{o}C
Characteristic length of the flow	d	0.06	m
Gravitational acceleration	g	9.8	m/s^2
Density	ρ	7800	kg/m^3
Viscosity	μ	0.001	$pa \cdot s$
Specific heat	c	465	$J/kg^{o}C$
Thermal conductivity of steel	k	35	$W/m^{o}C$
Latent heat	L	2.72×10^{5}	J/kg
Heat transfer coefficient	h_{∞}	1079.45	$W/m^{2o}C$
Morphology constant	C	1.8×10^6	m^{-2}

The comparison of temperature distribution in the EM caster between the model without EM force and with EM force is shown in Figures 4.6(a) and (b), respectively. The electromagnetic force affects the thickness of the solidified steel shell. At 0.5 meters below meniscus, its thickness is about 15 cm for EM continuous caster and is about 2 cm for the conventional continuous caster.

Table 4.2: Computation schemes

Scheme	Source Current		
	(Ampere)		
1	10000		
2	20000		
3	30000		
4	0		

Figure 4.7 shows the effect of electromagnetic force on the thickness of solidified steel shell. The thickness of the solidified steel shell increases by about 7 times in the EM casting comparing to the conventional casting.

Figure 4.8 and Figure 4.9 present respectively the temperature distribution on strand surface in the conventional caster and the EM caster. Using the EM caster, the temperature near the mould wall drops faster than that in the conventional caster.

Figure 4.10 shows the temperature profile at the end of the mould in conventional caster and in an EM caster, respectively. It is noted that an EM caster produces the lower temperature at the end of the mould.

Figure 4.11-4.14 show the effect of varying source current on the velocity field and temperature field. The effect of the velocity field is presented in Figure 4.11. It is shown that a higher source current generates a smaller recirculation zone further to the symmetry plane and the nozzle inlet. Using 30 kA source current may block inlet flow as show in Figure 4.11(c). The influence of source current on the temperature profile and the solidified steel shell are shown in Figure 4.13 and Figure 4.12, respectively. It is found that

the thickness of the solidified steel shell increases when the source current increases.

Figure 4.14 shows the investigation of different source current on the temperature profile at the end of mould. It is noted that the EM caster produces the lower temperature at the end of mould when compared with the conventional caster and the larger source current gives the lower temperature.

4.6 Concluding Remarks

An efficient mathematical model and numerical algorithm for simulating the coupled turbulent fluid flow, heat transfer and solidification in the EM continuous casting process has been developed and used in numerical studies of the casting process.

The studies clearly show that the electromagnetic field have significant influence on the flow field, temperature field, and the growth of the solidified steel shell. By increasing source current, the thickness of the solidified steel shell increases significantly.

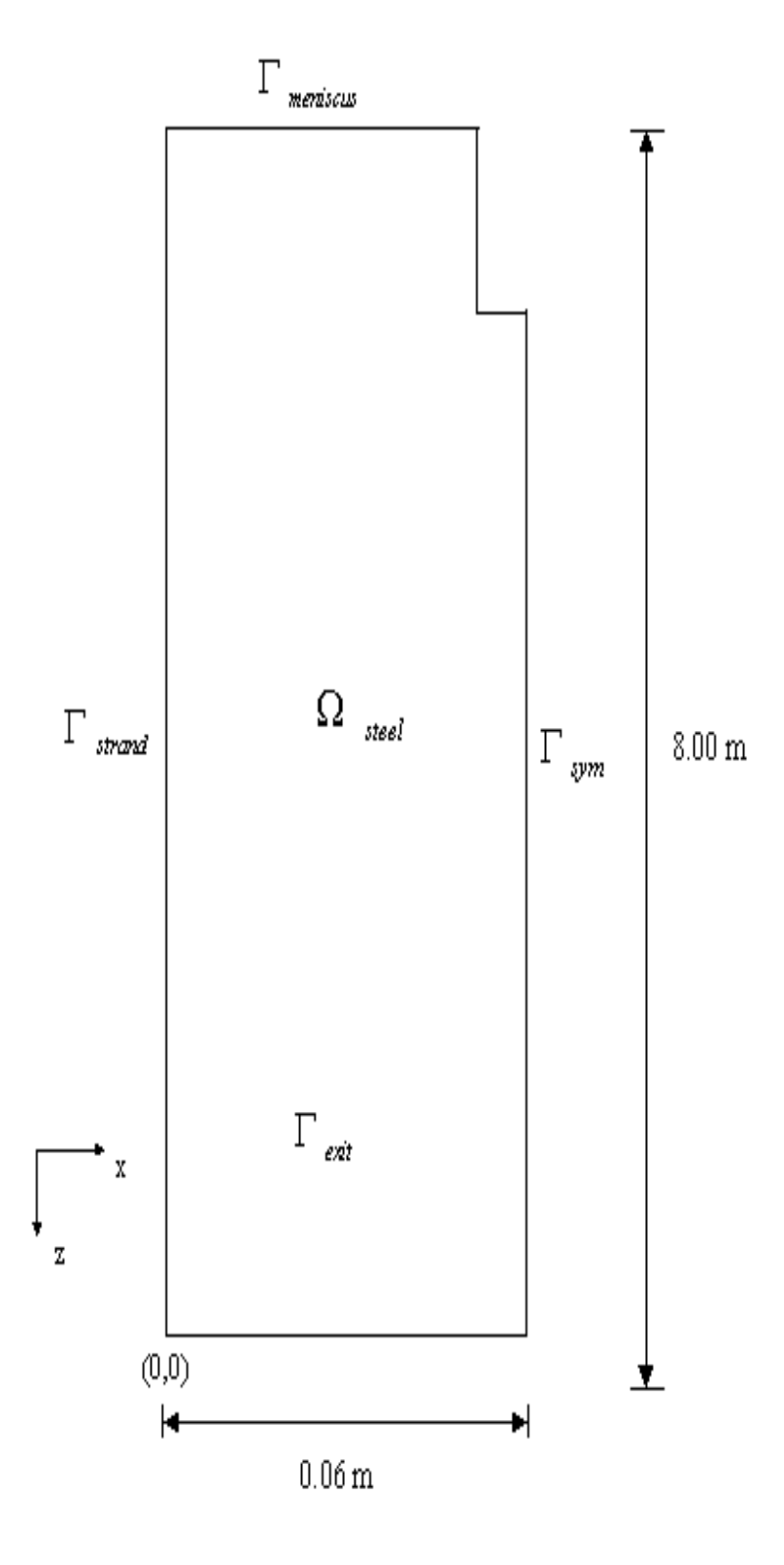


Figure 4.2: The computation domain and coordinate system.

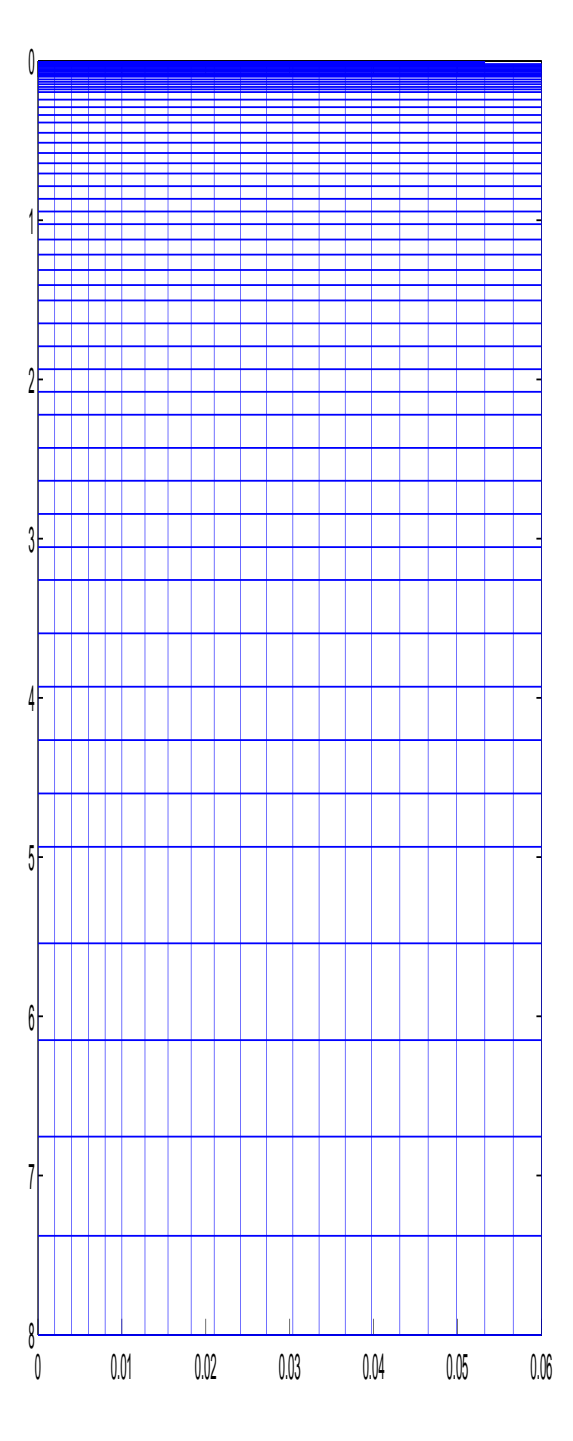


Figure 4.3: The finite element mesh for the coupled fluid flow-heat transfer problem.

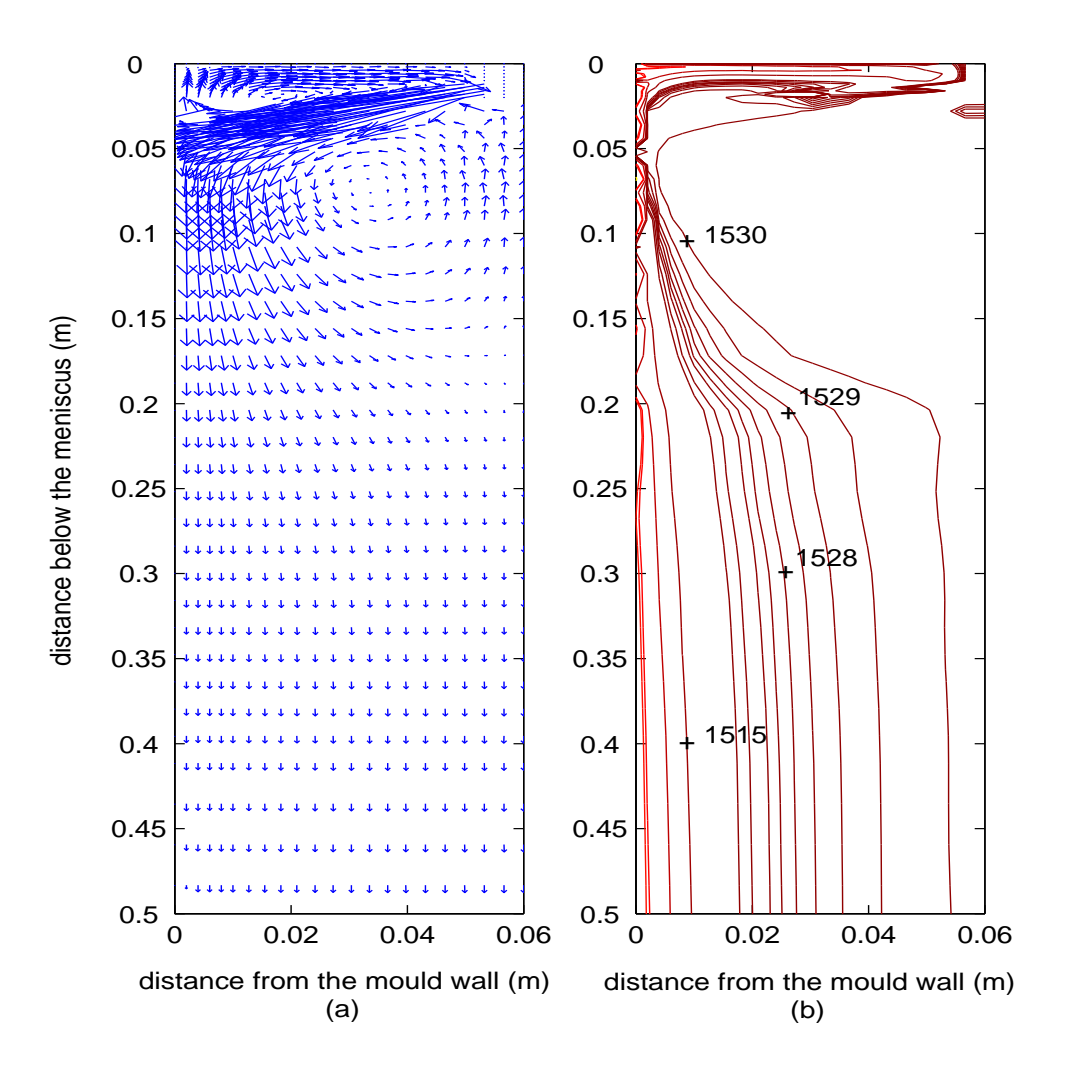


Figure 4.4: Vector plot of velocity vectors \mathbf{u} (m/s) and temperature contours $T({}^{\circ}C)$ when the coil current is off.

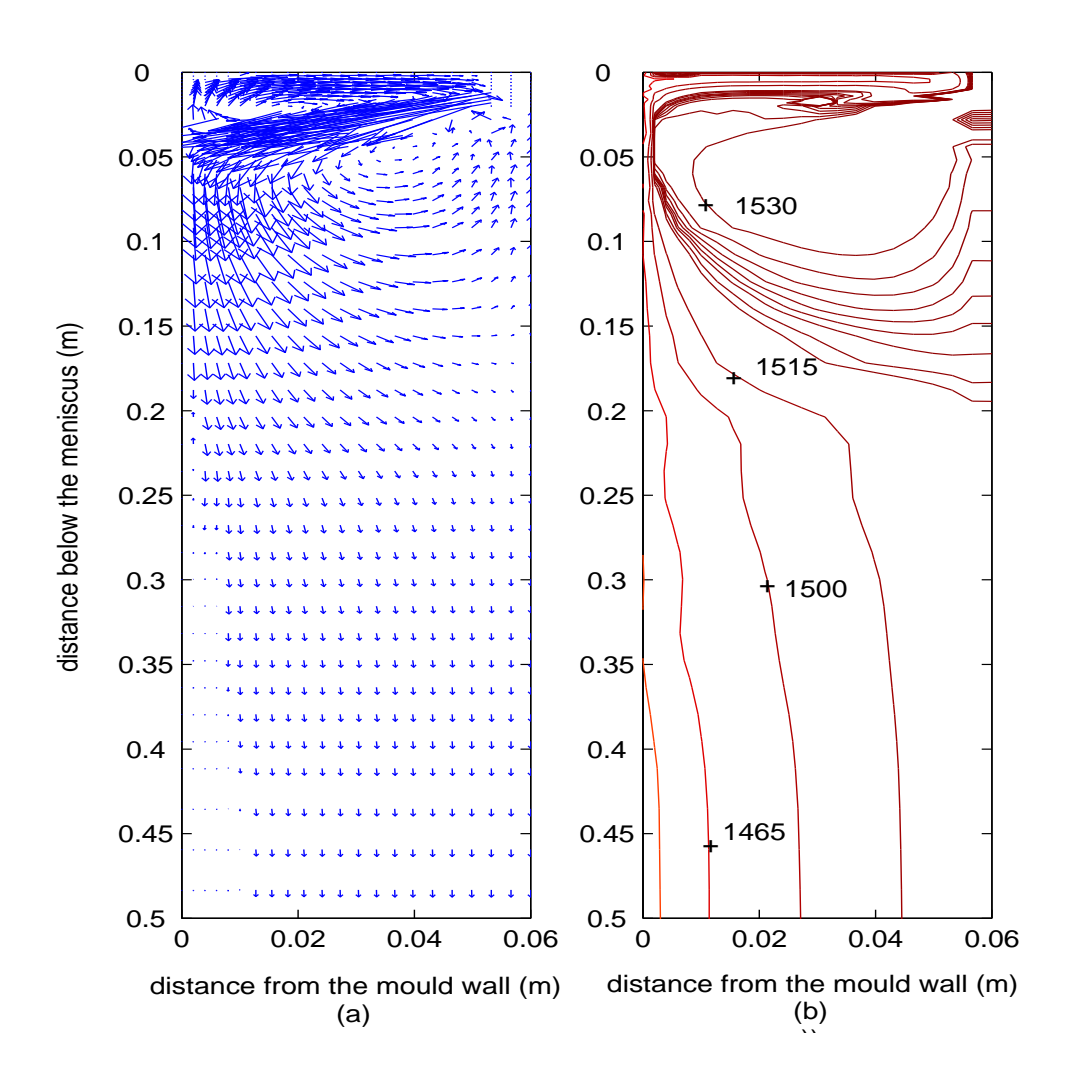


Figure 4.5: Velocity vectors ${\bf u}$ (m/s) and temperature contours $T(^{\circ}C)$ under 60 Hz magnetic field and 30000 A source current.

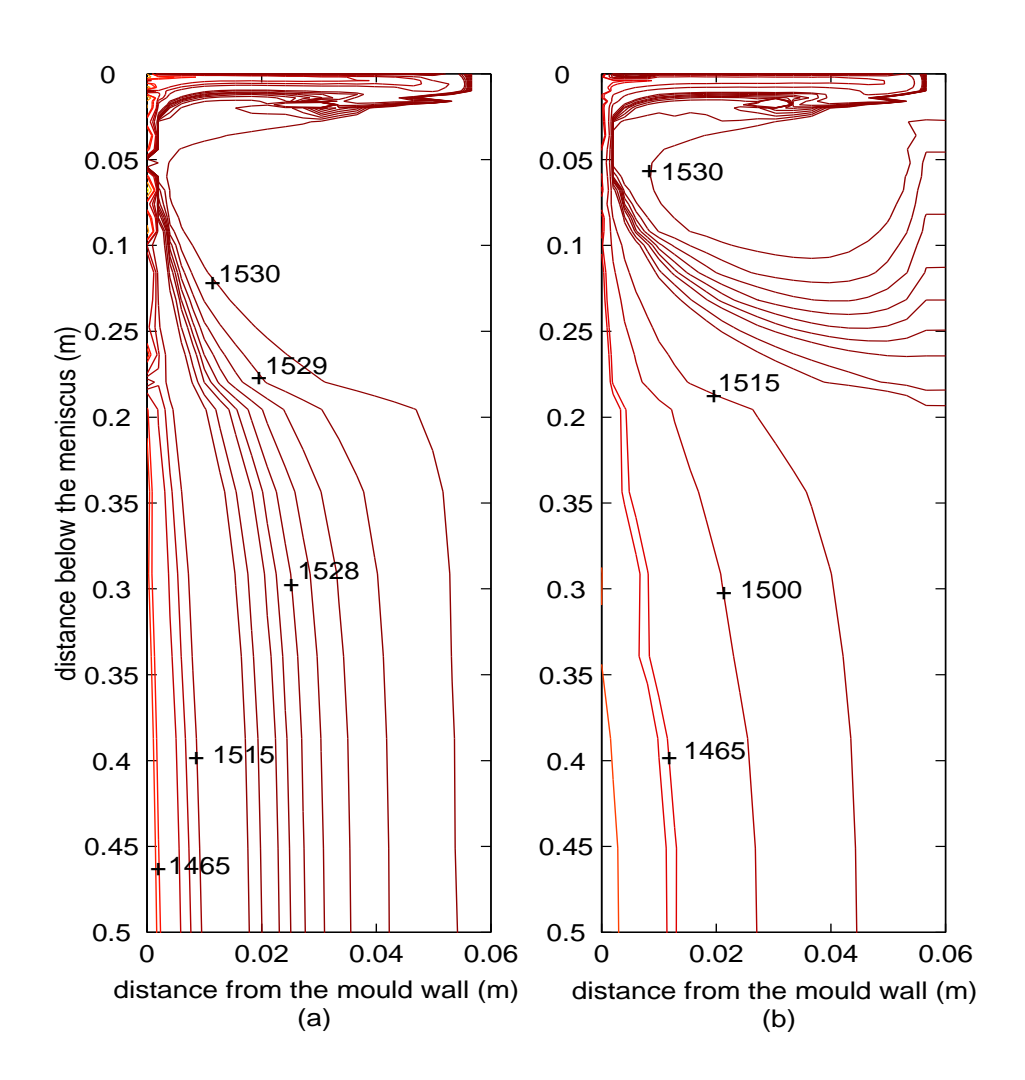


Figure 4.6: Temperature profile $T(^{\circ}C)$ in the liquid steel pool : (a) without EM force, (b) with EM force under 60 Hz magnetic field and 30000 A source current.

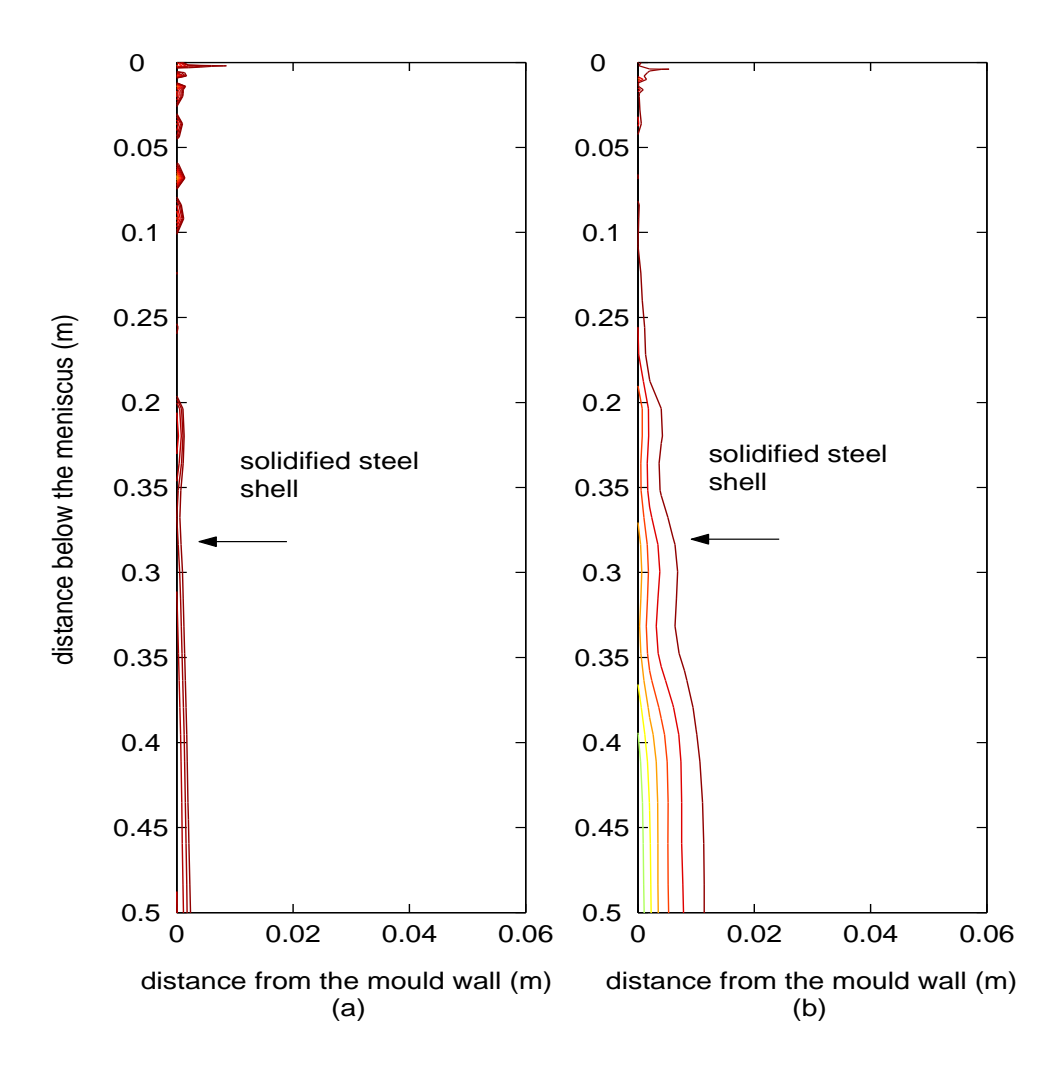


Figure 4.7: Thickness of solidified steel shell in (a) with no magnetic field, (b) under 60 Hz magnetic field and 30000 A source current.

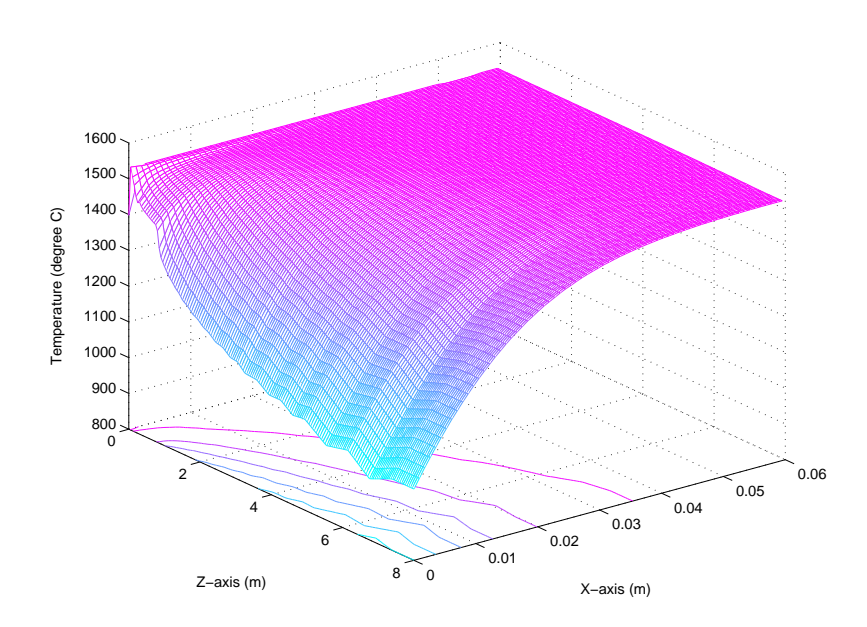


Figure 4.8: Temperature distribution of steel strand $T(^{\circ}C)$ in conventional continuous caster.

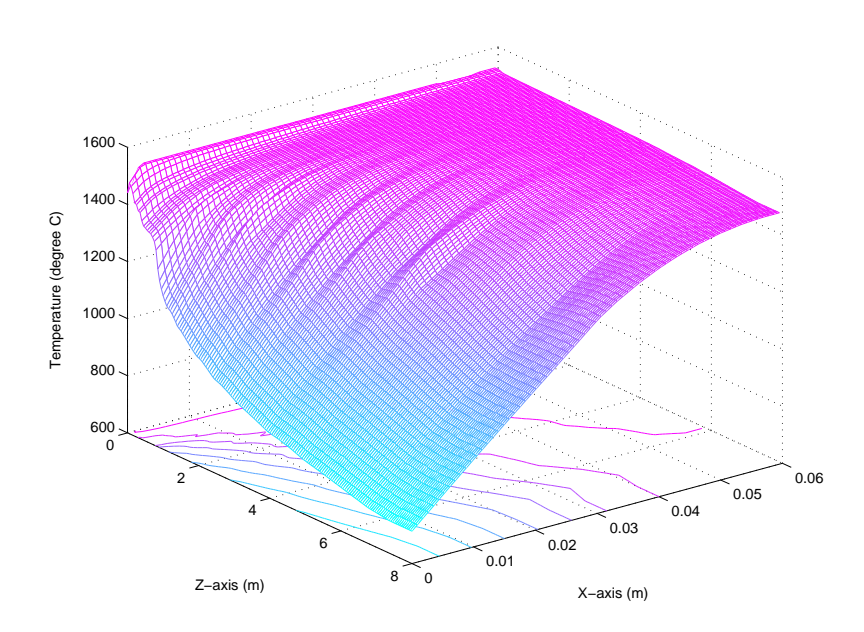


Figure 4.9: Temperature distribution of steel strand $T(^{\circ}C)$ in EM caster under 60 Hz magnetic field and 30000 A source current.

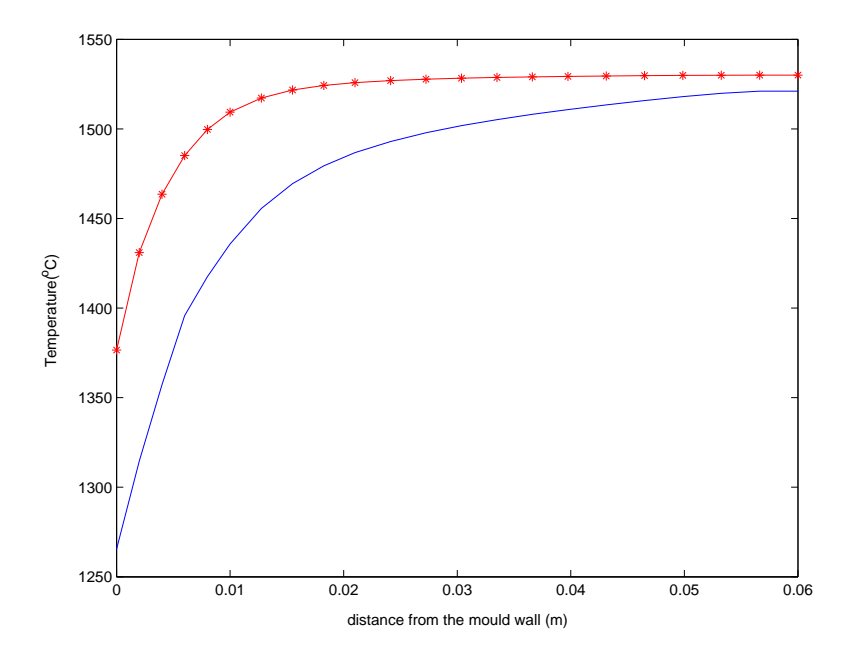


Figure 4.10: Temperature profile at the end of mould : label -*- for a model without EM force and —— for a model with EM force under 60 Hz magnetic field and 30000 A source current.

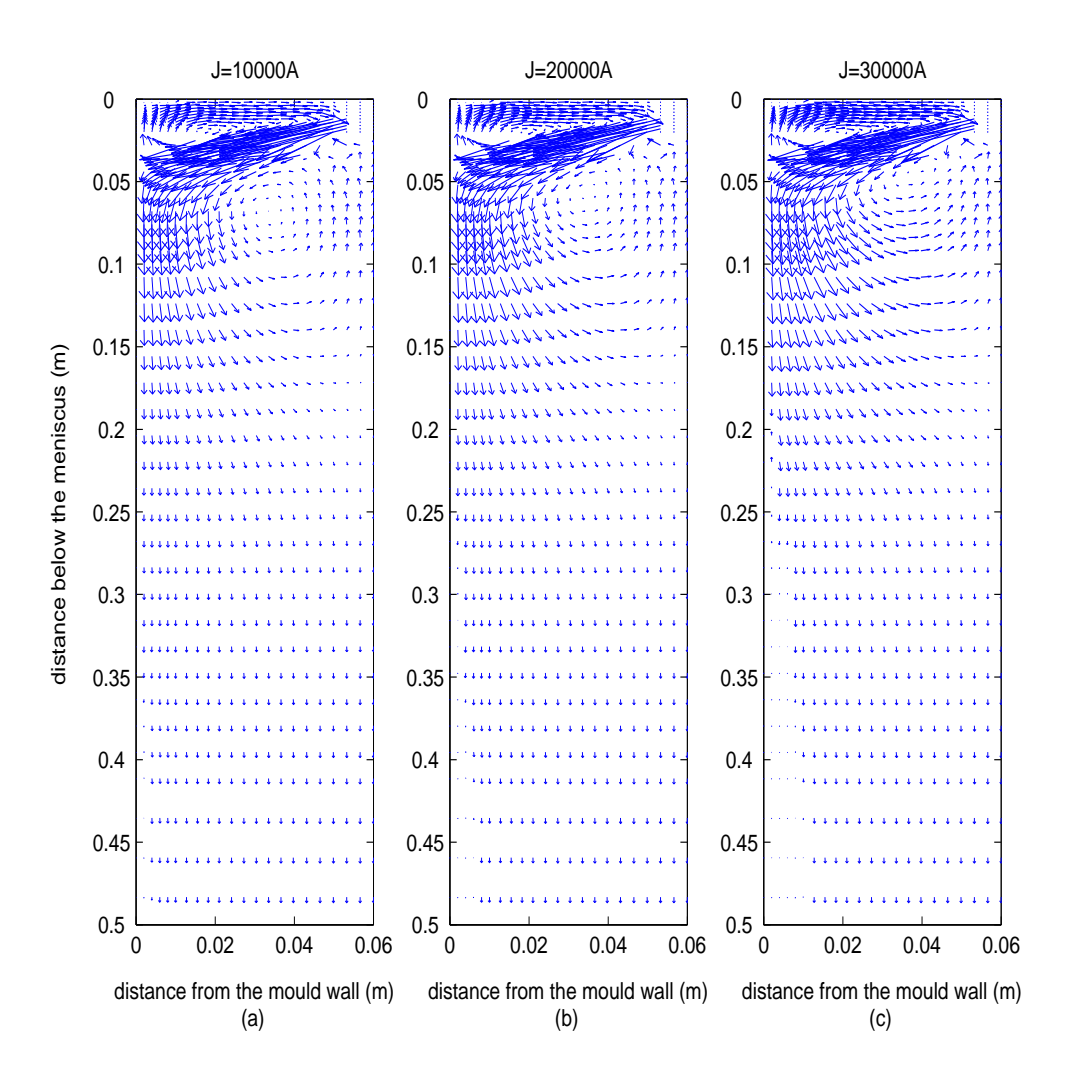


Figure 4.11: The velocity fields of molten steel in the process for three different source currents: (a) 10000 A, (b) 20000 A, and (c) 30000 A.

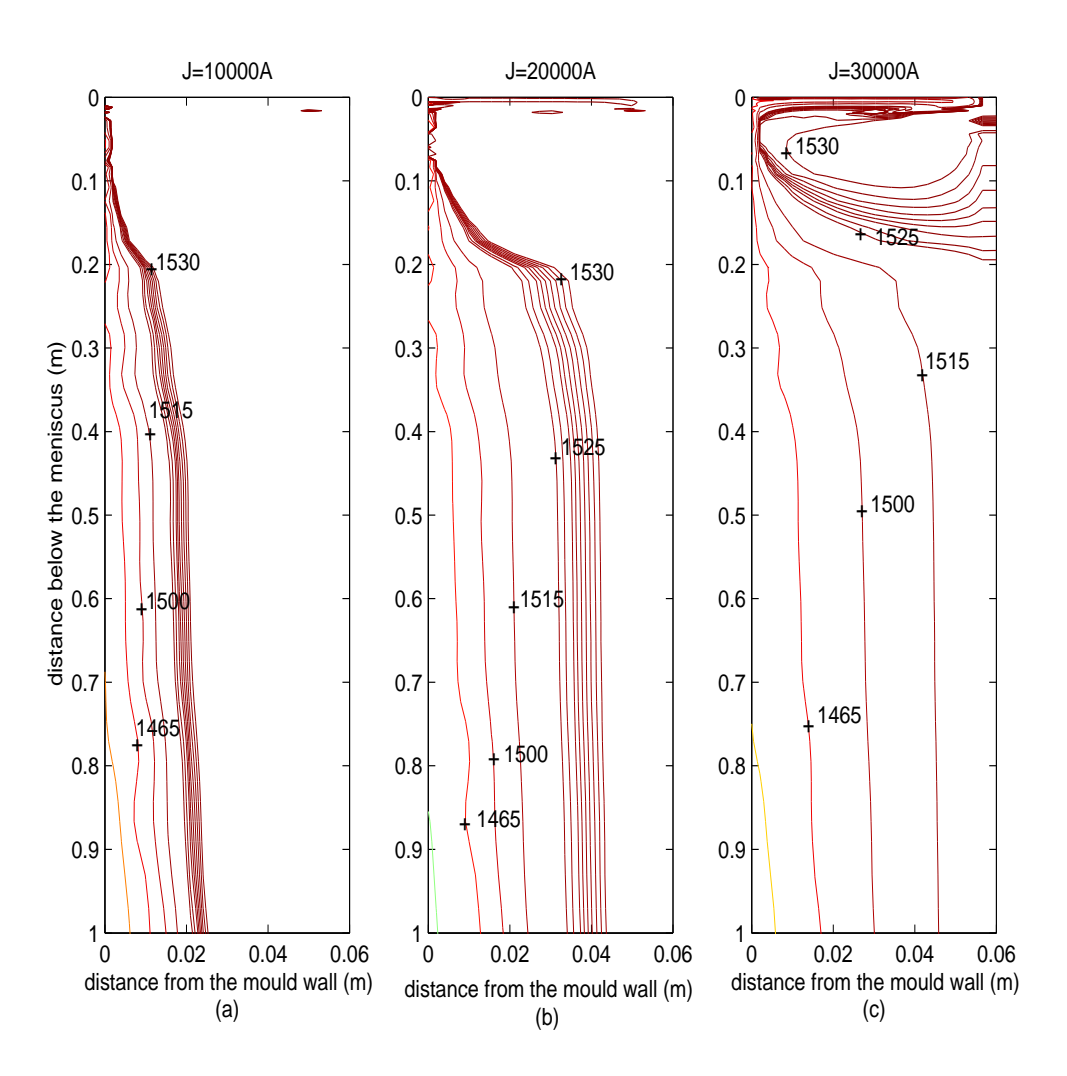


Figure 4.12: Temperature distributions of steel in the process for three different source currents: (a) 10000 A, (b) 20000 A, and (c) 30000 A.

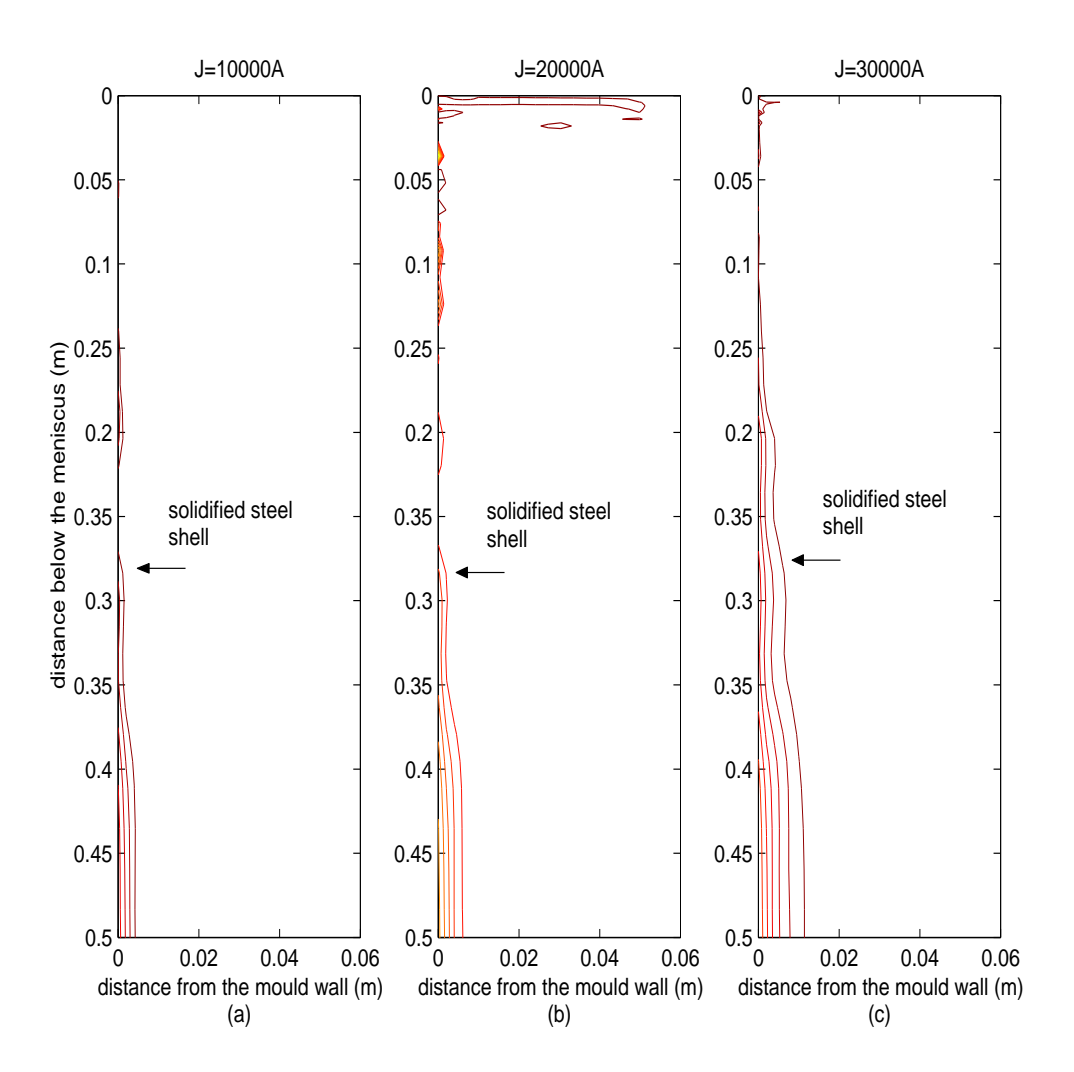


Figure 4.13: Thickness of solidified steel shell for different source currents : (a) 10000~A, (b) 20000~A, and (c) 30000~A.

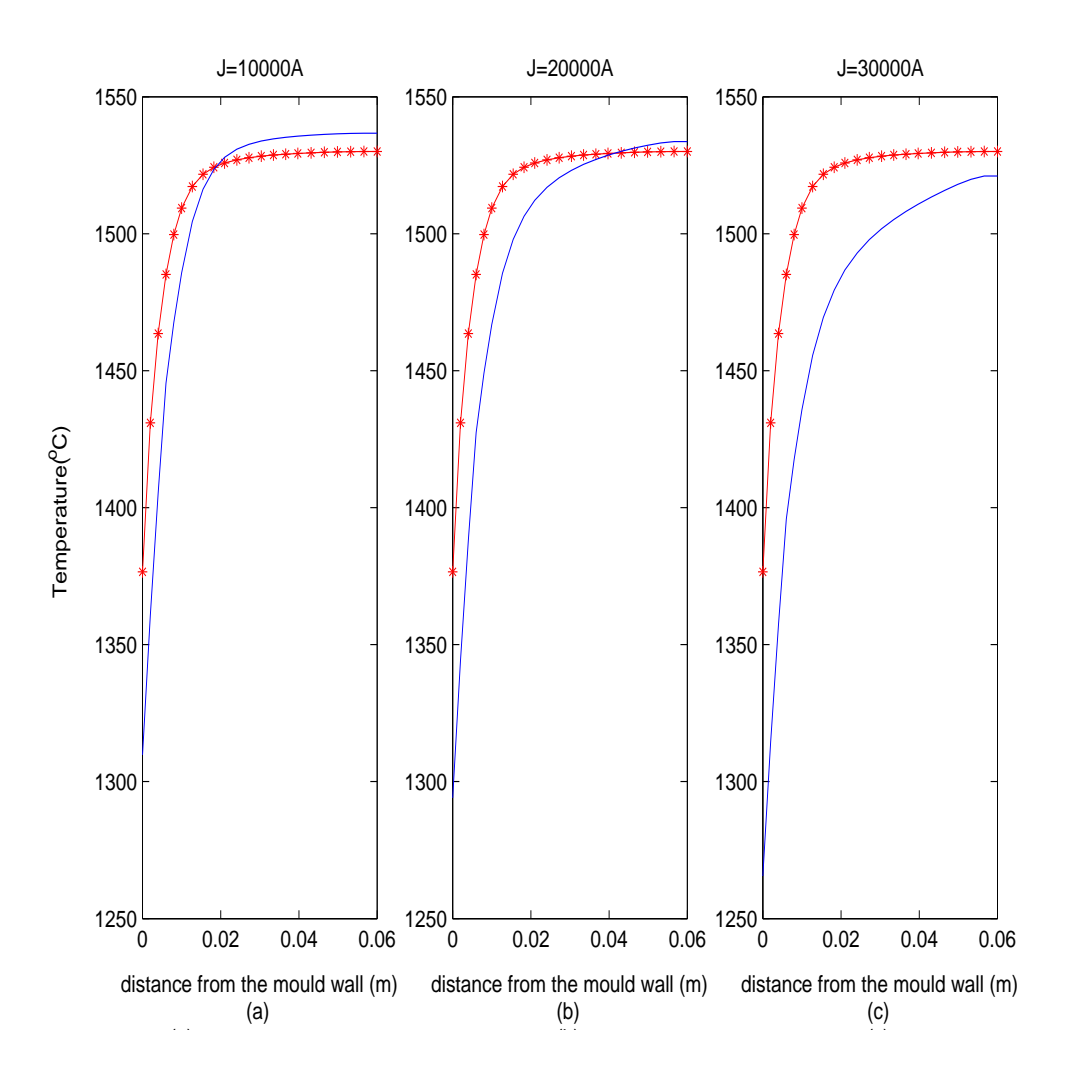


Figure 4.14: Temperature profile (${}^{\circ}C$) at the end of mould for different source currents: label -*- for a model without EM force, and —— for a model with EM force.

CHAPTER 5

DYNAMIC BEHAVIOR AT MENISCUS REGION

5.1 General Overview

In continuous casting process, the lubrication fluid or powder is added to the top surface of the liquid steel to facilitate the process. The phenomena in the region near the top surface, including the lubrication flux and molten steel, have significant influence on the quality of the casting products. Over the last few decades, many attempts have been made to study the mould flux behavior, including those due to Nakano et al. (1984) [58], Anzai et al. (1987) [59], Bommaraju and Saad (1990) [60], Sarademann and Schrewe (1991) [61], Nakato et al. (1991) [62], Li et al. (1995) [39], Mcdavid and Thomas (1996) [36], and Sha et al. (1996) [42]. However, only few attempts have been made to study the flow behavior in the meniscus region and the influence of the electromagnetic field imposed on the top surface. Thus, in this project, we study the influence of the electromagnetic field on the fluid flow phenomena in the meniscus region. The mathematical model is presented in section 5.2. In section 5.3, a moving finite element method for the solution of this problem is formulated. A numerical study of the flow pattern of the flux and steel under the influence of an electromagnetic field is given in the last section.

5.2 Mathematical Model

The field equations governing the fluid flow phenomena in the meniscus region include the continuity equation and the Navier-Stokes equations. The liquid steel and liquid flux are assumed as incompressible Newtonian fluids. Thus, the governing equations can be expressed as follows

$$u_{i,i} = 0 \quad \text{in} \quad \Omega \times \tau \tag{5.1}$$

Fac. of Grad. Studies, Mahidol Univ.

$$\rho\left(\frac{\partial u_i}{\partial t} + u_j u_{i,j}\right) + p_{,i} - (\mu(u_{i,j} + u_{j,i}))_{,j} = \rho g_i \quad \text{in} \quad \Omega \times \tau$$
 (5.2)

where $\Omega = \Omega_f \cup \Omega_s$ with Ω_f representing the flux region and Ω_s being the steel region; $\tau = [0, T]$; u and g denote respectively the fluid velocity and gravitational acceleration; the indices i, j refer to the x or z direction; p denotes the fluid pressure; ρ is the density of the fluid having different constant values in Ω_f and Ω_s ; μ denotes the fluid viscosity having different values in Ω_f and Ω_s .

In the electromagnetic continuous casting process, the electromagnetic coil is applied around the top part of the mould. The influence of electromagnetic field on the transport momentum is modelled by the addition of the electromagnetic force $\mathbf{F_{em}}$ to the momentum equations and the force is determined by

$$\mathbf{F_{em}} = \mathbf{J}_e \times \mathbf{B}.\tag{5.3}$$

As the lubrication oil or powder is a diamagnetic material [39, 63, 64], the effect of electromagnetic field on the flux region is not taken into account. Thus, the unified equations for the entire flux-steel region are as follows

$$u_{i,i} = 0 \quad \text{in} \quad \Omega \times \tau,$$
 (5.4)

$$\rho\left(\frac{\partial u_i}{\partial t} + u_j u_{i,j}\right) + \overline{p}_{,i} - (\mu(u_{i,j} + u_{j,i}))_{,j} = F_{em_i} \quad \text{in} \quad \Omega \times \tau, \tag{5.5}$$

where $\overline{p}=p-\rho gz$ and the electromagnetic force $\mathbf{F_{em}}$ is defined by

$$\mathbf{F}_{\mathbf{em}i} = \begin{cases} 0 & \text{in } \Omega_f \\ (\mathbf{J}_e \times \mathbf{B})_i & \text{in } \Omega_s \end{cases}$$
 (5.6)

Equations (5.4)-(5.5) constitute a system of three partial differential equations in terms of three coordinates and time dependent unknown functions u, v and p.

To completely define the problem, we also need to specify the boundary condition and initial condition for the velocity field of liquid flux and liquid steel. In a typical computation region as shown in Figure 5.1, we assume that the molten steel is fed to the system with inlet velocity u_s^0 , and the lubrication oil is continuously added at the top of the mould with velocity u_f^0 . The no-slip velocity condition and a pressure balance condition are imposed on the interface between flux and steel Γ_0 . On the symmetry boundary Γ_{sym} , the normal velocity \mathbf{u}_n and the derivative of tangential velocity \mathbf{u}_t are both zero.

On the nozzle wall Γ_n , the velocities of both flux and molten steel are set to zero, that is

$$\mathbf{u} = \mathbf{0}.\tag{5.7}$$

On the steel surface Γ_w , we assume that the steel is completely solidified. Thus, the solidified steel shell moves at the constant casting speed, i.e.

$$\mathbf{u} = (0, U_{cast}). \tag{5.8}$$

On the surface Γ'_w , the liquid flux moves at the same speed of the mould wall, namely

$$\mathbf{u} = (0, V). \tag{5.9}$$

where $V = A\omega cos(\omega t)$. On the exit boundary Γ_{exit} , the velocity is determined by the casting speed, i.e.

$$\mathbf{u} = (0, U_{cast}). \tag{5.10}$$

Thus, the flux and steel flow problem is governed by the following BVP:

BVP: Find u_i and p such that the field equations (5.4)-(5.5) are satisfied in the computation domain Ω and all boundary conditions are satisfied.

5.3 Moving Finite Element Formulation

Firstly, the continuity equation is weakened and replaced by

$$u_{i,i} = -\delta \overline{p},\tag{5.11}$$

where δ is a small positive number. For convenience in notation, we let

$$R = u_{i,i} + \delta \overline{p}, \tag{5.12}$$

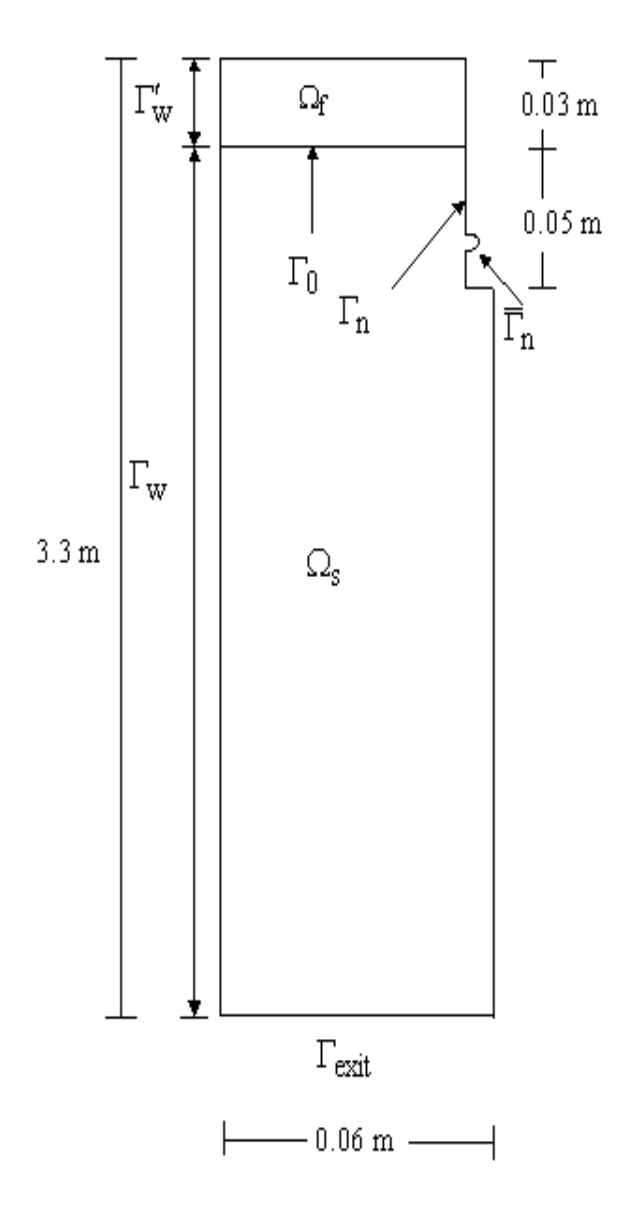


Figure 5.1: Computation domain.

$$R_{i} = \frac{\partial u_{i}}{\partial t} + u_{j}u_{i,j} + \frac{1}{\rho}\overline{p}_{,i} - (\nu(u_{i,j} + u_{j,i}))_{,j} - \frac{1}{\rho}F_{em_{i}}.$$
 (5.13)

In the moving finite element method, the mesh is allowed to deform, namely the node locations \mathbf{s}_j are assumed to be variables and are time dependent. The finite element basis functions are thus assumed to depend on s_j as well as on \mathbf{x} , i.e.,

$$\phi_i = \phi_i(\mathbf{x}, \mathbf{s}(t)), \tag{5.14}$$

where $\mathbf{s} = [\mathbf{s}_1, \mathbf{s}_2, \dots, \mathbf{s}_N]^T$ with N being the number of nodes. Thus, our finite element approximations of u_i and p are as follows

$$u_i(\mathbf{x},t) = \sum_{l=1}^{N} (u_i(t))_l \phi_l(\mathbf{x}, \mathbf{s}(t)); \qquad (5.15)$$

$$\bar{p}(\mathbf{x},t) = \sum_{l=1}^{N_p} (\bar{p}(t))_l \psi_l(\mathbf{x}, \mathbf{s}(t)). \tag{5.16}$$

Obviously, in order to determine $u(\mathbf{x},t)$ and $p(\mathbf{x},t)$, we need to determine $(u_i)_l$, p_l and $\mathbf{s}_1, \mathbf{s}_2, \dots, \mathbf{s}_N$. For this purpose, we need to construct a weak form of equations (5.4) and (5.5), respectively. The test space for equation (5.4) is chosen to be the space that p lies in. While, the test space for equation (5.5) is taken to be the space in which the function $\frac{\partial u}{\partial t}$ lies at each time instant, as proposed by Jimack for the solution of a convection-diffusion equation [65]. Now, following Jimack's work, by differentiating equation (5.15) with respect to time, we obtain

$$\frac{\partial u_i}{\partial t} = \sum_{l=1}^{N} \left[\frac{\partial u_i(t)_l}{\partial t} \phi_l + u_i(t)_l \frac{\partial \phi_l}{\partial t} \right]. \tag{5.17}$$

Differentiating equation (5.14) gives

$$\frac{\partial \phi_l}{\partial t} = (\nabla_{\mathbf{s}} \phi_l) \cdot \frac{d\mathbf{s}}{dt},\tag{5.18}$$

where $\nabla_{\mathbf{s}}$ denotes the gradient operator applied to the \mathbf{s} variable. Thus, the second term of equation (5.17) can be written as

$$\sum_{l=1}^{N} (u_i(t))_l \frac{\partial \phi_l}{\partial t} = \sum_{l=1}^{N} \dot{\mathbf{s}}_l \frac{\partial u_i}{\partial \mathbf{s}_l}$$
$$= \sum_{l=1}^{N} \dot{\mathbf{s}}_l \beta_{li}^T. \tag{5.19}$$

Thus, we obtain

$$\frac{\partial u_i}{\partial t} = \sum_{l=1}^{N} \left[\frac{\partial u_i(t)_l}{\partial t} \phi_l + \dot{\mathbf{s}}_l \cdot \beta_{li}^T \right], \tag{5.20}$$

where

$$\beta_{li} = \frac{\partial u_i}{\partial \mathbf{s}_l} = \left[\frac{\partial u_i}{\partial s_{lx}}, \frac{\partial u_i}{\partial s_{lz}} \right]^T. \tag{5.21}$$

Following Jimack (1996) [65] and Miller (1981) [66], we obtain

$$\beta_{li} = -\phi_l \nabla u_i. \tag{5.22}$$

Fac. of Grad. Studies, Mahidol Univ.

Now, in order to minimize the residual R given by (5.12) over all possible choice of p, the test space is chosen to be the space spanned by the functions

$$(\psi_1,\psi_2,\ldots,\psi_{N_p}).$$

To minimize the residual R_i given by (5.13) over all possible choice of $\frac{\partial u}{\partial t}$, the test space in two-dimensional cases is chosen, according to Jimack (1996) [65], as the space spanned by

$$\{\phi_1, (\beta_{1i})_x, (\beta_{1i})_z; \dots; \phi_N, (\beta_{Ni})_x, (\beta_{Ni})_z\},$$

where i = 1, 2. Thus, the weak forms of equations (5.12) and (5.13) could be obtained from the following formulae [67, 68],

$$(R, \psi_p) = 0,$$
 $(p = 1, 2, \dots, N_p),$ (5.23)

$$(R_i, \phi_m) = 0,$$
 $(i = 1, 2; m = 1, 2, ..., N),$ (5.24)

$$(R_1, (\beta_{m1})_k) + (R_2, (\beta_{m2})_k) = 0, \quad (k = 1, 2; m = 1, 2, \dots, N).$$
 (5.25)

where the inner product (\cdot, \cdot) is defined by equation (4.25). By substituting equations (5.15), (5.16), (5.20), and (5.22) into equations (5.23)-(5.25) and using the Green's formula, we have

$$\sum_{l=1}^{N} (\phi_{l,i}, \psi_p) u_{il} + \sum_{l=1}^{N_p} (\delta \psi_l, \psi_p) \bar{p}_l = 0,$$

$$\sum_{l=1}^{N} \left\{ (\phi_l, \phi_m) \dot{u}_{il} + \left(-\phi_l \frac{\partial u_i}{\partial x}, \phi_m \right) \dot{x}_l + \left(-\phi_l \frac{\partial u_i}{\partial z}, \phi_m \right) \dot{z}_l \right.$$

$$\left. + (u_j \phi_{l,j}, \phi_m) u_{il} + \nu(\phi_{l,j}, \phi_{m,j}) u_{il} + \nu(\phi_{l,i}, \phi_{m,j}) u_{jl} \right\}$$

$$\left. -\frac{1}{\rho} \sum_{l=1}^{N_p} \left\{ (\psi_l, \phi_{m,i}) \bar{p}_l - \rho B_p(\phi_m) \right\} = \left(\frac{1}{\rho} F_{em_i}, \phi_m \right),$$

$$\begin{split} \sum_{l=1}^{N} \left\{ \left(\phi_{l}, -\phi_{m} \frac{\partial u}{\partial x} \right) \dot{u}_{l} + \left(-\phi_{l} \frac{\partial u}{\partial x}, -\phi_{m} \frac{\partial u}{\partial x} \right) \dot{x}_{l} + \left(-\phi_{l} \frac{\partial u}{\partial z}, -\phi_{m} \frac{\partial u}{\partial x} \right) \dot{z}_{l} \right. \\ \left. + \left(u_{j} \phi_{l,j}, -\phi_{m} \frac{\partial u}{\partial x} \right) u_{l} + \nu \left(\phi_{l,j}, \left(-\phi_{m} \frac{\partial u}{\partial x} \right)_{,j} \right) u_{l} + \nu \left(\frac{\partial \phi_{l}}{\partial x}, \left(-\phi_{m} \frac{\partial u}{\partial x} \right)_{,j} \right) u_{jl} \\ \left. + \left(\phi_{l}, -\phi_{m} \frac{\partial v}{\partial x} \right) \dot{v}_{l} + \left(-\phi_{l} \frac{\partial v}{\partial x}, -\phi_{m} \frac{\partial v}{\partial x} \right) \dot{x}_{l} + \left(-\phi_{l} \frac{\partial v}{\partial z}, -\phi_{m} \frac{\partial v}{\partial x} \right) \dot{z}_{l} \\ \left. + \left(u_{j} \phi_{l,j}, -\phi_{m} \frac{\partial v}{\partial x} \right) v_{l} + \nu \left(\phi_{l,j}, \left(-\phi_{m} \frac{\partial v}{\partial x} \right)_{,j} \right) v_{l} + \nu \left(\frac{\partial \phi_{l}}{\partial z}, \left(-\phi_{m} \frac{\partial v}{\partial x} \right)_{,j} \right) u_{jl} \right\} \\ \left. - \frac{1}{\rho} \sum_{l=1}^{N_{p}} \left\{ \left(\psi_{l}, \frac{\partial}{\partial x} \left(-\phi_{m} \frac{\partial u}{\partial x} \right) \right) \bar{p}_{l} - \rho B_{p}^{1} \left(-\phi_{m} \frac{\partial u}{\partial x} \right) \\ \left. + \left(\psi_{l}, \frac{\partial}{\partial z} \left(-\phi_{m} \frac{\partial v}{\partial x} \right) \right) \bar{p}_{l} - \rho B_{p}^{2} \left(-\phi_{m} \frac{\partial v}{\partial x} \right) \right\} \\ \left. = \left(\frac{1}{\rho} F_{em_{x}}, -\phi_{m} \frac{\partial u}{\partial x} \right) + \left(\frac{1}{\rho} F_{em_{z}}, -\phi_{m} \frac{\partial v}{\partial x} \right), \end{split}$$

$$\begin{split} &\sum_{l=1}^{N} \left\{ \left(\phi_{l}, -\phi_{m} \frac{\partial u}{\partial z} \right) \dot{u}_{l} + \left(-\phi_{l} \frac{\partial u}{\partial x}, -\phi_{m} \frac{\partial u}{\partial z} \right) \dot{x}_{l} + \left(-\phi_{l} \frac{\partial u}{\partial z}, -\phi_{m} \frac{\partial u}{\partial z} \right) \dot{z}_{l} \right. \\ &\left. + \left(u_{j} \phi_{l,j}, -\phi_{m} \frac{\partial u}{\partial z} \right) u_{l} + \nu \left(\phi_{l,j}, \left(-\phi_{m} \frac{\partial u}{\partial z} \right)_{,j} \right) u_{l} + \nu \left(\frac{\partial \phi_{l}}{\partial x}, \left(-\phi_{m} \frac{\partial u}{\partial z} \right)_{,j} \right) u_{jl} \right. \\ &\left. + \left(\phi_{l}, -\phi_{m} \frac{\partial v}{\partial z} \right) \dot{v}_{l} + \left(-\phi_{l} \frac{\partial v}{\partial x}, -\phi_{m} \frac{\partial v}{\partial z} \right) \dot{x}_{l} + \left(-\phi_{l} \frac{\partial v}{\partial z}, -\phi_{m} \frac{\partial v}{\partial z} \right) \dot{z}_{l} \right. \\ &\left. + \left(u_{j} \phi_{l,j}, -\phi_{m} \frac{\partial v}{\partial z} \right) v_{l} + \nu \left(\phi_{l,j}, \left(-\phi_{m} \frac{\partial v}{\partial z} \right)_{,j} \right) v_{l} + \nu \left(\frac{\partial \phi_{l}}{\partial z}, \left(-\phi_{m} \frac{\partial v}{\partial z} \right)_{,j} \right) u_{jl} \right\} \end{split}$$

$$-\frac{1}{\rho} \sum_{l=1}^{N_p} \left\{ \left(\psi_l, \frac{\partial}{\partial x} \left(-\phi_m \frac{\partial u}{\partial z} \right) \right) \bar{p}_l - \rho B_p^{1*} \left(-\phi_m \frac{\partial u}{\partial z} \right) + \left(\psi_l, \frac{\partial}{\partial z} \left(-\phi_m \frac{\partial v}{\partial z} \right) \right) \bar{p}_l - \rho B_p^{2*} \left(-\phi_m \frac{\partial v}{\partial z} \right) \right\}$$

$$= \left(\frac{1}{\rho} F_{em_x}, -\phi_m \frac{\partial u}{\partial z} \right) + \left(\frac{1}{\rho} F_{em_z}, -\phi_m \frac{\partial v}{\partial z} \right), \quad (5.26)$$

where the boundary terms B_p , B_p^1 , B_p^2 , B_p^{1*} and B_p^{2*} are defined by

$$\begin{split} B_p(\phi_m) &= \int\limits_{\Gamma_{exit}} \frac{1}{\rho} \phi_m \psi_l \ d\Gamma \ p_l^*, \\ B_p^1 \left(-\phi_m \frac{\partial u}{\partial x} \right) &= \int\limits_{\Gamma_{exit}} \frac{1}{\rho} \left(-\phi_m \frac{\partial u}{\partial x} \right) \psi_l \ d\Gamma \ p_l^*, \\ B_p^2 \left(-\phi_m \frac{\partial v}{\partial x} \right) &= \int\limits_{\Gamma_{exit}} \frac{1}{\rho} \left(-\phi_m \frac{\partial v}{\partial x} \right) \psi_l \ d\Gamma \ p_l^*, \\ B_p^{1*} \left(-\phi_m \frac{\partial u}{\partial z} \right) &= \int\limits_{\Gamma_{exit}} \frac{1}{\rho} \left(-\phi_m \frac{\partial u}{\partial z} \right) \psi_l \ d\Gamma \ p_l^*, \\ B_p^{2*} \left(-\phi_m \frac{\partial v}{\partial z} \right) &= \int\limits_{\Gamma_{exit}} \frac{1}{\rho} \left(-\phi_m \frac{\partial v}{\partial z} \right) \psi_l \ d\Gamma \ p_l^*. \end{split}$$

Following equations $(5.26)_3$ and $(5.26)_4$, we have

$$\nu \left(\phi_{l,j}, \left(-\phi_m \frac{\partial u}{\partial x} \right)_{,j} \right) u_l + \nu \left(\frac{\partial \phi_l}{\partial x}, \left(-\phi_m \frac{\partial u}{\partial x} \right)_{,j} \right) u_{jl}$$

$$+ \nu \left(\phi_{l,j}, \left(-\phi_m \frac{\partial v}{\partial x} \right)_{,j} \right) v_l + \nu \left(\frac{\partial \phi_l}{\partial z}, \left(-\phi_m \frac{\partial v}{\partial x} \right)_{,j} \right) u_{jl}$$

$$= \left\{ -\nu \left(\frac{\partial \phi_{l}}{\partial x}, \frac{\partial u}{\partial x} \frac{\partial \phi_{m}}{\partial x} \right) + \frac{1}{2}\nu \left(\frac{\partial \phi_{l}}{\partial z}, \frac{\partial u}{\partial z} \frac{\partial \phi_{m}}{\partial x} \right) - \nu \left(\frac{\partial \phi_{l}}{\partial z}, \frac{\partial u}{\partial x} \frac{\partial \phi_{m}}{\partial z} \right) \right\} u_{l}$$

$$+ \left\{ -\frac{1}{2}\nu \left(\frac{\partial \phi_{l}}{\partial x}, \frac{\partial v}{\partial x} \frac{\partial \phi_{m}}{\partial x} \right) + \nu \left(\frac{\partial \phi_{l}}{\partial z}, \frac{\partial v}{\partial z} \frac{\partial \phi_{m}}{\partial x} \right) - 2\nu \left(\frac{\partial \phi_{l}}{\partial z}, \frac{\partial v}{\partial x} \frac{\partial \phi_{m}}{\partial z} \right) - \nu \left(\frac{\partial \phi_{l}}{\partial x}, \frac{\partial u}{\partial x} \frac{\partial \phi_{m}}{\partial z} \right) \right\} v_{l},$$

$$(5.27)$$

$$\left(\psi_{l}, \frac{\partial}{\partial x} \left(-\phi_{m} \frac{\partial u}{\partial x}\right)\right) \bar{p}_{l} + \left(\psi_{l}, \frac{\partial}{\partial z} \left(-\phi_{m} \frac{\partial v}{\partial z}\right)\right) \bar{p}_{l}$$

$$= \left(\frac{\partial \psi_{l}}{\partial x}, -\phi_{m} \frac{\partial u}{\partial x}\right) \bar{p}_{l} + \left(\frac{\partial \psi_{l}}{\partial z}, -\phi_{m} \frac{\partial v}{\partial x}\right) \bar{p}_{l}, \qquad (5.28)$$

$$\nu\left(\phi_{l,j}, \left(-\phi_m \frac{\partial u}{\partial z}\right)_{,j}\right) u_l + \nu\left(\frac{\partial \phi_l}{\partial x}, \left(-\phi_m \frac{\partial u}{\partial z}\right)_{,j}\right) u_{jl}$$
$$+\nu\left(\phi_{l,j}, \left(-\phi_m \frac{\partial v}{\partial z}\right)_{,j}\right) v_l + \nu\left(\frac{\partial \phi_l}{\partial z}, \left(-\phi_m \frac{\partial v}{\partial z}\right)_{,j}\right) u_{jl}$$

$$= \left\{ \nu \left(\frac{\partial \phi_{l}}{\partial x}, \frac{\partial u}{\partial x} \frac{\partial \phi_{m}}{\partial z} \right) - 2\nu \left(\frac{\partial \phi_{l}}{\partial x}, \frac{\partial u}{\partial z} \frac{\partial \phi_{m}}{\partial x} \right) - \frac{1}{2} \nu \left(\frac{\partial \phi_{l}}{\partial z}, \frac{\partial u}{\partial z} \frac{\partial \phi_{m}}{\partial z} \right) - \nu \left(\frac{\partial \phi_{l}}{\partial z}, \frac{\partial v}{\partial z} \frac{\partial \phi_{m}}{\partial x} \right) \right\} u_{l}$$

$$+ \left\{ \frac{1}{2} \nu \left(\frac{\partial \phi_{l}}{\partial x}, \frac{\partial v}{\partial x} \frac{\partial \phi_{m}}{\partial z} \right) - \nu \left(\frac{\partial \phi_{l}}{\partial x}, \frac{\partial v}{\partial z} \frac{\partial \phi_{m}}{\partial x} \right) - \nu \left(\frac{\partial \phi_{l}}{\partial z}, \frac{\partial v}{\partial z} \frac{\partial \phi_{m}}{\partial z} \right) \right\} v_{l}, \quad (5.29)$$

$$\left(\psi_{l}, \frac{\partial}{\partial x} \left(-\phi_{m} \frac{\partial u}{\partial z}\right)\right) \bar{p}_{l} + \left(\psi_{l}, \frac{\partial}{\partial z} \left(-\phi_{m} \frac{\partial v}{\partial z}\right)\right) \bar{p}_{l}$$

$$= \left(\frac{\partial \psi_{l}}{\partial x}, -\phi_{m} \frac{\partial u}{\partial z}\right) \bar{p}_{l} + \left(\frac{\partial \psi_{l}}{\partial z}, -\phi_{m} \frac{\partial v}{\partial z}\right) \bar{p}_{l}. \tag{5.30}$$

Fac. of Grad. Studies, Mahidol Univ.

for m = 1, 2, 3, ..., N and $p = 1, 2, 3, ..., N_p$. The system of equations (5.26) can be expressed in matrix form as

$$C\mathbf{u} + \delta C_p \mathbf{p} = 0, \tag{5.31}$$

$$E\dot{\mathbf{u}} + E_1\dot{\mathbf{s}} + (A + D_u)\mathbf{u} + C_1\mathbf{p} = \mathbf{F}_1, \tag{5.32}$$

$$E_2\dot{\mathbf{u}} + E_s\dot{\mathbf{s}} + (A^* + D_u^*)\mathbf{u} + C_2\mathbf{p} = \mathbf{F}_2, \tag{5.33}$$

where the coefficient matrices are given by

$$C_p = ((c_p)_{lm})_{N_p \times N_p}$$
 with $(c_p)_{lm} = \int_{\Omega} \psi_l \psi_m \, d\Omega$,

$$C = \begin{bmatrix} c_{lm}^1 \\ c_{lm}^2 \end{bmatrix}_{2N \times N_p}^T \quad \text{with} \quad c_{lm}^k = \int_{\Omega} \frac{\partial \phi_l}{\partial x_k} \psi_m \, d\Omega \quad (k = 1, 2),$$

$$C_1 = \frac{1}{\rho} \begin{bmatrix} \bar{c}_{lm} - c_{lm}^1 \\ \\ \bar{c}_{lm} - c_{lm}^2 \end{bmatrix}_{2N \times N_n} \text{ with } \bar{c}_{lm} = \int_{\Gamma_{exit}} \phi_l \psi_m \, d\Gamma,$$

$$C_{2} = \frac{1}{\rho} \begin{bmatrix} -\frac{\partial u}{\partial x} c_{lm}^{*1} - \frac{\partial v}{\partial x} c_{lm}^{*2} - (\frac{\partial u}{\partial x} + \frac{\partial v}{\partial x}) \bar{c}_{lm} \\ -\frac{\partial u}{\partial z} c_{lm}^{*1} - \frac{\partial v}{\partial z} c_{lm}^{*2} - (\frac{\partial u}{\partial z} + \frac{\partial v}{\partial z}) \bar{c}_{lm} \end{bmatrix}_{2N \times N_{p}} \text{ with } \bar{c}_{lm}^{*k} = \int_{\Omega} \frac{\partial \psi_{m}}{\partial x_{k}} \phi_{l} d\Omega(k = 1, 2),$$

$$E = \begin{bmatrix} e_{lm} & 0 \\ & & \\ 0 & e_{lm} \end{bmatrix}_{2N \times 2N} \quad \text{with} \quad e_{lm} = \int_{\Omega} \phi_l \phi_m \, d\Omega,$$

$$E_{1} = \begin{bmatrix} -\frac{\partial u}{\partial x}e_{lm} & -\frac{\partial u}{\partial z}e_{lm} \\ -\frac{\partial v}{\partial x}e_{lm} & -\frac{\partial v}{\partial z}e_{lm} \end{bmatrix}_{2N\times2N}$$

$$E_{2} = \begin{bmatrix} -\frac{\partial u}{\partial x}e_{lm} & -\frac{\partial v}{\partial x}e_{lm} \\ -\frac{\partial u}{\partial z}e_{lm} & -\frac{\partial v}{\partial z}e_{lm} \end{bmatrix}_{2N\times2N}$$

$$E_{s} = \begin{bmatrix} \left[(\frac{\partial u}{\partial x})^{2} + (\frac{\partial v}{\partial x})^{2} \right]e_{lm} & \left(\frac{\partial u}{\partial x}\frac{\partial u}{\partial z} + \frac{\partial v}{\partial x}\frac{\partial v}{\partial z} \right)e_{lm} \\ (\frac{\partial u}{\partial x}\frac{\partial u}{\partial z} + \frac{\partial v}{\partial x}\frac{\partial v}{\partial z})e_{lm} & \left[(\frac{\partial u}{\partial z})^{2} + (\frac{\partial v}{\partial z})^{2} \right]e_{lm} \end{bmatrix}_{2N\times2N}$$

$$A = \begin{bmatrix} a_{lm} & 0 \\ & & \\ 0 & a_{lm} \end{bmatrix}_{2N \times 2N} \quad \text{with} \quad a_{lm} = \int_{\Omega} \phi_l (u_x \frac{\partial \phi_m}{\partial x} + u_z \frac{\partial \phi_m}{\partial z}) d\Omega,$$

$$A^* = \begin{bmatrix} -\frac{\partial u}{\partial x} a_{lm} & -\frac{\partial v}{\partial x} a_{lm} \\ \\ -\frac{\partial u}{\partial z} a_{lm} & -\frac{\partial v}{\partial z} a_{lm} \end{bmatrix}_{2N \times 2N}$$

$$D_{u} = \begin{bmatrix} 2d_{lm}^{11} + d_{lm}^{22} & d_{lm}^{12} \\ & & \\ d_{lm}^{21} & d_{lm}^{11} + 2d_{lm}^{22} \end{bmatrix}_{2N \times 2N} \text{ with } d_{lm}^{kj} = \int_{\Omega} \nu \frac{\partial \phi_{l}}{\partial x_{k}} \frac{\partial \phi_{m}}{\partial x_{j}} d\Omega \ (k, j = 1, 2),$$

$$D_{u}^{*} = \begin{bmatrix} d_{11}^{*} & d_{12}^{*} \\ d_{11}^{*} & d_{12}^{*} \\ d_{21}^{*} & d_{22}^{*} \end{bmatrix}_{2N \times 2N}$$

$$d_{11}^{*} = -\frac{\partial u}{\partial x} d_{lm}^{11} - \frac{\partial u}{\partial x} d_{lm}^{22} + \frac{1}{2} \frac{\partial u}{\partial z} d_{lm}^{21},$$

$$d_{12}^{*} = -\frac{1}{2} \frac{\partial v}{\partial x} d_{lm}^{11} - 2 \frac{\partial v}{\partial x} d_{lm}^{21} - \frac{\partial u}{\partial x} d_{lm}^{12} + \frac{\partial v}{\partial z} d_{lm}^{21},$$

$$d_{21}^{*} = -2 \frac{\partial u}{\partial z} d_{lm}^{11} - \frac{1}{2} \frac{\partial u}{\partial z} d_{lm}^{22} + \frac{\partial u}{\partial x} d_{lm}^{12} - \frac{\partial v}{\partial z} d_{lm}^{21},$$

$$d_{22}^{*} = -\frac{\partial v}{\partial z} d_{lm}^{11} - \frac{\partial v}{\partial z} d_{lm}^{22} + \frac{1}{2} \frac{\partial v}{\partial x} d_{lm}^{12},$$

$$F_1 = \begin{bmatrix} f_l^1 \\ \\ f_l^2 \end{bmatrix}_{2N \times 1} \qquad f_l^1 = \int_{\Omega} \frac{1}{\rho} (F_{em})_x \phi_l \, d\Omega,$$
 with
$$f_l^2 = \int_{\Omega} \frac{1}{\rho} (F_{em})_z \phi_l \, d\Omega,$$

$$\begin{bmatrix}
f_{l}^{2} \\
\end{bmatrix}_{2N \times 1} \qquad f_{l}^{2} = \int_{\Omega} \frac{1}{\rho} (F_{em})_{z} \phi_{l} d\Omega,$$

$$F_{2} = \begin{bmatrix}
f_{l1}^{1} + f_{l2}^{1} \\
f_{l1}^{2} + f_{l2}^{2}
\end{bmatrix}_{2N \times 1} \qquad \text{with} \qquad f_{lk}^{m} = \int_{\Omega} \frac{1}{\rho} (-\frac{\partial u_{k}}{\partial x_{j}}) (F_{em})_{k} \phi_{l} d\Omega \quad (k, j = 1, 2),$$

$$(5.34)$$

Further, the system of equations (5.31)-(5.33) can be rewritten as

$$C\mathbf{u} + \delta C_p \mathbf{p} = 0, \tag{5.35}$$

$$E\dot{\mathbf{u}} + E_1\dot{\mathbf{s}} + K_1\mathbf{u} + C_1\mathbf{p} = \mathbf{F}_1, \tag{5.36}$$

$$E_2\dot{\mathbf{u}} + E_s\dot{\mathbf{s}} + K_2\mathbf{u} + C_2\mathbf{p} = \mathbf{F}_2, \tag{5.37}$$

where K_1 and K_2 are defined in equations (5.32) and (5.33). From equation (5.31), we may determine the pressure \mathbf{p} by

$$\mathbf{p} = -\frac{1}{\delta} C_p^{-1} C \mathbf{u}. \tag{5.38}$$

By substituting equation (5.38) into equations (5.32) and (5.33), we obtain a new system of equations (5.39) and (5.40) for \mathbf{u} and \mathbf{s}

$$E\dot{\mathbf{u}} + E_1\dot{\mathbf{s}} + K_1\mathbf{u} - \frac{1}{\delta}C_1C_p^{-1}C\mathbf{u} = \mathbf{F}_1, \tag{5.39}$$

$$E_2 \dot{\mathbf{u}} + E_s \dot{\mathbf{s}} + K_2 \mathbf{u} - \frac{1}{\delta} C_2 C_p^{-1} C \mathbf{u} = \mathbf{F}_2, \tag{5.40}$$

which can be expressed in shorter form as

$$A(\mathbf{Y})\dot{\mathbf{Y}} = \mathbf{G},\tag{5.41}$$

where $\mathbf{Y} = [u_1, v_1, x_1, z_1; \dots; u_N, v_N, x_N, z_N]^T$ in which (u_l, v_l) denotes the velocity at the l^{th} node located at (x_l, z_l) .

The above nonlinear system (5.41) can be solved by using Euler's backward difference scheme with variable time step. Let \mathbf{Y}_n be the solution and Δt_n be the time increment at time step n, we have

$$A(\mathbf{Y}_{n+1})(\mathbf{Y}_{n+1} - \mathbf{Y}_n) = \mathbf{G}_{n+1} \triangle t_n. \tag{5.42}$$

The iterative solution of the system (5.43) at iteration i is defined by

$$A(\mathbf{Y}_{n+1}^{i})(\mathbf{Y}_{n+1}^{i+1} - \mathbf{Y}_{n}) = \mathbf{G}_{n+1}^{i} \triangle t_{n}.$$
 (5.43)

5.4 Numerical Studies

A computer program based on the algorithm presented in the previous section is developed for the solution of the two-phase flow in the continuous casting process. A numerical investigation has been undertaken to analyze the effect of electromagnetic field on the flow pattern. In this study, the computational domain is the square billet which has a mould half width of 0.06 meters and a depth of 0.8 meters. Since the mould is symmetrical about two planes which pass through the central line of the mould, the computation region could be limited to one quadrant and its boundary consists of several parts as shown in Figure 5.1. The casting parameters and the computational schemes for investigating the effect of electromagnetic field are shown in Table 5.1 and Table 5.2, respectively. The finite element mesh consists of 1324 elements and 1410 nodes as shown in Figure 5.2.

The results for flux flow and steel flow at the meniscus region in the continuous casting process are given in Figures 5.3 and 5.4. Figure 5.3(a) presents liquid flux flow and steel flow for the model without source current.

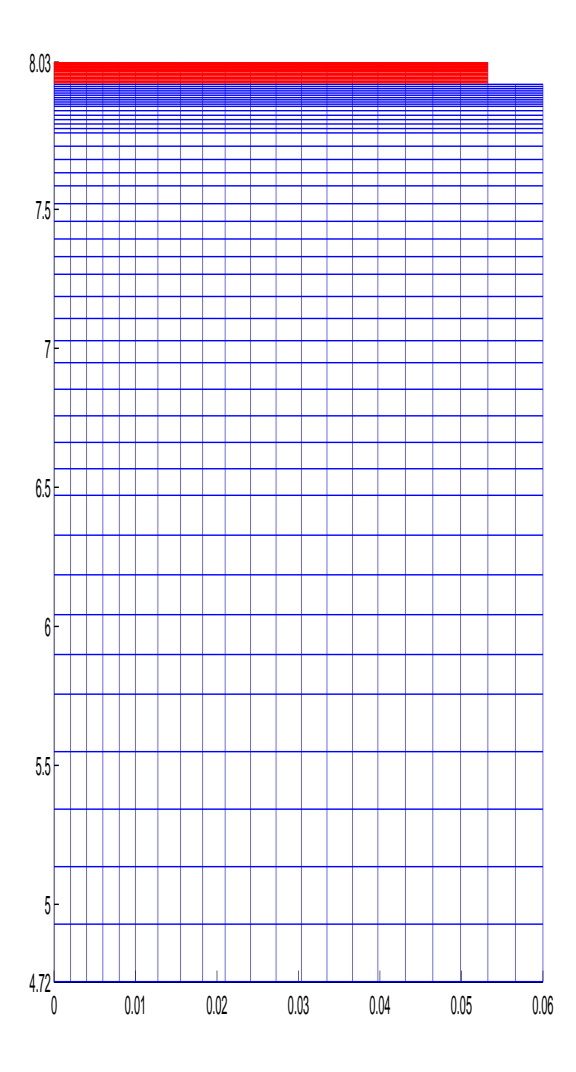


Figure 5.2: Generating mesh for flux and steel.

There is a recirculation zone at the center of flux region. We also investigated the effect of source current on the flow patterns of liquid flux and steel. The results as shown in Figure 5.4 (a), (b) and (c) present the flow pattern of liquid flux labelled by black color and liquid steel labelled by red color. It is noted that no circulation zone occurs in the flux region for the model with source current. Larger magnitude of source current produces higher speed upward velocities of liquid flux and steel near the meniscus region.

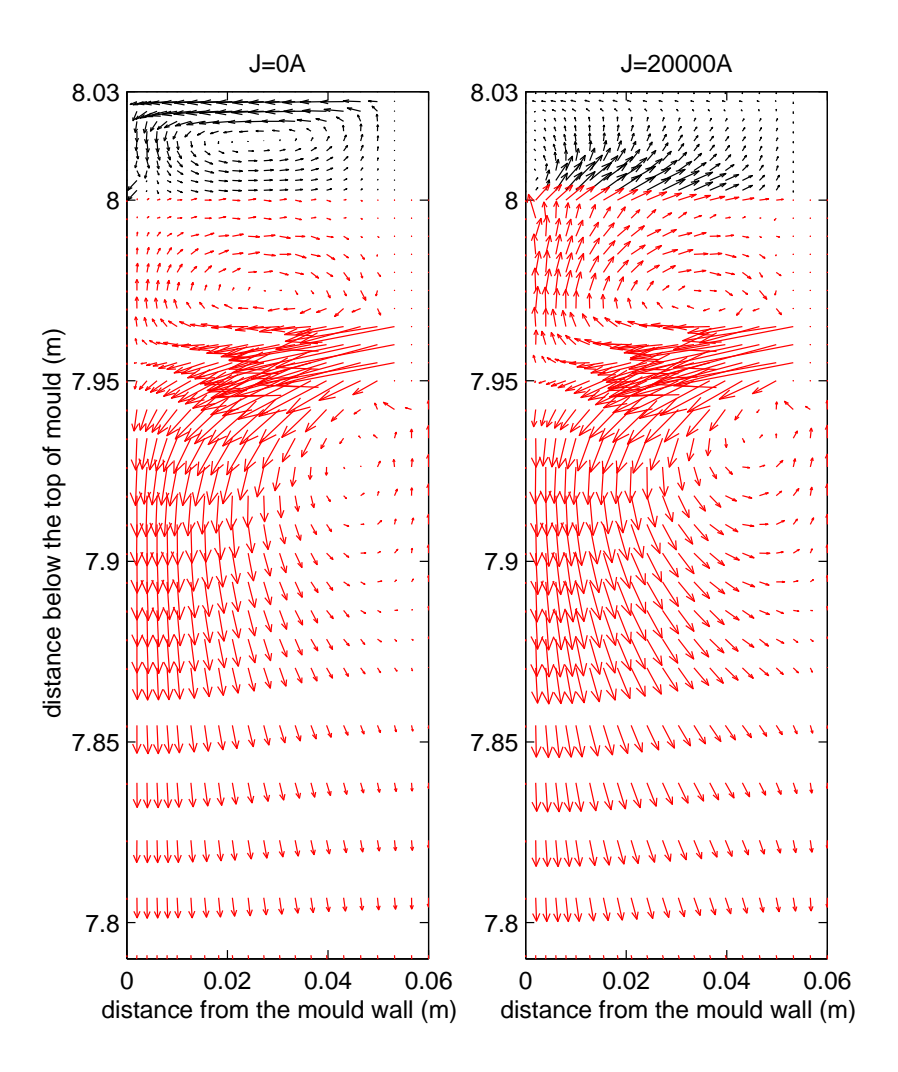


Figure 5.3: Flow patterns of liquid flux (labelled by black color) and liquid steel (labelled by red color) in (a) conventional casting process and (b) EM casting process.

5.5 Concluding Remarks

An efficient mathematical model and a numerical algorithm, based on a moving finite element formulation, has been developed to study the coupled flux flow and steel flow in the meniscus region. The results obtained from this section could be used as an initial solution for the determination the meniscus shape.

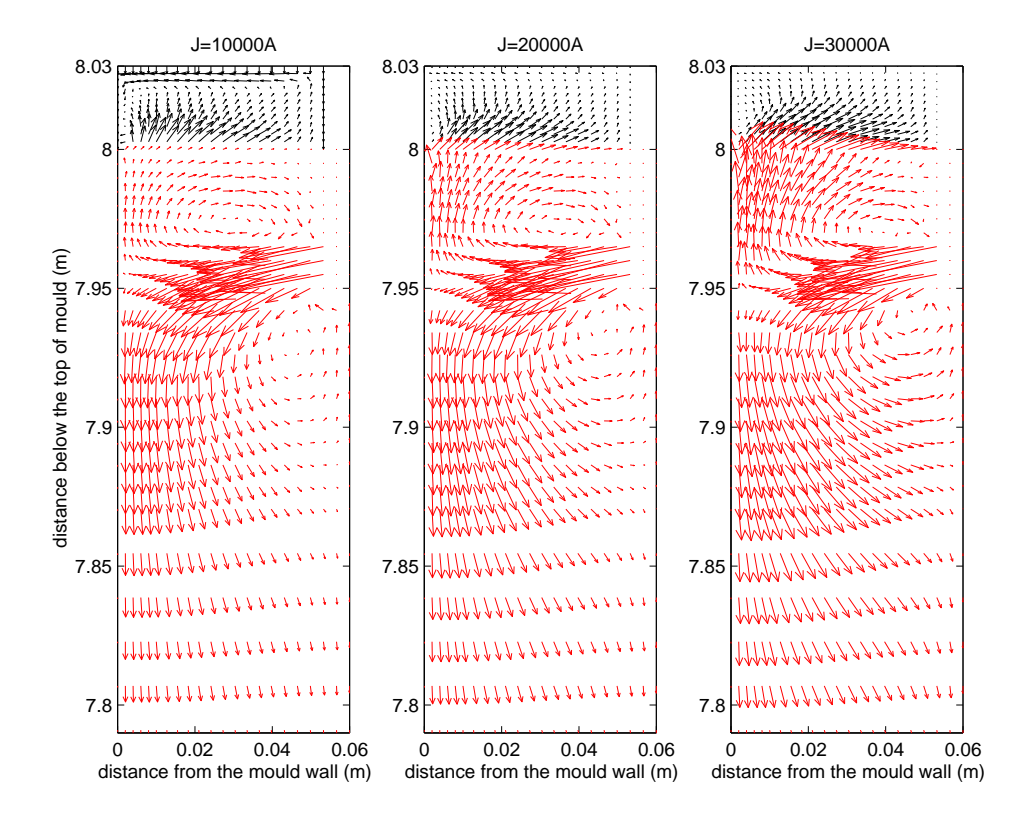


Figure 5.4: Flow patterns of liquid flux (labelled by black color) and liquid steel (labelled by red color) for different source currents (a) 10000 A (b) 20000 A and (c) 30000 A.

Table 5.1: Parameters used in numerical simulation

Parameter	symbol	Value	Unit
Density of flux	$ ho_f$	2930	kg/m^3
Viscosity of flux	μ_f	0.5	$pa \cdot s$
Density of steel	$ ho_s$	7800	kg/m^3
Viscosity of steel	μ_s	0.001	$pa \cdot s$
Casting speed	U_{cast}	0.032	m/s
Nozzle port angle	_	30 down	degree
Velocity of mould wall	V	$A\omega\cos(\omega t)$	m/s
Angular frequency of mould oscillation	ω	$30*\left(\frac{2\pi}{60}\right)$	rad/s

Table 5.2: Computation schemes

Scheme	Source Current	
	(Ampere)	
1	10000	
2	20000	
3	30000	
4	0	

CHAPTER 6

SUMMARY AND CONCLUSIONS

6.1 Concluding Remarks

This research focused on the development of mathematical models and numerical techniques for study of fluid flow, multi-phase heat transfer and electromagnetic stirring in the electromagnetic continuous casting process. The results achieved and gained from the research are summarized as follows,

- 1. A finite element method has been developed for the solution of the two-dimensional electromagnetic problem in the electromagnetic continuous casting process. A commercial package FEMLAB is used to calculate the electromagnetic field, the induced current and the electromagnetic force. The effect of magnetic frequency and source current on electromagnetic force have been investigated. Some conclusions from the numerical studies are as follows
 - (a) The frequency of magnetic field has a significant effect on the electromagnetic force. With a higher frequency of magnetic field, the electromagnetic force increases.
 - (b) The electromagnetic force occurring in the mould is strongly governed by the source current. With an increase of source current, the electromagnetic force increases.
- 2. A finite element method is used to solve the two-dimensional coupled fluid flow and heat transfer with solidification problem in the electromagnetic continuous casting process. The mathematical models with and without the effect of electromagnetic force have been established and implemented numerical in computers. The effects of electromagnetic field on the flow field

and the solidification of steel have been investigated. The results obtained by both models are compared, and it is found that the electromagnetic force has significant influences on the flow field and temperature field in the continuous casting process. From the numerical studies, it can be concluded that the source current has a significant effect on the flow field and solidification of steel in the electromagnetic continuous casting process. With increasing the source current, the recirculation flow occurred in the mould moves far away from the mould wall and the thickness of the solidification steel shell increases.

3. A two-phase flow model for the meniscus region and a corresponding numerical technique were developed based on the moving finite element method. The effect of turbulence is not taken into account in the model. The simulated results from the model clearly show the flow pattern of flux and steel in the continuous casting process. In the lubrication oil domain at the top part of the mould, a recirculation flow zone occurs due to the effect of steel flow. The meniscus shape could be roughly determined.

6.2 Further Works

In this work, a robust two-dimensional model was developed to study the coupled fluid flow and heat transfer with solidification occurring in the electromagnetic continuous steel casting. However, in the real world problem, the mechanism of the continuous casting process is three dimensional in nature. Thus, it is useful to undertake further work to develop three dimensional mathematical model for the electromagnetic continuous casting process.

REFERENCES

- [1] Thailand Iron and Steel Industry Club (TISIC). 1995. p. 15-32.
- [2] Irving WR. Continuous casting of steel. The institute of materials 1993.
- [3] Wiwatanapataphee, B. Mathematical model of fluid flow and heat transfer in continuous steel casting process. Ph.D. Thesis, School of Mathematics. Perth, Curtin University of Technology 1998:168.
- [4] Wiwatanapataphee B, Wu YH, Archapitak J, Siew PF and Unyong B. A numerical study of the turbulent flow of molten steel in a domain with a phase-change boundary. J Comput Appl Math 2004;116:307-319.
- [5] Natarajan TT, Kaddah NE. Finite element analysis of electromagnetically driven flow in sub-mold stirring of steel billets and slabs. ISIJ Int 1998;38(7):680-9.
- [6] Birat JP and Chonè J. Electromagnetic stirring on billet, bloom, and slab continuous casters: state of the art in 1982. Ironmaking Steelmaking 1983;10(6):269-81.
- [7] Nakata H, Inoue T, Mori H, Ayata K, Murakami T, Kominami T, Improvement of billet surface quality by ultra-high-frequency electromagnetic casting. ISIJ Int 2002;42:264-72.
- [8] Toh T, Takeuchi E, Hojo M, Kawai H, and Matsumura S. Electromagnetic control of initial solidification in continuous casting of steel by low frequency alternating magnetic field. ISIJ Int 1997;37(11):1112-9.
- [9] Miyoshino I, Takeuchi E, Yano H, Sakane J, Saeki T, Kajioka H, Influence of electromagnetic pressure on the early solidification in a continuous casting mold. ISIJ Int 1989;29:1040-7.

[10] Thomas BG, Zhang L. Mathematical modeling of fluid flow in continuous casting ISIJ Int 2001;41(10):1181-93.

- [11] Yokoya S, Takagi S, Iguchi M, Asako Y, Westoff R, Hara S. Swirling effect in immersion nozzle on flow and heat transport in billet continuous casting mold. ISIJ Int 1998;38(8):827-33.
- [12] Yokoya S, Westoff R, Asako Y, Hara S, Szekely J. Numerical study of immersion nozzle outlet flow pattern with swirling flow in continuous casting. ISIJ Int 1994, 34(11):889-95.
- [13] Henkes RAWM, Hoogendoorm CJ. Comparison of turbulence models for natural convection boundary layer along a heated vertical plate. Int J Heat Mass Transfer 1989;32(1):157-69.
- [14] Li BQ. Numerical simulation of flow and temperature evolution during the initial phase of steady-state solidification. J Mater Process Tech 1997;71:402-13.
- [15] Yang H, Zhao L, Zhang H, Deng K, Li W, and Gan Y. Mathematical simulation on coupled flow, heat, and solute transport in slab continuous casting process. Metall Mater Trans B 1998;29B:1345-56.
- [16] Lee JE, Han HN, Oh KH, Yoon JK. A fully coupled analysis of fluid flow, heat transfer and stress in continuous round billet casting. ISIJ Int 1999;39(5):435-44.
- [17] Takatani K, Tanizawa Y, Mizukami H and Nishimura K. Mathematical Model for transient fluid flow in a continuous casting mold ISIJ Int 2001;41(10):1252-61.
- [18] Thomas BG, Yuan Q, Sivaramakrishnan S, Shi T, Vanka SP and ASSAR MB. Comparison of four methods to evaluate fluid velocities in continuous slab casting mold ISIJ Int 2002;41(10):1262-71.

- [19] Garnier, M. Electromagnetic processing of liquid materials in Europe. ISIJ Int 1990;30(1):1-7.
- [20] Kolesnichenko AF. Electromagnetic processes in liquid material in the USSR and East European countries. ISIJ Int 1990;30(1):8-26.
- [21] Nakanishi K. Japanese state of the art continuous casting process. ISIJ Int 1996;36(Supplement):S14-7.
- [22] Makarov S, Ludwig R and Apelian D. Electromagnetic separation techniques in metal casting I. Conventional methods. IEEE T Magn 2000;36(4):2015-21.
- [23] Trindade LB, Vilela ACF, Filho AFF, Vilhena MTMB and Soares RB. Numerical model of electromagnetic stirring for continuous casting billets. IEEE T Magn 2002;38(6):3658-60.
- [24] Na X, Zhang X and Gan Y. Mathematical analysis and mumerical simulation of high frequency electromagnetic field in soft contact continuous casting mold. ISIJ Int 2002;42(9):974-81.
- [25] Genma N, Soejima T, Saito T, Masayasu K, Kaihara Y, Hirohiko F, et al. The linear-motor type in-mold electromagnetic stirring technique for the slab continuous caster. ISIJ Int 1989, 29(12): 1056 - 1062.
- [26] Trophime C, Masse P and Etay J. MHD3D: A numerical code for the strong coupling in magnetohydrodynamic application to an EM stirrer. IEEE T Magn 1996;32(3):1006-9.
- [27] Fujisaki K and Ueyama T. Magnetohydrodynamic calculation of In-Mold electromagnetic stirring. IEEE T Magn 1997;33(2).
- [28] Fujisaki K, Ueyama T, Toh T, Uehara M and Kobayashi S. Magnetohydrodynamic calculation for electromagnetic stirring of molten metal. IEEE T Magn 1998;34(4).

[29] Li BQ. Solidification processing of materials in magnetic fields 1998. Availabe from: http://www.tms.org/pubs/journals/JOM/9802.html.

- [30] Dumont B and Gagnoud A. 3-D finite element method with impedance boundary condition for the modeling of molten metal shape in electromagnetic casting. IEEE T Magn 2000;36(4).
- [31] Fujisaki K. Consideration of heat transfer and solidification in 3-D MHD calculation. IEEE T Magn 2000;36(4):1300-04.
- [32] Li B, Okane T and Umeda T. Modeling of molten metal flow in a continuous casting process considering the effects of argon gas injection and static magnetic field application. Metall Mater Trans B 2000;31(6):1491-530.
- [33] Park HS, Nam H and Yoon JK. Numerical analysis of fluid flow and heat transfer in parallel type mold of a thin slab caster. ISIJ Int 2001;41(9):974-80.
- [34] Park J, Jeong H, Kim H and Kim J. Laboratory scale continuous casting of steel billet with high frequency magnetic field. ISIJ Int 2002;42(4):385-91.
- [35] Kim H, Park JP, Jeong H and Kim J. Continuous casting of billet with high frequency electromagnetic field. ISIJ Int 2002;42(2):171-7.
- [36] McDavid RM, Thomas BG. Flow and Thermal behavior of the top surface flux/powder layers in continuous casting molds. Metall Mater Trans B 1996;27B:672-85.
- [37] Nakano T, Fuji M, Nagano K, Matsuyama T and Masuo N. Model analysis of melting process of mold powder for continuous casting of steel. Technical Report, Nippon Steel Technical Report 1987;34(7):21-30.
- [38] Nakata H and Etay J. Meniscus shape of molten steel under alternating magnetic field. ISIJ Int 1992;32(4):521-8.

- [39] Li T, Nagaya S, Sassa K, and Asai S. Study of meniscus behavior and surface properties during casting in a high-frequency magnetic field. Metall Mater Trans B 1995;26B:353-9.
- [40] Lucus T. Optimisaion of steel flow in moulds. CFX Update Autumn 1998 Available from:http://www-waterloo.ansys.com/cfx/pdf/pdf0295.pdf.
- [41] Thomas BG. Continuous Casting: Modeling. The encyclopedia of advanced materials 2. 2001.
- [42] Sha H, Diedrichs R and Schwerdtfeger K. Dynamic behavior of a liquid/liquid interface at an oscillating wall. Metall Mater Trans B 1996;27B:305-14.
- [43] FEMLAB electromagnetic module Version 2.3 (2002)
- [44] Aboutalebi MR, Amano S, Guthric RIL. Coupled turbulent flow heat and solute transport in continuous casting process. Metall Mater Trans B 1995;26B:731-44.
- [45] Launder BE. On the computation of convective heat transfer in complex turbulent flows. ASME J Heat Transfer 1998;110:1112-28.
- [46] Reddy MP and Reddy JN. Numerical simulation for forming processes using a coupled fluid flow and heat transfer model. Internat J Numer Methods Eng 1992;35(5):1229-45.
- [47] Prandtl L. Uber ein neues formelsystem fur die ausgebildete turbulenz (On a new formation for the fully developed turbulence). Nachr Akad Wiss (Report of Academy of Sciences) Gottingen, Germany 1945.
- [48] Kolmogonov AN. Equations of turbulent motion of incompressible fluid. IZV Akad Nauk USSR Ser Phys 1942;6:56-8 (translated into English by Spalding DB, as Imperial College, Mechanical Engineering Department Report ON/6, 1968, London, U.K.)

- [49] Harlow FH and Nakayama PI. Turbulence transport equations. Phys Fluids 1967;10(11):2323-8.
- [50] Launder DB, Spalding DB. The numerical computation of turbulent flows. Comput Methods Appl Mech Eng 1974:269-89.
- [51] Lumley JL. Turbulence modelling. J Appl Maths 1983;50:1097-103.
- [52] Saffman PG A model for inhomogeneous turbulen flow. Proc Royal Soc London A317:417-33.
- [53] Rodi W and Spalding DB. A two-parameter model of turbulence and its application to free jets. Warme-und Stofubertragung 1970;3(2):85-95.
- [54] Ferziger JH. Simulation of incompressible turbulent flows. Comput Phys 1987;69:1-48.
- [55] Jaeger M and Dhatt G. An extended $k \varepsilon$ dinite element model. J Numer Methods Fluids 1992, 14:1325-45.
- [56] Jones WP and Launder BE. The calculation of low-Reynolds number phenomena with a two-equation model of turbulence. Internat J Heat Mass Transfer 1973, 16:1113-9.
- [57] Wu YH, Hill JM and Flint PJ. A noval finite element method for heat transfer in the continuous caster. Austral Math Soc Serie B, 35:263-88.
- [58] Nakano T, Kishi T, Koyama K, Komai T and Naitoh S. Trans Iron Steel Inst Jpn 1984;24(11):950-6.
- [59] Anzai E, Ando T, Shigezumi T, Ikeda M, and Nakano T. Hydrodynamic behavior of molten powder in meniscus zone of continuous casting mold. Nippon Steel Technical Report 1987;34(7):31-40.
- [60] Bommaraju R and Saad E. Steelmaking Conf Proc ISS-AIME, Warrendale, PA 1990;73:281-96.

- [61] Sardemann J and schrewe H. Steelmaking Conf Proc ISS-AIME, Warrendale, PA 1991;74:719-29.
- [62] Nakato H, Takeuchi S, Fujii T, Nozaki T, Washio M. Steelmaking Conf Proc. ISS-AIME, Warrendale, PA 1991;74:639-46.
- [63] Li T, Sassa K, and Asai S. Surface Quality Improvement of Continuously Cast Metals by Imposing Intermittent High Frequency Magnetic Field and Synchronizing the Field with Mold Oscillation. ISIJ Int 1996;36(4):410-6.
- [64] Kawamoto M, Tsukaguchi Y, Nishida N, Kanazawa T and Hiraki S. Improvement of the initial stage of solidification by using mild cooling mold powder. ISIJ Int 1997;37(2):134-9.
- [65] Jimack PK. A best approximation property of the moving finite element method. Siam J Numer 1996;33(6):2286-302.
- [66] Miller K and Miller RN. Moving finite elements I Siam J Numer Anal 1981;18(6)
- [67] Gelinas RJ, Doss SK and Miller K. The moving finite element method:Applications to general partial differential equations with multiple large gradients. J Comput Phys 1981;40:202-49.
- [68] Miller MJ. Moving finite elements. Clarendon Press 1994.

APPENDIX

ACCEPTED PAPERS FOR PUBLICATION

- 1. A moving finite element method for simulating the flow of molten steel and flux in the continuous casting process, , Computational Mathematics and Modeling, special volume of the East-West Journal of Mathematics, published in 2003.
- 2. A finite element scheme for the determination of electromagnetic force in continuous steel casting, International Journal of Computational and Numerical Analysis and Applications, in press, (accepted in May 2004)

Computational Mathematics and Modeling, pp. 21-28

A MOVING FINITE ELEMENT METHOD FOR SIMULATING THE FLOW OF MOLTEN STEEL AND FLUX IN THE CONTINUOUS CASTING PROCESS

Jutatip Archapitak[†], Benchawan Wiwatanapataphee[†], Yong Hong Wu^{*}, I Ming Tang[†]

*Faculty of Science, Mahidol University, Rama VI, Bangkok 10400
*Department of Mathematics, Curtin University of Technology, Perth, Australia

Abstract

A moving finite element method is developed for solving a fluid flow problem arising from the continuous steel casting process. The governing equations consist of the continuity equation and the Navier-Stokes equations. The formulation of the method is cast within the framework of the weighted residual method. A numerical technique based on the moving finite element method is developed to simulate the flow of molten steel and flux in the casting process.

Keywords - moving finite element, weight residual method, continuous casting

1. Introduction

The continuous steel casting process is an industrial process involving heat transfer, fluid flow and solidification. Figure 1 shows the essential feature of the continuous casting process. Molten steel flows from a tundish through a nozzle into a water-cooled mould and the solidified steel is continuously extracted from the bottom of the mould at a constant casting speed. During the casting process, mould powder is added at the top of the mould, and the mould oscillates vertically to facilitate the process and to prevent the steel from sticking to the mould wall.

The control of heat transfer and fluid flow is essential for the success of the process. Improper cooling strategy may cause internal defects, breakout of molten steel and surface cracks. Over the last couple of decades, many studies have been carried out to model various aspects of the continuous casting process. These studies have resulted in a fundamental understanding of the physics of the continuous casting process and led to the development of some essential methods for the design of the continuous casting process. However, many phenomena occurring in the caster, such as the formation of oscillation marks and the meniscus behavior, have still not been fully understood nor well controlled. Several studies on the phenomena at the meniscus in the continuous casting process have been carried out, including those by Laki et al. (1984), Nakana et al (1987), Morisue et al (1993), Mac David & Thomas (1996), Keisuke et al (2000). These studies have led to a better understanding on the mechanics of the meniscus phenomena. However,

A MOVING FINITE ELEMENT METHOD FOR SIMULATING THE FLOW OF $\ \ldots$ 22

sophisticated numerical techniques for the simulation of the meniscus shape and oscillation mark formulation as well as molten flux-steel flow have yet to be developed. The purpose of this work is to develop a model for the flows of liquid flux and liquid steel, and to develop a numerical algorithm based on the moving finite element method to solve the problem.

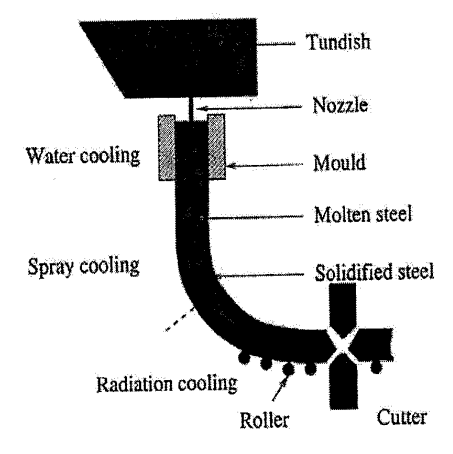


Figure 1. The continuous steel casting process.

2. Governing equations

The equations governing the flow of liquid flux and liquid steel include the continuity equation and the Navier - Stoke equations that can be expressed as follows,

$$u_{i,i} = 0$$
 in Ω , (1)

$$u_{i,j} = 0 \qquad \text{in} \quad \Omega,$$

$$\rho \left(\frac{\partial u_i}{\partial t} + u_j u_{i,j} \right) + p_{,i} - (\mu(u_{i,j} + u_{j,i}))_{,j} = 0 \quad \text{in} \quad \Omega$$
(2)

where we have used, and will continue to use throughout this paper, the index notation with repeated literal index representing summation over the index range; $\Omega = \Omega_f \cup \Omega_s$ with Ω_f representing the flux region and Ω_s being the steel region; u and g denote respectively the fluid velocity and gravitational acceleration; the index i refers to the x or z direction; $p = \overline{p} - \rho gz$ with \bar{p} denoting the fluid pressure; ρ is the density of fluid which has different constant values in Ω_f and Ω_s ; μ denotes the fluid viscosity having different values in Ω_f and Ω_s .

Equations (1) - (2) constitute a system of three partial differential equations in terms of three coordinates and time dependent unknown functions u_x, u_z and p. To completely define the problem, we also need to specify the boundary conditions and initial conditions for the velocity field of liquid flux and liquid steel. In a typical computational region as shown in Figure 2, we

23

J. ARCHAPITAK, B. WIWATANAPATAPHEE, Y. H. WU and I MING TANG

assume that the molten steel is fed to the system with inlet velocity U_s^0 , and the flux is continuously added at the top of the mould with velocity U_f^0 . The no-slip velocity condition and a pressure balance condition are imposed on the flux – steel interface Γ_0 . On the nozzle wall Γ_n , the velocities of molten steel and flux are zero, that is

$$u = \mathbf{0} \tag{3}$$

On the surface Γ_w , the solidified steel and flux move at the constant casting speed, i.e.,

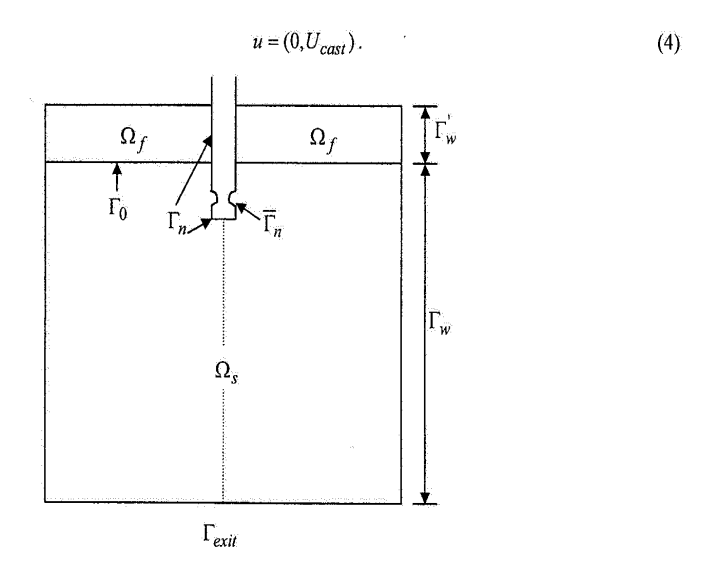


Figure 2. The computation domain

On the surface Γ_w , the liquid flux moves with the mould velocity, i.e.,

$$u = (0, U_{mould}). (5)$$

On the exit boundary Γ_{exit} , the velocity is determined by the casting speed, namely

$$u = (0, U_{cast}). (6)$$

Now, the problem to be solved can be stated as the following boundary value problem:

BVP: Find u and p such that equations (1)-(2) and boundary conditions (3)-(6) are satisfied.

2. Numerical method

Firstly, the continuity equation is weakened and replaced by

$$u_{i,i} = -\delta p , \qquad (7)$$

where δ is a small positive number. For convenience in notation, let

$$R = u_{i,i} + \delta p \,, \tag{8}$$

24 A MOVING FINITE ELEMENT METHOD FOR SIMULATING THE FLOW OF

$$R_i = \frac{\partial u_i}{\partial t} + u_j u_{i,j} + \frac{1}{\rho} P_{,i} - \left(\frac{\mu}{\rho} (u_{i,j} + u_{j,i}) \right)_{,j}, \tag{9}$$

In moving finite element methods, the mesh is allowed to deform, namely the node locations s_j are assumed to be variables and are time dependent. The finite element basis functions are thus assumed to depend on s_j as well as on x, i.e.,

$$\phi_i = \phi_i(\mathbf{x}, \mathbf{s}) \,, \tag{10}$$

where $\mathbf{s} = [\mathbf{s}_1, \mathbf{s}_2, ..., \mathbf{s}_N]^T$ with N being the number of nodes. Thus, our finite element approximations of u and p are as follows

$$u_i(\mathbf{x},t) = u_{li}(t)\phi_l(\mathbf{x},\mathbf{s}(t)), \qquad (11)$$

$$p(\mathbf{x},t) = p_I(t)\psi_I(\mathbf{x},\mathbf{s}(t)). \tag{12}$$

Obviously, in order to determine $u(\mathbf{x},t)$ and $p(\mathbf{x},t)$, we need to determine u_{li} , p_{l} and $\mathbf{s}_{1},\mathbf{s}_{2},...,\mathbf{s}_{N}$. For this purpose, we need to construct a weak form of (1) and (2) for which the trial solutions of $u(\mathbf{x},t)$ and $p(\mathbf{x},t)$ take the form of (11) and (12) respectively. The test space for equation (1) is chosen to be the space that p lies in. While, the test space for equation (2) is taken to be the space in which the function $\frac{\partial u}{\partial t}$ lies in at each time instant, as proposed by Jimack for the solution of a convection-diffusion equation [5]. Now following Jimack, by differentiating (11) with respect to time, we obtain

$$\frac{\partial u_i}{\partial t} = \dot{u}_{li} \phi_l + u_{li} \nabla_{\mathbf{s}} \phi_l \cdot \dot{\mathbf{s}} = \dot{u}_{li} \phi_l + \dot{\mathbf{s}}_{l} \cdot \boldsymbol{\beta}_{li}, \tag{13}$$

where the gradient operator $\nabla_{\mathbf{s}}$ applies to the \mathbf{s} variables and

$$\beta_{li} = \frac{\partial u_i}{\partial s_l} = \left(\frac{\partial u_i}{\partial s_{lx}}, \frac{\partial u_i}{\partial s_{lz}}\right). \tag{14}$$

Following Miller[10] and Jimack [5], we obtain

$$\beta_{li} = \nabla_l u_i = u_{kl} \nabla_l \phi_k = -u_{kl} \phi_l \nabla \phi_k = -\phi_l \nabla u_i. \tag{15}$$

Now, in order to minimize the residual of equation (1) over all possible choice of p, the test space is chosen to be the space spanned by the functions

$$(\psi_1,\psi_2,...,\psi_{N_n})$$
.

While, to minimize the residual of equation (2) over all possible choice of $\frac{\partial u}{\partial t}$, the test space in two-dimensional cases is chosen, according to Jimack [5], as the space spanned by

$$\big\{\phi_1,(\beta_{1i})_x,(\beta_{1i})_z;...;\phi_N,(\beta_{Ni})_x,(\beta_{Ni})_z\big\},$$

where i = 1, 2. Thus, the weak forms of (1) and (2) are as follow,

J. ARCHAPITAK, B. WIWATANAPATAPHEE, Y. H. WU and I MING TANG

25

$$(R, \Psi_j) = 0,$$
 $(j = 1, 2, ..., N_p),$ (16)

$$(R_i, \phi_{ij}) = 0$$
, $(i = 1, 2; j = 1, 2, ..., N)$, (17)

$$(R_1, (\beta_{j1})_k) + (R_2, (\beta_{j2})_k) = 0, \quad (k = 1, 2; j = 1, 2, ..., N).$$
 (18)

From above, through a long derivation, we obtain

$$C\mathbf{u} + \delta C_{p}\mathbf{p} = 0, \qquad (19)$$

$$M \dot{\mathbf{u}} + M_1 \dot{\mathbf{s}} + K_1 \mathbf{u} + C_1 \mathbf{p} = 0,$$
 (20)

$$M_2 \dot{\mathbf{u}} + M_s \dot{\mathbf{s}} + K_2 \mathbf{u} + C_2 \mathbf{p} = 0,$$
 (21)

which form a system of $(4N + N_p)$ equations for the solution of the nodal values of $u(\mathbf{x},t)$ and $p(\mathbf{x},t)$ as well as **s**. From equation (19)

$$\mathbf{p} = -\frac{1}{\delta} C_p^{-1} C \mathbf{u} , \qquad (22)$$

on using which, equations (20) and (21) become

$$M\dot{\mathbf{u}} + M_1\dot{\mathbf{s}} + K_1\mathbf{u} - \frac{1}{8}C_1C_p^{-1}C\mathbf{u} = 0,$$
 (23)

$$M_2 \dot{\mathbf{u}} + M_s \dot{\mathbf{s}} + K_2 \mathbf{u} - \frac{1}{8} C_2 C_p^{-1} C \mathbf{u} = 0$$
 (24)

Equations (23) and (24) can be expressed in shorter form as

$$A(\mathbf{Y})\dot{\mathbf{Y}} = \mathbf{G} \,, \tag{25}$$

where $\mathbf{Y} = [u_1, v_1, x_1, z_1; ...; u_N, v_N, x_N, z_N]^T$ in which (u_i, v_i) denotes the velocity at the *i*th node; (x_i, z_i) is the position of the *i*th node. System (25) is then solved by using Euler's backward difference scheme with variable time step. Let Y_n be the solution and Δt_n be the time increment at time step n, we have

$$A(\mathbf{Y}_{n+1})(\mathbf{Y}_{n+1} - \mathbf{Y}_n) = \mathbf{G}_{n+1} \Delta t_n.$$
 (26)

By using an iterative scheme, the iterative solution of equation (26) at iteration i is defined by

$$A(\mathbf{Y}_{n+1}^{i})(\mathbf{Y}_{n+1}^{i+1} - \mathbf{Y}_{n}) = \mathbf{G}_{n+1}^{i} \Delta t_{n}.$$
 (27)

4. Numerical example

For the continuous steel caster under consideration, the mould is symmetrical about two planes that pass through the central line of the mould. Thus the computation region could be limited to one quadrant and its boundary consists of several parts as shown in Figure 2. The caster has a mould half width of 875 mm, a narrow - face half width of 118 mm, a depth of 800 mm. The casting parameters are as shown in Table 1. Figure 3 shows the flow patterns of liquid flux and steel for three different velocities of mould wall stroke. The results indicate that the average velocity of liquid flux above the meniscus surface increases when the velocity of the stroke of

26 A MOVING FINITE ELEMENT METHOD FOR SIMULATING THE FLOW OF

mould wall increases, and that the flow of liquid steel dominates the shape of the meniscus surface.

Parameter	Value	Unit
Density of Steel ρ_s	7800	kg/m^3
Density of Flux ρ_f	2930	kg/m^3
Viscosity of Steel μ _s	0.001	Pa·s
Viscosity of Flux μ _f	0.5	Pa·s

Table 1. Parameter used in the numerical example

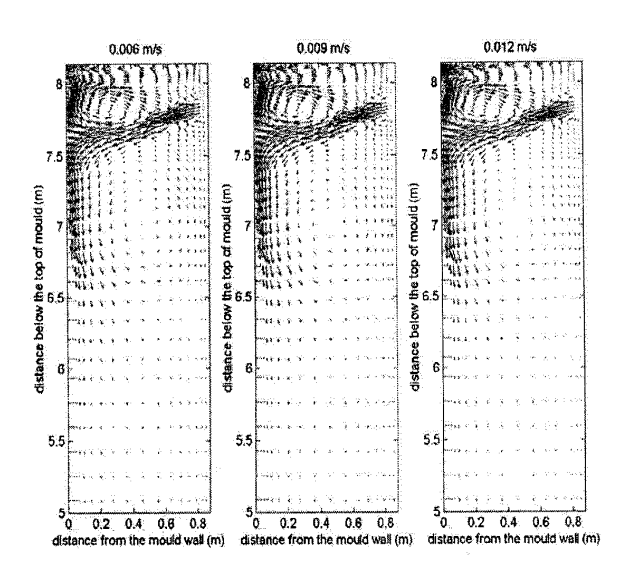


Figure 3. The velocity vector for strokes of mould wall at 0.006 m/s, 0.009 m/s, and 0.012 m/s.

5. Conclusions

A mathematical model and a numerical technique, based on a moving finite element formulation, have been developed to study the flow of liquid flux and liquid steel and to predict the meniscus shape. The meniscus refers to the interface between the liquid flux and the liquid steel. Three different strokes of mould wall have been used in this study to investigate their impact on the fluid velocity field and the meniscus shape. It should be addressed here that, the formulation in this paper focuses only on fluid flow. However, in practice, the problem involves not only fluid flow but also heat transfer and electromagnetic stirring. Thus, in our future work, we will take into account the effect of temperature field and electromagnetic field to get more accurate results of the meniscus shape and flow field above and below the meniscus region.

Acknowledgements

We are very grateful to The Thailand Research Fund (TRF) and National Metal and Materials Technology Center National Science and Technology Development Agency for their financial support.

References

- J.K. Brimacombe, I.V.Samarasekera, J.E.Laid(eds.), Continuous casting: Heat flow, solidification and crack formation, Iron and Steel Society, AIME 2 (1983). J.K. Brimacombe, I.V.Samarasekera, J.E.Laid(eds.), Continuous casting: Heat flow, solidification and crack formation, Iron and Steel Society, AIME 2 (1983).
- [2] S.K. Choudhary, D. Mazumdar, Mathematical modeling of fluid flow, heat transfer and solidification phenomena in continuous casting of steel, Steel Research 66 (5) (1995) 199-205.
- [3] Dunont B, and Gagnoud A, 3D Finite Element Method with Impedance Boundary Condition for the Modeling of Molten Metal Shape in Electromagnetic Casting IEEE Transactions on magnetics, Vol.36, No.4, July 2000.
- [4] P.J.Flint, A three-dimensional finite difference model of heat transfer, fluid flow and solidification in the continuous slab caster, Steel making Conference model of heat transfer, fluid flow and solidification in the continuous slab caster, Steel making Conference processing (1990) 481-490.
- [5] P.K. Jimack, A best approximation property of the moving finite element method, SIAM J. NUMER. ANAL. Vol. 33, No.6, pp.2286-2302, December 1996.
- [6] J.E. Lait, J.K. Brimacombe, F. Weinberg, Continuous casting, TMS AIME New York (1973) 171-196
- [7] J.E. Lait, J.K. Brimacombe, F. Weinberg, *Mathematical modeling of heat flow in the continuous casting of steel*, Ironmaking and Steelmaking(Quarterly) 2 (1974) 90-97.
- [8] M. Larrecq, C. Sagiez., M.Wanin, Influence of convective heat transfer on solidification in the mould, Proceeding of inter. Conference of Solidification technology in the foundry and cast house, (1983) 536-54.
- [9] K. Miller and R.N. Miller, Moving finite elements I, Siam J. Numer. Anal., Vol.18, No.6, December 1981.
- [10] E.A. Mizikar, Mathematical heat-transfer model for solidification of continuously cast steel slabs, Transactions of TMS-AIME 239(1967) 1747-1753.
- [11] A.Perkins, W.R. Irving, Two dimensional heat transfer model for continuous casting, The Metals Society (1975)187-199.
- [12] R. Taylor, K.C. Mills, Physical properties of casting powders: part 3 thermal conductivities of casting powders, Ironmaking and Steelmaking 15 (1988)187-194
- [13] B. Wiwattanapataphee, Mathematical Modeling of fluid flow and Heat Transfer in continuous casting process, Ph.D Thesis, Curtin Uni. of Tech., 1998.
- [14] B. Wiwattanapataphee, and Yong Hong Wu, A new Petrov Galerkin finite element method for transient mass and heat transport with solidification, submitted.
- [15] B. Wiwattanapataphee, and Yong Hong Wu, A Finite Element method for the Coupled Turbulent Mass and Heat Flow, 2000. Anderson, J. D. Jr., Modern Compressible Flow With Historical Prospective, McGraw-Hill, New York, 1982.
- [16]Y-H. Wu, J.M. Hill, P.J. Flint, A noval finite element method for heat transfer in the continuous caster, J. Austral. Math. Soc. Ser. B 35 (1994) 263-288.

†A FINITE ELEMENT SCHEME FOR THE DETERMINATION OF ELECTROMAGNETIC FORCE IN CONTINUOUS STEEL CASTING

J. Archapitak¹, B. Wiwatanapataphee¹, Y. H. Wu^{2*} and I. M. Tang³

Department of Mathematics, Faculty of Science, Mahidol University, Bangkok 10400, Thailand. e-mail: g4237665@student.mahidol.ac.th

²Department of Mathematics and Statistics, Curtin University of Technology, GPO Box U 1987, Perth, WA6845, Australia. e-mail: yhwu@maths.curtin.edu.au

³Department of Physics, Faculty of Science, Mahidol University, Bangkok, 10400, Thailand. e-mail: scmit@mahidol.ac.th

Abstract: This paper is concerned with the determination of the electromagnetic force acting on molten steel in the continuous steel casting process. The governing equations for the electromagnetic field are formulated in terms of the magnetic vector potential and the electric scalar potential. For two-dimensional cases, the transient magnetic field is shown to be governed by a parabolic type boundary value problem. Based on Galerkin's method, a finite element scheme is developed to solve the boundary value problem. The numerical results obtained demonstrate that the induced electromagnetic force always acts inward to sustain the molten steel. The effects of source current and magnetic frequency on the magnitude of the induced electromagnetic force are also presented in this paper.

AMS Subj. Classification: 65N30

Key Words: continuous casting, electromagnetic field, Lorentz force.

^{*}Corresponding author

[†]Paper to appear in International Journal of Computational and Numerical Analysis and Applications accepted in May, 2004.

1. Introduction

Continuous casting is an industrial process for converting molten steel to solid steel products. As shown in Figure 1, in the continuous casting process, molten steel is poured continuously from a tundish through a submerged entry nozzle into a water-cooled casting mould where intensive cooling results in a thin solidified steel shell to form around the edge of the casting. The solidified steel shell with a liquid pool in the center is then continuously withdrawn from the bottom of the mould at a constant speed. The product is supported by a set of rollers, after leaving the mould, and cooled down by water sprays. When the completely solidified casting has attained the desired length, it is cut off with a cutter.

The process involves many complex phenomena such as turbulent flow, heat transfer with phase change and formation of oscillation marks on steel surface. These phenomena interact one with another and thus the modelling of the continuous casting process constitutes one of the most outstanding mathematical modelling problems. Over the last few decades, extensive studies have been carried out worldwide to model various aspects of the continuous casting process, particularly on the heat transfer and steel solidification process [1,10], the turbulent flow phenomena [9, 11, 12] and the formation of oscillation marks [2, 7]. Although previous studies have led to a significant advance in the continuous casting technology, many problems still occur in the industrial process. One of the problems, which has not been fully understood and under control, is the so-called oscillation marks formation.

To minimize the depth of oscillation marks on steel surface and to improve steel quality, considerable efforts have been made worldwide in recent years, particularly in Europe and Japan, to develop electromagnetic casting technologies to utilize the electromagnetic field to influence the casting process [3, 4, 6, 8]. Many experiments show that the external electromagnetic field [5, 8, 13] has significant influence on the formation and the depth of oscillation marks. In electromagnetic casting, a coil is mounted around the casting mould. The magnetic field generated from the source current through the coil induces the electric current in molten steel. This current heats the liquid in terms of joule heating and generates a body force in the molten steel, which is the so called electromagnetic force or Lorentz force, $\mathbf{F}_r = \mathbf{J} \times \mathbf{B}$, where \mathbf{J} and \mathbf{B} are respectively the induced current density and magnetic flux density. The Joule heat and the body force act on the molten steel and consequently influence the flow of the liquid, the steel solidification process, and the formation of oscillation marks on steel surface.

In an attempt to incorporate the effect of the electromagnetic field into our recently developed model for the coupled fluid flow and heat transfer

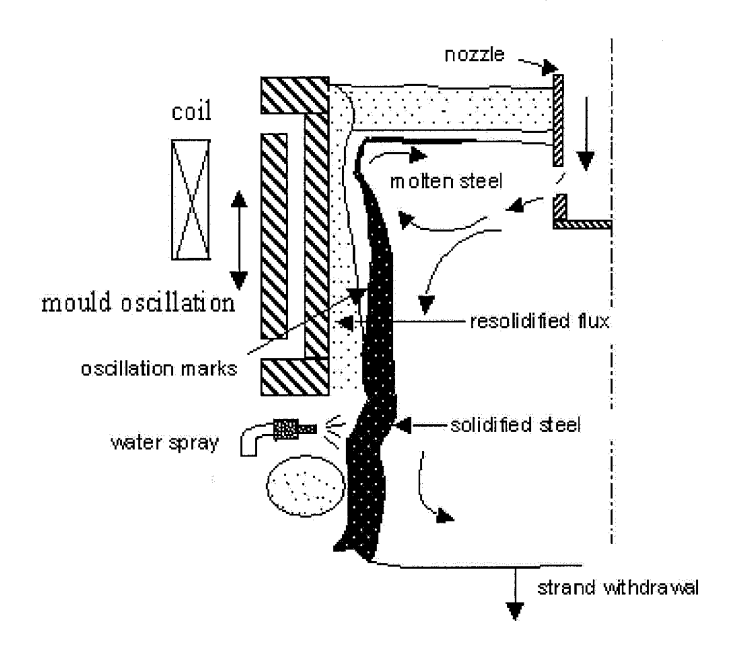


Figure 1: The continuous steel casting process.

in the continuous steel casting process [12], a finite element based numerical scheme has been developed for the calculation of the electromagnetic force and is presented in this paper. The rest of the paper is organized as follows. In section two, we construct the boundary value problem for the determination of the electromagnetic field in the continuous casting process. In section three, we develop a finite element scheme for the determination of the electromagnetic field and derive the formula for the determination of the electromagnetic force using the finite element solution of the magnetic field. In section four, a numerical study is carried out to demonstrate the influence of various electromagnetic field parameters on the electromagnetic force induced in molten steel.

2. Governing Equations for the Electromagnetic Field

The governing equations for the electromagnetic field include the Maxwell equations and the constitutive equations. Let ${\bf H}$ and ${\bf E}$ denote respectively the magnetic field and the electric field. Then the Maxwell equations are

$$\nabla \times \mathbf{H} = \mathbf{J} + \frac{\partial \mathbf{D}}{\partial t},\tag{1}$$

$$\nabla \times \mathbf{E} = -\frac{\partial \mathbf{B}}{\partial t},\tag{2}$$

$$\nabla \cdot \mathbf{B} = 0, \tag{3}$$

$$\nabla \cdot \mathbf{D} = \rho_d, \tag{4}$$

where $\mathbf{J}, \mathbf{D}, \rho_d$ and \mathbf{B} denote respectively current density, electric displacement, free charge density and magnetic flux density. The magnetic flux density \mathbf{B} and the electric displacement \mathbf{D} are respectively related to the magnetic field \mathbf{H} and the electric field \mathbf{E} by the following constitutive equations

$$\mathbf{B} = \mu \mathbf{H},\tag{5}$$

$$\mathbf{D} = \varepsilon \mathbf{E},\tag{6}$$

where μ and ε are magnetic permeability and permittivity respectively. Another constitutive equation relating the current density with \mathbf{E} , \mathbf{B} and the velocity \mathbf{v} of the conducting media is as follows

$$\mathbf{J} = \sigma(\mathbf{E} + \mathbf{v} \times \mathbf{B}) + \rho_d \mathbf{v} + \mathbf{J_s},\tag{7}$$

where σ is the electroconductivity. As molten steel is a good conductor, the transient term in equation (1) can be neglected and we thus have

$$\nabla \times \mathbf{H} = \mathbf{J},\tag{8}$$

$$\nabla \cdot \mathbf{J} = 0, \tag{9}$$

where equation (9) is obtained by noting that the divergence of the curl of any vector field is identical to zero. Further simplification is to neglect the displacement current ρ_d and the flow-induced current $\sigma \mathbf{v} \times \mathbf{B}$. Thus, we have

$$\mathbf{J} = \sigma \mathbf{E} + \mathbf{J_s},\tag{10}$$

and equation (4) is identical to equation (9) by noting equations (6) and (10). Hence, our problem becomes to determine $\bf B$ and $\bf J$ by solving the following equations

$$\nabla \times \left(\frac{\mathbf{B}}{\mu}\right) = \mathbf{J},\tag{11}$$

$$\nabla \times \left(\frac{\mathbf{J} - \mathbf{J_s}}{\sigma}\right) = -\frac{\partial \mathbf{B}}{\partial t},\tag{12}$$

$$\nabla \cdot \mathbf{B} = 0, \tag{13}$$

$$\nabla \cdot \mathbf{J} = 0. \tag{14}$$

In this work, we solve the problem by firstly formulating the problem in terms of a potential function. From equation (13) and noting that the divergence

of the curl of any vector field is identical to zero, we can determine ${\bf B}$ by a magnetic vector potential ${\bf A}$, namely

$$\mathbf{B} = \nabla \times \mathbf{A},\tag{15}$$

and hence equation (11) becomes

$$\nabla \times \left(\frac{1}{\mu} \nabla \times \mathbf{A}\right) = \mathbf{J}.\tag{16}$$

Substituting equation (15) into equation (12) yields

$$\nabla \times \left(\frac{\mathbf{J} - \mathbf{J_s}}{\sigma} + \frac{\partial \mathbf{A}}{\partial t} \right) = 0, \tag{17}$$

which indicates that the vector field $\left(\frac{\mathbf{J}-\mathbf{J_s}}{\sigma}+\frac{\partial \mathbf{A}}{\partial t}\right)$ is conservative and consequently, there exists a scalar potential ϕ such that

$$\frac{\mathbf{J} - \mathbf{J_s}}{\sigma} + \frac{\partial \mathbf{A}}{\partial t} = -\nabla \phi, \tag{18}$$

or

$$\mathbf{J} = \mathbf{J_s} - \sigma \frac{\partial \mathbf{A}}{\partial t} - \sigma \nabla \phi. \tag{19}$$

Substituting equation (19) into equations (16) and (14), we end up with two equations for the determination of A and ϕ , namely

$$\nabla \times (\frac{1}{\mu} \nabla \times \mathbf{A}) = -\sigma \frac{\partial \mathbf{A}}{\partial t} - \sigma \nabla \phi + \mathbf{J_s}, \tag{20}$$

$$\nabla \cdot (-\sigma \frac{\partial \mathbf{A}}{\partial t} - \sigma \nabla \phi + \mathbf{J_s}) = 0.$$
 (21)

In this work, we are concerned with two-dimensional problems with ${\bf A}, {\bf J}$ and ϕ taking the following forms

$$\mathbf{A} = (0, A_y(x, z), 0), \mathbf{J} = (0, J_y(x, z), 0), \ \phi = \text{constant}.$$
 (22)

With equation (22), equation (21) is satisfied automatically and equation (20) becomes

$$\frac{\partial A_y}{\partial t} = \frac{1}{\sigma \mu} \nabla^2 A_y - \frac{1}{\sigma} J_{s_y},\tag{23}$$

or in index notation

$$A_{y,t} = \frac{1}{\sigma\mu} A_{y,jj} - \frac{1}{\sigma} J_{sy}. \tag{24}$$

For the case of sinusoidal source current, i.e.

$$J_{sn} = j_s(x, z)e^{i\omega t},\tag{25}$$

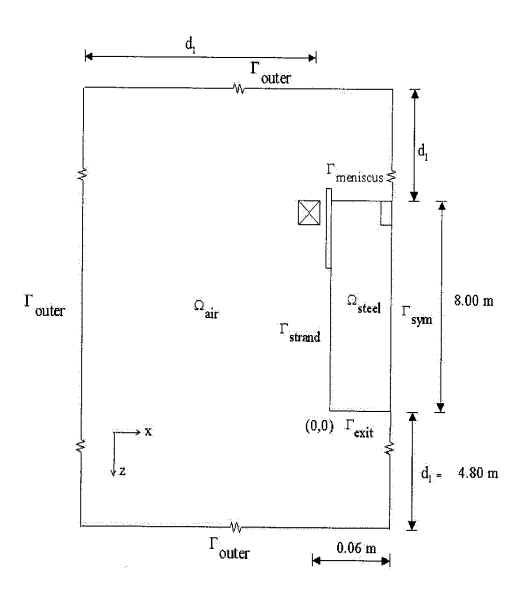


Figure 2: The computation domain for the electromagnetic problem.

equation (23) admits solution of the following form

$$A_y = a(x, z)e^{i\omega t}. (26)$$

By substituting equation (26) into equation (24), we have

$$a_{,jj} - \beta^2 a = \mu j_s. \tag{27}$$

where $\beta^2 = \sigma \mu \omega i$. To completely define the problem, boundary conditions must be given to specify the value of a(x,z) on the boundary. We consider here a typical casting system as shown in Figure 2. On the outer boundary, a is set to zero, which implies that the effect of induction on the magnetic field at these locations is negligible. To insure good accuracy, an appropriate distance d_1 measured from the outer boundary to the inductor is needed and, for the example under investigation, d_1 is taken to be 4.8 meter.

3. Finite Element Solution of the Magnetic Field

To solve equation (27) numerically, we first develop the following corresponding variational boundary value problem using the weighted residual technique

VBVP: Find $a \in H_0^1(\Omega)$ such that $\forall w \in H_0^1(\Omega)$

$$(a_{,j}, w_{,j}) + \beta^2(a, w) = -\mu(j_s, w),$$
 (28)

where w is the so-called weight function or test function; (\cdot,\cdot) denotes the inner product on the square integrable function space $L^2(\Omega)$ and $H^1_0(\Omega)$ is defined as follows

$$H^1_0(\Omega) = \left\{ v \, \middle| \, v, \frac{\partial v}{\partial x}, \frac{\partial v}{\partial z} \in L^2(\Omega) \text{ and } v = 0 \text{ on } \partial \Omega \right\}.$$

To solve the VBVP problem, we pose the problem into an N-dimensional subspace, namely, approximate a and w by

$$a = \sum_{i=1}^{N} a_i \phi_i$$
 , $w = \sum_{i=1}^{N} w_i \phi_i$, (29)

Substituting the second equation of (29) into equation (28), we have

$$\{(a_{,j},\phi_{k,j})+\beta^2(a,\phi_k)+(j_s,\phi_k)\}w_k=0.$$

As w and consequently w_k are arbitrary, we have for $k = 1, 2, \dots, N$

$$(a_{,j},\phi_{k,j}) + \beta^2(a,\phi_k) = -(j_s,\phi_k).$$
 (30)

Now by substituting the first equation of (29) into equation (30), we have for $k = 1, 2, \dots, N$ that

$$\sum_{i=1}^{N} \left[(\phi_{i,j}, \phi_{k,j}) + \beta^{2}(\phi_{i}, \phi_{k}) \right] a_{i} = -(j_{s}, \phi_{k}),$$

which can be written in matrix form as

$$\mathbf{Ma} = \mathbf{F} \tag{31}$$

where

$$\mathbf{M} = \{m_{ik}\}\ \text{with}\ m_{ik} = (\phi_{i,j}, \phi_{k,j}) + \beta^2(\phi_i, \phi_k)$$

$$\mathbf{F} = \{f_k\}$$
 with $f_k = -(j_s, \phi_k)$.

Once the finite element solution of a(x,z) is found from system (31), the magnetic vector potential, the magnetic flux density **B** and the current density **J** can be determined from equations (15), (19), (22), (25), and (26) as follows

$$\mathbf{A} = e^{i\omega t}[0, \ a(x, z), \ 0], \tag{32}$$

$$\mathbf{B} = \nabla \times \mathbf{A} = e^{i\omega t} \left[-\frac{\partial a}{\partial z}, \ 0, \ \frac{\partial a}{\partial x} \right] := \mathbf{b}(x, z) \ e^{i\omega t}, \tag{33}$$

$$\mathbf{J} = \mathbf{J_s} - \sigma \frac{\partial \mathbf{A}}{\partial t} - \sigma \nabla \phi = e^{i\omega t} [0, j_s - \sigma \omega ai, 0].$$
 (34)

Consequently, the Lorentz force can be determined by

$$\mathbf{F}_{r} = \mathbf{J} \times \mathbf{B},$$

$$= (j_{s} - \sigma \omega ai) \nabla a \ e^{2\omega it},$$

$$:= \mathbf{f}_{r}(x, z) e^{2\omega it}.$$
(35)

4. Numerical Studies

The numerical example under investigation is a rectangular caster which has a width of 0.12 m and a depth of 0.8 m in the x-z plane. The computation region is as given in Figure 2. The finite element mesh, constructed from the FEMLAB graphic subroutine, has 23180 elements and 11856 nodes. The parameters used in the computation are chosen to have values as follows: conductivity of steel $\sigma_s = 7.14 \times 10^5 \ \Omega^{-1} m^{-1}$; magnetic permeability in vacuum $\mu = 4\pi \times 10^{-7} \mathrm{Henry}/m$; magnetic permittivity in vacuum $\varepsilon = 8.8540 \times 10^{-12} \mathrm{Farad}/m$; magnetic field frequency $f = 60 - 100 \ \mathrm{Hz}$; source current density $j_s = 1000000 - 3000000 \ A/m^2$.

Figure 3 shows the contour plot of the finite element solution of a(x,z) from which the transient magnetic vector potential can be determined by equation (32). Figures 4 and 5 show respectively the magnetic flux density vector $\mathbf{b}(x,z)$ and the Lorentz force vector $\mathbf{f}_r(x,z)$ as defined in equations (33) and (35). Figures 6 and 7 show respectively the influences of the source current and the magnetic field frequency on the magnitude of the Lorentz force $|\mathbf{f}_r(x,z)|$ on a horizontal section 0.05 m below the meniscus.

The results show that the Lorentz force acts on the molten steel basically in the horizontal direction toward the central plane. This force will contribute to preventing molten steel from sticking to the mould wall and smoothing the steel casting surface. The results have also demonstrated that the magnitude of the force could be increased by increasing the source current and the magnetic field frequency.

With the Lorentz force determined, the influence of electromagnetic field on heat transfer and fluid flow in continuous casting can be simulated by incorporating this body force into our recently developed heat transfer-fluid flow model [12].

Acknowledgments

The first author is supported by the Thailand Research Fund (TRF) through the Royal Golden Jubilee Ph.D. Program (contract number PHD/0134/2543, 3· M· MU/43/B·1). The financial support is gratefully acknowledged.

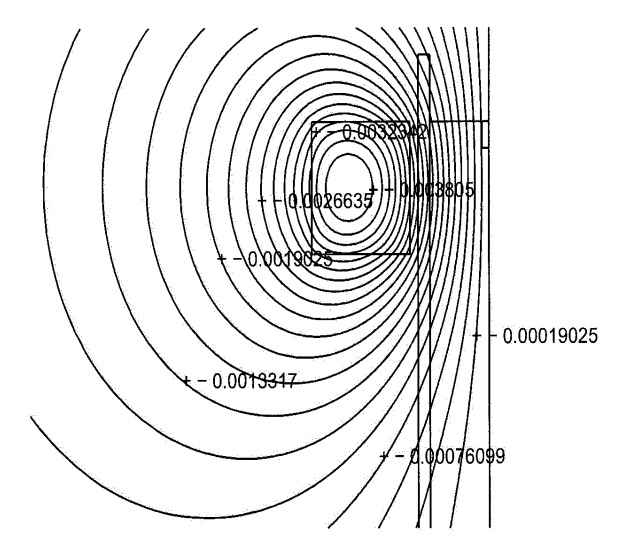


Figure 3: The contour plot of a(x,z) at $j_s=1000000\ A/m^2$ and frequency $f=60\ {\rm Hz}.$

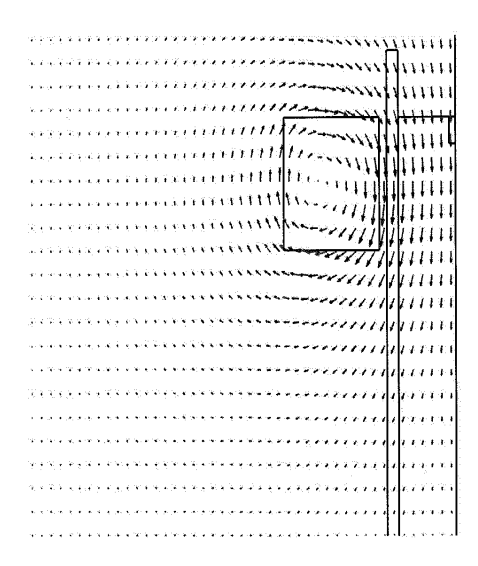


Figure 4: The magnetic flux density vector $\mathbf{b}(x,z)$ at $j_s=1000000~A/m^2$ and frequency $f=60~\mathrm{Hz}.$

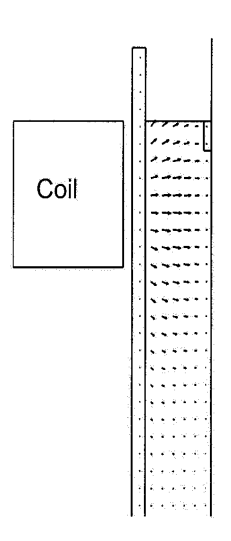


Figure 5: The electromagnetic force vector $\mathbf{f}_r(x,z)$ at $j_s=1000000~A/m^2$ and frequency $f=60~\mathrm{Hz}.$

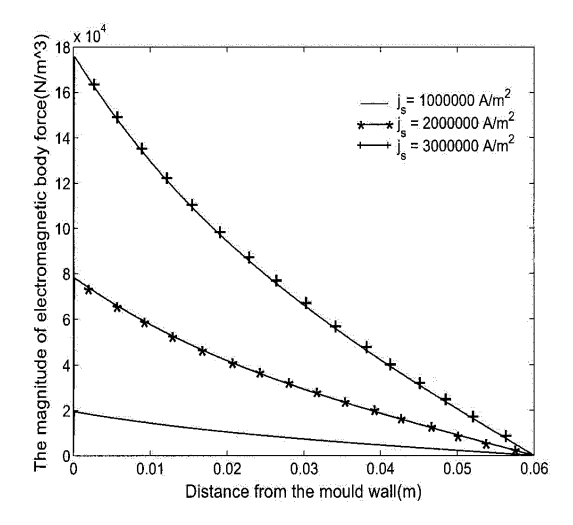


Figure 6: The influence of source current on the magnitude of the electromagnetic force at frequency $f=60~{\rm Hz}.$

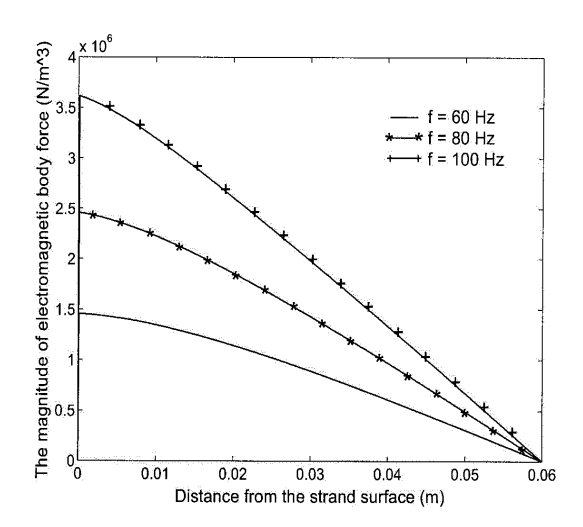


Figure 7: The influence of the frequency of magnetic field on the magnitude of the electromagnetic force at $j_s = 1000000 \ A/m^2$.

References

- [1] J.M. Hill and Y.H. Wu, On a nonlinear stefan problem arising in the continuous casting of steel, *Acta Mechanica*, **107** (1994), 183-198.
- [2] J.M. Hill, Y.H. Wu and B. Wiwatanapataphee, Mathematical analysis of the formation of oscillation marks in the continuous steel casting, *Engineering Mathematics*, **36(4)** (1999), 311-326.
- [3] D.R. Jenkins and De Hoog F.R., Calculation of the magnetic field due to the electromagnetic stirring of molten steel, *Numerical Methods in Engineering 96*, John Wiley and Sons Ltd, (1994), 332-336.
- [4] H. Kim, J.P. Park, H. Jeong, J. Kim, Continuous casting of billet with high frequency electromagnetic field, ISIJ International, 42 (2002), 171-177.
- [5] B. Li and F. Tsukihashi, Effect of static magnetic field application on the mass transfer in sequence slab continuous casting process, *ISIJ Interna*tional, 41 (2001), 844-850.
- [6] T.J. Li, K. Sassa and S. Asai, Surface quality improvement of continuous cast metals by imposing intermitten high frequency magnetic field and synchronising the field with mould oscillation, ISIJ International, 36(4) (1996), 410-416.
- [7] K. Schwerdtfeger and H. Sha, Depth of oscillation marks forming in continuous casting of steel, Metallurgical and Materials Transactions B, 31B (2000), 813-826.

1

- [8] P. Sivesson, G. Hallen and B. Widell, Improvement of inner quality of continuously cast billets using electromagnetic stirring and thermal soft reduction, *Ironmaking and Steelmaking*, 25(3) (1998), 239-246.
- [9] B.G. Thomas, L.J. Mika and F.M. Najjar, Simulation of fluid flow inside a continuous slab-casting machine, Metallurgical and Materials Transactions B, 21 (1990), 387-300.
- [10] Y.H. Wu, J.M. Hill and P. Flint, A novel finite element method for heat transfer in the continuous caster, J. Austral. Math. Soc. Ser. B, 35 (1993), 263-288.
- [11] Y.H. Wu and B. Wiwatanapataphee, An exponentially fitted enthalpy control volume algorithm for coupled fluid flow and heat transfer, ANZIAM Journal, 32E (2000), 1580-1598.
- [12] B. Wiwatanapataphee, Y.H. Wu, J. Archapitak and P.F. Siew, A numerical study of the turbulent flow of molten steel in a domain with a phase-change boundary, *Journal of Computational and Applied Mathematics*, 166(1) (2003), 307-319.
- [13] Y. Zhou, K. Sassa and S. Asai, Substitute function for mould oscillation replaced by imposition of an intermitten magnetic field in a continuous caster, *Tdtsu to Hagane-J. of the Iron&Steel Institute of Japan*, **85(6)** (1999), 460-465.

BIOGRAPHY

NAME Miss Jutatip Archapitak

DATE OF BIRTH 8 May 1977

PLACE OF BIRTH Bangkok, Thailand

INSTITUTIONS ATTENDED Mahidol University, 1995–1998:

Bachelor of Science (Mathematics)

(Second class honours)

Mahidol University, 1999–2004:

Doctor of Philosophy (Mathematics)

SCHOLARSHIPS Development and Promotion of Science and

Technology Talents Project (DPST),

Thailand, 1997–2000

The Royal Golden Jubilee Ph.D. Program

scholarship from the Thailand Research

Fund, Thailand, 2001–2004

HOME ADDRESS 74 Tedsabarn Sai 3 Road, Watkunlaya

Thonburi, Bangkok 10600 Thailand

E-MAIL jutatiparchapitak@yahoo.com